



**UNIVERSIDAD NACIONAL AUTÓNOMA DE MÉXICO**  
PROGRAMA DE MAESTRÍA Y DOCTORADO EN CIENCIAS MÉDICAS,  
ODONTOLÓGICAS Y DE LA SALUD  
FACULTAD DE MEDICINA  
CAMPO DE CONOCIMIENTO: CIENCIAS MÉDICAS

BIOMARCADORES AVANZADOS DE RESONANCIA MAGNÉTICA COMO  
FACTORES PRONÓSTICOS PARA LA SOBREVIVENCIA DE PACIENTES CON  
GLIOBLASTOMA MULTIFORME.

TESIS  
QUE PARA OPTAR POR EL GRADO DE DOCTOR EN CIENCIAS

PRESENTA:  
M. EN C. ERNESTO ALEJANDRO ROLDAN VALADEZ

TUTOR PRINCIPAL:  
DR. LUIS CAMILO RÍOS CASTAÑEDA  
PROGRAMA DE MAESTRÍA Y DOCTORADO EN CIENCIAS MÉDICAS,  
ODONTOLÓGICAS Y DE LA SALUD

MIEMBROS DEL COMITÉ TUTOR:  
DR. ANTONIO VILLA ROMERO  
FACULTAD DE MEDICINA

DR. SERGIO MORENO JIMÉNEZ  
PROGRAMA DE MAESTRÍA Y DOCTORADO EN CIENCIAS MÉDICAS,  
ODONTOLÓGICAS Y DE LA SALUD

MÉXICO, D.F. JUNIO 2014



Universidad Nacional  
Autónoma de México

Dirección General de Bibliotecas de la UNAM

**Biblioteca Central**



**UNAM – Dirección General de Bibliotecas**  
**Tesis Digitales**  
**Restricciones de uso**

**DERECHOS RESERVADOS ©**  
**PROHIBIDA SU REPRODUCCIÓN TOTAL O PARCIAL**

Todo el material contenido en esta tesis esta protegido por la Ley Federal del Derecho de Autor (LFDA) de los Estados Unidos Mexicanos (México).

El uso de imágenes, fragmentos de videos, y demás material que sea objeto de protección de los derechos de autor, será exclusivamente para fines educativos e informativos y deberá citar la fuente donde la obtuvo mencionando el autor o autores. Cualquier uso distinto como el lucro, reproducción, edición o modificación, será perseguido y sancionado por el respectivo titular de los Derechos de Autor.

## Índice

<b>Resumen .....</b>	<b>4</b>
<b>Abstract .....</b>	<b>5</b>
<b>Introducción .....</b>	<b>6</b>
<b>Proyecto de tesis .....</b>	<b>8</b>
<b>Avances del proyecto de tesis .....</b>	<b>63</b>
<b>Anexos (artículos publicados) .....</b>	<b>112</b>
<b>Conclusiones .....</b>	<b>142</b>

## RESUMEN

La evaluación por imagen de los tumores cerebrales implica la obtención de secuencias convencionales que convencionales consisten en el T1 con y sin gadolinio (medio de contraste), el T2, la difusión y la secuencia Flair. Entre los años 2006 y 2009, diversas publicaciones en revistas especializadas de neurología e imagenología, presentaron la propuesta de incluir secuencias para “análisis avanzado” en el estudio de los tumores cerebrales.

Estas secuencias están representadas por: la secuencia de difusión y su post proceso para medir el *Coefficiente de Difusión Aparente (ADC)*; la *perfusión cerebral*, que permite cuantificar *el volumen y el flujo sanguíneo cerebral (CBV, CBF)*; la *espectroscopia*, que permite cuantificar diferentes metabolitos en el tumor y zona peritumoral, y dar evidencia de infiltración en áreas que todavía no presentan realce al contraste. La última técnica de análisis avanzado es la secuencia *tensor de difusión (DTI)*, que mide la orientación tridimensional del movimiento de las moléculas de agua en el tejido nervioso y con ello, crea mapas cuantitativos y permite medir diferentes biomarcadores.

Esta tesis presenta el protocolo de investigación realizado para el análisis avanzado de secuencias de resonancia magnética en el estudio de sobrevida de pacientes con glioblastoma multiforme; dos artículos originales en proceso de revisión que representan los avances realizados hasta el momento de presentación y tres artículos originales publicados en revistas indexadas como parte de los productos del proyecto de investigación.

## ABSTRACT

Imaging evaluation of brain tumors implies the acquisition of magnetic resonance imaging (MRI) sequences known as conventional; they are represented by the T1-weighted before and after gadolinium administration, T2-weighted, diffusion and Flair. Between 2006 and 2009, several publications in indexed journals in the fields of neurology and imaging proposed the inclusion of sequences for the “Advanced Analysis” of brain tumors.

This group of images comprises the sequences of diffusion, and its image postprocessing to measure the *apparent diffusion coefficient* (ADC); the *perfusion weighted imaging* (PWI), which allows the calculation of cerebral blood flow and cerebral blood volume; the *spectroscopy* (MRS) which quantifies several brain metabolites in the tumor and peritumoral regions given evidence of infiltrated areas of brain tissue, still not showing enhance after contrast administration. The last advance sequence is the diffusion tensor imaging (DTI), that measures the 3D movement of water molecules in brain tissue; with this sequence it is possible to create quantitative maps that derive up to eleven different biomarkers.

In this thesis, we present the original research protocol proposed at the National Institute of Neurology and Neurosurgery for the study of survival in patients with glioblastoma multiforme using advanced biomarkers of MRI; the full text of two manuscripts currently under review as part of the advances of the project and three full-text, published, original articles as evidence of the products of this research project.

## Introducción

Los tumores gliales de alto grado (glioblastoma multiforme) representan el tipo más común de tumor cerebral maligno alcanzando el 40-50% de las neoplasias cerebrales primarias. Los esquemas actuales para el tratamiento de estos tumores implica la combinación de cirugía con radioterapia/quimioterapia adyuvante. Sin embargo, el pronóstico global para estos tumores es pobre todavía a pesar de los tratamientos agresivos, especialmente en pacientes con gliomas de alto grado (IV) cuyo promedio de supervivencia después de la cirugía es de solamente 8-9 meses en México y en hospitales de países desarrollados alcanza una media de supervivencia de hasta 14 meses. El pronóstico de los pacientes varía significativamente dependiendo de la histología y del tratamiento empleado. En la actualidad existen publicaciones discordantes, ya que aún con el mismo diagnóstico patológico y tratamientos equivalentes, algunos pacientes tienen un resultado relativamente favorable mientras que otros tienen un pronóstico muy pobre.

Entre los años 2006 y 2009, diversas publicaciones en revistas especializadas de neurología e imagenología, presentaron la propuesta de complementar con secuencias para “análisis avanzado” las imágenes convencionales de resonancia magnética que hasta la fecha se adquieren en el estudio de tumores cerebrales, las secuencias convencionales consisten en el T1 con y sin medio de contraste, el T2 con gadolinio, la difusión y la secuencia Flair.

El tejido tumoral que muestra reactividad al medio de contraste (realce) se le conoce como tejido tumoral viable, y las regiones de tejido cerebral que muestran una señal hiperintensa en las secuencias T2 y Flair, se les conoce como áreas de edema vasogenico, que debido al comportamiento histológico de este tipo de tumores, no descarta tener infiltración microscópica peritumoral.

Las secuencias de análisis avanzado están representadas por el post proceso de la difusión para medir la velocidad de las moléculas de agua en el área de interés, lo que se conoce como Coefficiente de Difusión Aparente (ADC); la perfusión cerebral, técnica con la que puede cuantificarse el volumen y el flujo sanguíneo cerebral, el primero de ellos, al ser cuantificado en el área de tumor se le conoce como volumen tumoral relativo, y es el biomarcador utilizado para evaluar la respuesta a los nuevos agentes quimioterapéuticos; la siguiente técnica la representa la espectroscopia, en la que se pueden cuantificar metabolitos en el área tumoral y peritumoral, lo que puede dar evidencia de infiltración tumoral aun en áreas que no presentan realce al contraste. La ultima técnica de análisis avanzado esta representada por la secuencia llamada tensor de difusión, con la cual, es posible medir la orientación tridimensional del movimiento de las moléculas en los axones y demás componentes del tejido nervioso y con ello, realizar no solo la representación tridimensional de tractos cerebrales, sino también la creación de mapas cuantitativos, que sometidos a análisis estadístico multivariado, pueden descubrir nuevos

comportamientos en el tejido cerebral infiltrado por tumor, para este proyecto, glioblastoma multiforme, que pueden apoyar el diagnóstico de la supervivencia en los pacientes.

Es importante comprender los factores que contribuyen positiva o negativamente al pronóstico de los pacientes con lesiones cerebrales gliales de alto grado. Sin embargo, pocos estudios a nivel internacional han analizado los factores pronósticos de estas lesiones con biomarcadores avanzados de resonancia magnética, no conocemos un estudio similar que haya sido desarrollado en México hasta la fecha.

Con este proyecto se pretende demostrar la utilidad clínica de nuevos biomarcadores derivados de las secuencias avanzadas de resonancia magnética. Como parte del proyecto, deberemos conocer previamente el comportamiento del tejido cerebral normal al ser evaluado con estos nuevos biomarcadores.



INSTITUTO NACIONAL DE NEUROLOGÍA Y NEUROCIROGÍA  
MANUEL VELASCO SUÁREZ  
DIRECCIÓN DE INVESTIGACIÓN

Insurgentes Sur 3877  
Col. La Fama, C.P. 14269  
Mexico, D.F., Tel. 56-06-14-07  
www.innn.salud.gob.mx

### PROTOCOLO DE INVESTIGACIÓN CLÍNICA

No.: 84/11  
Octubre 16 de 2012.

DEPARTAMENTO QUE PROPONE: Neuroquímica

TITULO DEL PROTOCOLO:

**Biomarcadores avanzados de resonancia magnética como factores pronósticos para la sobrevida de pacientes con glioblastoma multiforme.**

*(3ª modificación para comité científico del INNN)*

INVESTIGADOR PRINCIPAL	SERVICIO	CARGO (extensión telefónica y correo electrónico)	FIRMA
<u>Dr. Ernesto Roldán Valadez</u>	<u>Depto. Neuroquímica</u>	Alumno Doctorado Ext. 2006 <u>ernest.rolدان@usa.net</u>	_____

COAUTORES:

Dr. Sergio Moreno      Radioneurocirugía      Jefatura      \_\_\_\_\_

TUTOR: Dr. Camilo Ríos Castañeda      Departamento de Neuroquímica



**Glosario de términos médicos relacionados al protocolo**

Anisotropía	Es la propiedad general de la materia según la cual determinadas propiedades físicas, tales como: elasticidad, temperatura, conductividad, velocidad de propagación de la luz, etc. varían según la dirección en que son examinadas. Algo anisótropo podrá presentar diferentes características según la dirección. La (opuesta de isotropía)
Biopsia	procedimiento en el que se extraen muestras de tejido (con una aguja o durante una cirugía) para examinarlas con un microscopio y determinar si existen células cancerosas o anormales.
Difusión	es el proceso de movimiento molecular.
Escala Karnofsky	también llamada KPS, es la forma típica de medir la capacidad de los pacientes con cáncer de realizar tareas rutinarias. Los puntajes de la escala de rendimiento de Karnofsky oscilan entre 0 y 100. Un puntaje más alto significa que el paciente tiene mejor capacidad de realizar las actividades cotidianas. La KPS se puede usar para determinar el pronóstico del paciente, medir los cambios en la capacidad del paciente para funcionar o decidir si un paciente puede ser incluido en un estudio clínico.
Gamma Knife	tipo de radiocirugía que usa rayos gamma para tratar el cáncer de cerebro.
Glioma	(Del griego glia, liga). Tumor desarrollado a expensas del tejido nervioso, de consistencia blanda, cuya estructura se asemeja a la de la neuroglia.
Glioblastoma	Variedad de glioma formada por tejido nervioso en estado embrionario y de evolución maligna. Al lado del glioblastoma multiforme (Bailey y Cushing) o heteromorfo (Del Río Hortega) o espongiblastoma multiforme (Globus y Strauss) de células monstruosas y poliformes, se describe el glioblastoma isomorfo (Del Río Hortega) formado por células indiferenciadas.
Infiltración	acumulación de una sustancia en un tejido en el que no se encuentra en condiciones fisiológicas. Acumulación de elementos celulares en la reacción inflamatoria o de elementos tumorales.
IRM/MRI	imágenes por resonancia magnética (su sigla en inglés es) - procedimiento de diagnóstico que utiliza una combinación de imanes grandes, radiofrecuencias y una computadora para producir imágenes detalladas de los órganos y las estructuras internas del cuerpo.
radiocirugía	tipo de tratamiento de radiología terapéutica que usa haces de radiación muy focalizados para tratar cáncer y otras lesiones en un tratamiento de sesión única.
Tomografía	de las palabras griegas "cortar o seccionar" (tomos) y "escribir" (graphein), en medicina nuclear, es un método para separar la interferencia del área de interés mediante la imagen de una sección transversal del objeto.
Tomografía computarizada	(También llamada CT o CAT.) - procedimiento de diagnóstico por imágenes que utiliza una combinación de rayos X y tecnología de computadoras para producir imágenes transversales (a menudo llamadas "rebanadas"), tanto horizontales como verticales, del cuerpo. Una CT muestra imágenes detalladas de cualquier parte del cuerpo, incluyendo los huesos, los músculos, la grasa y los órganos. La CT es más detallada que los rayos X generales.

## 1) ANTECEDENTES

### ***Epidemiología del glioblastoma multiforme***

Los tumores gliales de alto grado (glioblastoma multiforme) representan el tipo más común de tumor cerebral maligno y representan el 40-50% de las neoplasias cerebrales primarias en adultos (1). En las últimas tres décadas, tanto en Estados Unidos de Norteamérica (EUA) como en otros países industrializados se ha observado un incremento en la mortalidad, secundario a una mayor incidencia de tumores cerebrales primarios.(2, 3) En EU, la incidencia de cáncer del cerebro se ha incrementado 1.2% por año desde 1973 y la mortalidad se ha incrementado 0.7% por año. Esto ha sido más evidente en los pacientes mayores de 60 años, en que la incidencia se incrementa 2.5% por año desde 1980. En este mismo grupo de pacientes se observa una mayor frecuencia de tumores agresivos de origen glial, en particular el glioblastoma multiforme y el astrocitoma anaplásico.(2-4) Varios autores consideran que este incremento es artificial y arguyen que la incidencia se ha incrementado debido al considerable avance en la técnica de neuroimagen ocurrido desde los años 70s, que permite un diagnóstico preciso y evita los diagnósticos erróneos, así como a un incremento en la densidad de población.

Aunque la incidencia de los tumores cerebrales es de solamente 17,000 casos por año, estos representan un problema médico considerable, ya que hasta un 60% de estos son malignos.(5) En EUA se reportan en promedio aproximadamente 12,000 nuevos casos por año, ubicándolo como el tumor intra-axial cerebral más frecuente.(6)

Los gliomas de alto grado representan la segunda causa de mortalidad por cáncer en adultos jóvenes, menores de 35 años, son la cuarta causa de muerte en menores de 54 años, y la principal causa de pérdida de la capacidad productiva en esta población.(5) La edad media de diagnóstico son los 65 años con un promedio de supervivencia de 10 meses, la supervivencia media a 5 años desde el tiempo del diagnóstico es alrededor del 3.3% solamente. Esta cifra es aun más baja, de 3.5 meses para mayores de 65 años. Aproximadamente 2% de los pacientes son mayores de 65 años y solo 15% de ellos son menores de 45 años, de estos alrededor del 10 sobrevive más de 2 años.(6)

En México poco se sabe sobre la epidemiología de los tumores del SN, ya que los datos publicados a la fecha sobre los diversos tipos de gliomas rara vez mencionan el grado de malignidad de los mismos, además al ser efectuados en hospitales del Distrito Federal (DF) que por sus características de población concentran a pacientes adultos o niños (locales o foráneos) y no a ambos, por lo que dejan de ser representativos de la población general.(7) En el Instituto Nacional de Neurología y Neurocirugía (INNN) de la ciudad de México, el glioblastoma multiforme (GBM) representa el 9% de todas las

neoplasias intracraneales y el 28% de los gliomas.(8) Estadísticas aun no publicadas del departamento de Radioneurocirugía del INNN refieren la incidencia del GBM en hasta 104 casos al año con una frecuencia de ingresos por casos nuevos de 1-2 casos por semana. Alrededor del 30% de los casos se refieren en menores de 45 años de edad, lo cual contrasta con el 15% que se menciona en la literatura mundial. La sobrevida media al año del diagnóstico en el INNN es del 10% aproximadamente y a 18 meses del 5% aproximadamente.(9)

<b>Clasificación de la OMS para los astrocitomas</b>
Grado I-OMS: Astrocitoma pilocítico
Grado II-OMS: Astrocitoma difuso (de bajo grado)
Grado III-OMS: Astrocitoma anaplásico
Grado IV-OMS: Glioblastoma multiforme

Los tres tipos histopatológicos más frecuentes son el glioblastoma multiforme, el astrocitoma anaplásico y el oligodendroglioma anaplásico. El glioblastoma multiforme constituye la forma más agresiva de los astrocitomas (tumor grado IV-OMS).

### **Clasificación de los tumores cerebrales**

Determinación de la malignidad según las características histológicas del tumor.

<b>Tumores de evolución lenta (Bajo grado)</b>
Tumores de grado I benignos, de crecimiento lento y circunscriptos. Tumores de grado II De crecimiento lento, pero con límites imprecisos, o de extensión.
<b>Tumores de evolución rápida (alto grado)</b>
Tumores de grado III Tumores anaplásicos, su evolución es más rápida. Tumores de grado IV Tumores malignos, muestran signos histológicos de crecimiento muy rápido en todas las regiones examinadas.

CLASIFICACIÓN HISTOLÓGICA DE LOS TUMORES DEL SISTEMA NERVIOSO

Tumores del tejido glial	Tumores de las meninges	Tumores de células germinales	Tumores de la región selar	Otros
Tumores astrocíticos				
Astrocitoma				
<b>Glioblastoma multiforme</b>				
Tumores oligodendrogiales				
Oligodendroglioma		Germinoma		Tumores metastásicos
Tumores ependimales	Meningioma	Carcinoma embrional	Adenoma pituitario	Tumores de las vainas nerviosas
Ependimoma	Hemangiopericitoma	Teratoma	Carcinoma pituitario	Schwannoma
Tumores del plexo coroides	Tumor melanocítico	Tumor del seno endodérmico	Craneofaringioma	Neurofibroma
Papiloma	Hemangioblastoma			Linfoma primario del SNC
Carcinoma				
Tumores embrionarios				
Meduloblastoma				
Tumores del parénquima pineal				

## **Diagnóstico Clínico**

Los tumores cerebrales causan síntomas variados. En general, se distinguen las manifestaciones derivadas de la hipertensión intracraneal, y los síntomas secundarios a la expansión tumoral, estos últimos denominados *signos focales*, que dependen de la estructura anatómica afectada.

- *Síntomas de hipertensión intracraneal*
  - Visión doble
  - Dolor en una extremidad
  - Cefalea
  - Vómitos
  - Edema de pupila y alteraciones visuales
  - Trastornos del comportamiento (irritabilidad, labilidad emocional, fallos en el discernimiento, alteraciones de la memoria, falta de iniciativa, indiferencia a las costumbres sociales.)
- *Síndromes focales*: Son manifestaciones que orientan la localización de la lesión.

La presentación más común de los astrocitomas malignos es con déficit neurológico (68%) y de éstos la afección de la vía piramidal la más común (45%) también pueden presentarse con cefalea (54%) y crisis convulsivas (26%). Los síntomas anteriormente mencionados son debido a afección indirecta de dichas vías pues son atribuidos principalmente al edema vasogénico y a la inflamación perilesional producida. Existe información que indica que los síntomas clínicos y la historia natural de la enfermedad tienen un curso más agresivo en pacientes de edad avanzada que en los menores de 45 años pero esto aún está por comprobarse.(10)

## **Diagnóstico por Imagen del GBM**

El diagnóstico se realiza mediante exámenes imagenológicos como la tomografía axial computarizada (TAC) o la resonancia magnética (RM), las cuales permiten conocer la localización y el tamaño del tumor y además sugerir la naturaleza del mismo, pero es la biopsia la que indica el tipo exacto de tumor. Antes de la tomografía (TC) muchos de esos pacientes eran catalogados erróneamente como portadores de enfermedades neurodegenerativas o cerebrovasculares.(3, 4)

### **Evaluación convencional con RM: Volumetría 3D y edema perilesional**

La evaluación convencional es aquella proporcionada por las secuencia T1 post gadolinio para delinear la enfermedad macroscópica (volumen tumoral) (11), y el edema perilesional en cuantificado en la secuencia T2 (12).

El uso de la volumetría cerebral mediante resonancia magnética ha sido reportado en patologías que pertenecen a diferentes especialidades médicas, por ejemplo, la esclerosis múltiple <sup>(13)</sup>, alcoholismo (13), Alzheimer y deterioro cognitivo leve (14), esquizofrenia (14-16), el trastorno por déficit de atención con hiperactividad (17-19), síndrome de Tourette (17), el autismo (20-22), el síndrome de Appert (23), el síndrome de Down (24), el síndrome de Rett (25), retardo del crecimiento intrauterino (26), y trastornos de conducta (27).

En el caso de los tumores cerebrales, la importancia de la volumetría está basada en el conocimiento de que el área de realce por el ácido de gadolinio-diethylenetriaminepentaacético (Gd-DTPA) generalmente se asume que corresponde a la masa principal de tejido de tumor activo, sin embargo una evaluación global también debería considerarse en aquellos casos con un componente quístico o necrótico. La imagen anatómica que se usa en RM es el método más extensamente aceptado para determinar el blanco para el tratamiento en la radioterapia y la cirugía (28), ver figura 1.

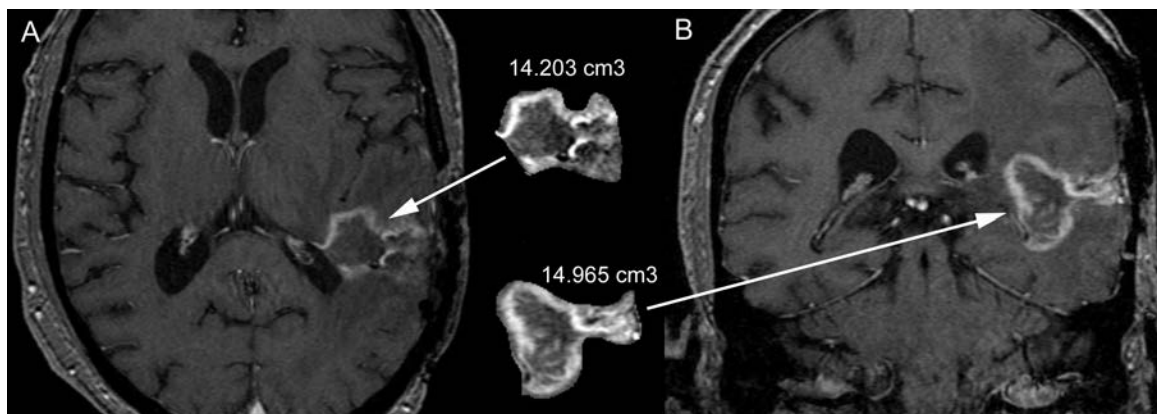


*Figura 1. Ejemplo de la aplicación de la volumetría para cuantificación de un tumor cerebral en secuencia T1 postgadolinio en los planos axial (A) y coronal (B). Se observa en ambos casos una imagen representativa del volumen en cada plano, el tumor presenta formas irregulares, que impiden la aplicación de formulas para cálculo del volumen (por ejemplo la fórmula del volumen para la esfera o la elipse no se aplican a este caso).*

En el INNN, la evaluación convencional de GBM incluye: localización, volumen tumoral en secuencia T1 post gadolinio, volumen tumoral incluido el edema perilesional en T2, y el índice de edema tumoral (volumen tumoral en secuencia T1/volumen tumoral incluido el edema en secuencia T2).

### ***Utilización del Análisis Avanzado por Resonancia Magnética en la evaluación de GBM***

El concepto de “análisis avanzado” es de reciente aplicación en la evaluación con RM de tumores cerebrales, fue publicado por primera vez por investigadores del departamento de radiología de “University of Pennsylvania School of Medicine” en octubre de 2006,(29) en una revista especializada en imagenología (*Radiographics*) y al año siguiente, 2007, una publicación en una revista clínica (*Neurologic Clinics*) del departamento de radiología del Brigham and Women’s Hospital de Harvard Medical School en Boston, Estados Unidos, presentó también una revisión de la aplicación clínica de estas técnicas avanzadas.(30)

Aunque en la actualidad exista mas de una docena de variables que se pueden cuantificar con RM, las secuencias de RM consideradas actualmente en el “análisis avanzado” para la evaluación diagnóstica, progresión tumoral y/o respuesta a los diferentes tratamientos son:

- ✓ Difusión,
- ✓ Perfusión,
- ✓ Tensor de Difusión, y
- ✓ Espectroscopia

A continuación se presenta una breve descripción de estas técnicas de RM.

#### ***Biomarcadores de la Espectroscopia por Resonancia Magnética***

La espectroscopia por resonancia magnética (ERM) es una técnica que nos permite cuantificar diversos metabolitos e interpretarlos de manera cualitativa y/o cuantitativa (31). El objetivo principal de la ERM es brindar una herramienta para mejorar la sensibilidad y especificidad de una gran variedad de patologías, actualmente es utilizada principalmente en el sistema nervioso central y puede ser utilizada en otras regiones anatómicas como son próstata, glándula mamaria, hígado y tumores de partes blandas.

La ERM más utilizada es la del núcleo del hidrógeno. La técnica se basa en las diferencias mínimas que se encuentran en las frecuencias de resonancia de los núcleos de hidrógeno dependiendo de su entorno, a este fenómeno se le denomina “desplazamiento químico” (32, 33).

Cada núcleo de  $^1\text{H}$  otorga una amplia gama de información ya que de manera suimultánea son detectados varios metabolitos y neurotransmisores; la localización o resonancia de los compuestos más relevantes en partes por millón (ppm) se resumen en la siguiente tabla (34):

Metabolito	Pico (ppm)	Descripción
<b>N-Acetilaspártato (NAA)</b>	2.02	Marcador de densidad e integridad neuronal y viabilidad axonal.
<b>Colina (Cho)</b>	3.22	Componente del metabolismo de fosfolípidos de membrana celular, refleja proliferación celular.
<b>Creatina (Cr)</b>	3.02 y 3.94	Utilizado como referencia, debido a que es el metabolito más estable y constante en sus valores.
<b>Mioinositol (ml)</b>	3.56	Marcador glial en los astrocitos, producto de la degradación de mielina, refleja volumen celular.
<b>Lactato (Lac)</b>	1.33 y 4.1	Indicador de glicolisis anaeróbica
<b>Lípidos</b>	0.8 - 1.3	Indican necrosis y/o disrupción de la vaina de mielina.
<b>Alanina</b>	1.49	Aminoácido no esencial presente en el cerebro.

A pesar del éxito de la ERM clínica y la disponibilidad de la ERM en la mayoría de los equipos de resonancia magnética en los hospitales, esta técnica no es utilizada tan ampliamente como podría serlo (35, 36).

Puesto que las neoplasias primarias son propensas a infiltrar el tejido cerebral circundante, el examen de áreas fuera de la zona de realce del tumor han probado ser promisorias (37), estas mediciones son obtenidas con espectroscopia.

El índice de cho/NAA mayor a 1.0 en el tejido cerebral residual o circundante a una lesión tumoral ya conocida, es el biomarcador de espectroscopia mas comúnmente aceptado y ha mostrado una exactitud de hasta el 100% para representar el tejido tumoral (37).

Varios puntos de corte han sido sugeridos para este biomarcador, aunque no hay todavía un consenso. Por ejemplo, algunos estudios han reportado un índice de Cho/NAA de más de 1.90 con un tiempo de eco largo (sensibilidad 83%; especificidad 88%) como punto de corte para lesiones de alto grado (38).

Otros biomarcadores de espectroscopia que han sido propuestos para lesiones gliales incluyen el porcentaje de lípidos, el índice de lactato/creatina, colina/creatina, mioinositol/Naa y N-acetilaspártato/creatina (39, 40). La presencia de lípidos y/o lactato en gliomas no tratados sugiere la presencia de un tumor grado IV (41).

La figura 2 muestra la utilidad de la ERM, en el diagnóstico del GBM.



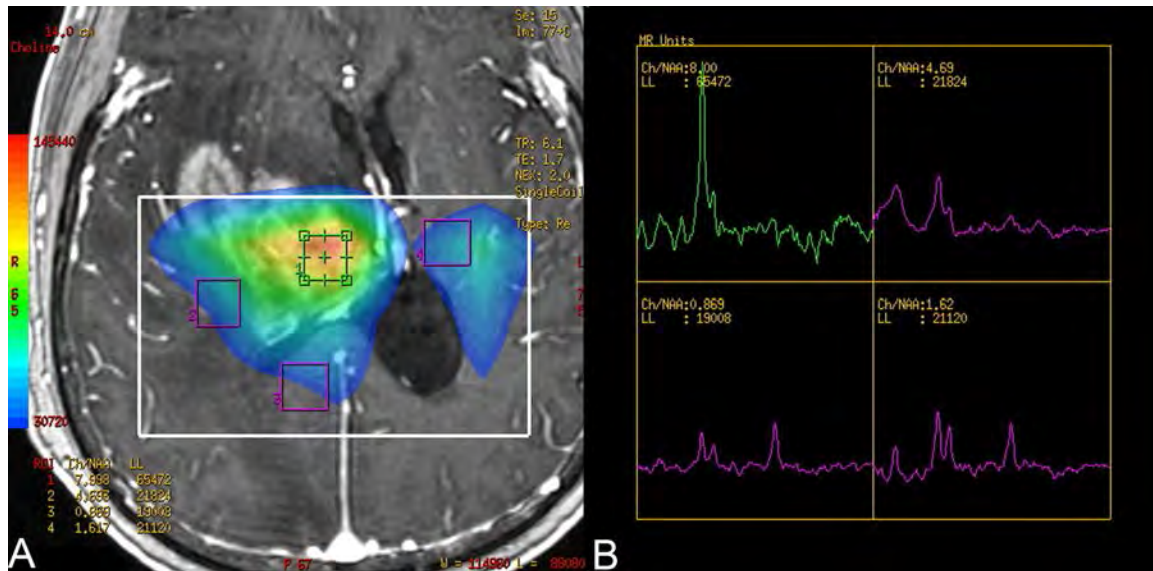


Fig. 2 - Espectroscopia multivoxel, A) mapa de color del índice de Cho/NAA en una muestra de cuatro voxels, B) espectros que muestran la elevación del índice de Cho/NAA en diferentes regiones: en el interior de la zona con realce del tumor (8.0), en el sitio de edema peritumoral (4.69) dando evidencia de un patrón de infiltración peritumoral. El estudio histopatológico reportó una lesión glial grado IV (glioblastoma). (Imágenes procesadas en la Unidad de RM del hospital Médica Sur).

### **Importancia de la Medición de Lípidos y Lactato en el Tejido Tumoral**

La presencia de lípidos ha sido correlacionada con la formación de necrosis donde la muerte celular resulta en el rompimiento de membranas.(42) Este aumento en la concentración de lípidos ha sido observado en tumores de alto grado, particularmente en el glioblastoma multiforme.(43)

Una publicación reciente demostró aumento en la concentración de lípidos casi exclusivamente en los gliomas de alto grado, y muy raramente presente en gliomas de bajo grado. Estas regiones han coincidido además con zonas que muestran aumento de volumen cerebral relativo, demostrado también con RM.(44)

La metodología para cuantificar la concentración de grasa con espectroscopia en el hígado, se ha demostrado que puede sustituir a la biopsia hepática para cuantificar la grasa.(45) Esta misma metodología de cuantificación se utilizara en el tejido cerebral esperando una alta correlación con la cuantificación que se realice en la pieza quirúrgica utilizando métodos de morfometría por el departamento de neuroquímica del INNN.

El lactato, producto final de la glucólisis no oxidativa ha sido correlacionado con niveles de oxígeno bajos o hipoxia en el tejido tumoral.(46) Los gliomas se caracterizan por presentar extensas zonas de hipoxia y necrosis.(47) La hipoxia es un promotor poderoso de la angiogénesis y de la infiltración tumoral a través de la activación de genes críticos para estas funciones.(48-51) La angiogénesis condicionada por la hipoxia condiciona un círculo vicioso de degeneración de microvasculatura inmadura y anormal que no puede funcionar adecuadamente y condiciona más hipoxia tumoral, resultando en necrosis.(52)

La aplicación clínica de la medición de lactato y lípidos está orientada por tanto a la diferenciación del glioma en bajo y alto grado. Esta es una información metabólica que va más allá de la imagen anatómica.

### ***Coefficiente de Difusión Aparente obtenido con secuencia de difusión***

La difusión, es un método de adquisición de imágenes que evalúa el movimiento microscópico de las moléculas de agua. Normalmente, este movimiento es desorganizado (o aleatorio) y se le denomina “movimiento browniano” (40).

Para generar una imagen de difusión, el equipo de resonancia aplica un gradiente magnético en una determinada dirección espacial que sirve para realinear las moléculas de agua estacionarias, haciendo que éstas emitan una señal. Así tras la aplicación de gradientes sensibles a la difusión, el agua normalmente en movimiento se evidencia como una pérdida en la intensidad de señal, y se observa un incremento en la intensidad de señal en aquellas regiones en las que las moléculas de agua permanecen estacionarias (53, 54).

Para cuantificar el grado de movimiento del agua, es necesario procesar las imágenes de difusión y obtener mapas del denominado “coeficiente de difusión aparente” (CDA) (31), definido también como la longitud del camino promedio de difusión de agua dentro de cada voxel, y está determinado por las barreras del tejido a la difusión en una escala de aproximadamente 10  $\mu\text{m}$ .

El CDA es inversamente proporcional a la densidad celular, presumiblemente a causa de la tortuosidad del espacio intersticial y la limitación resultante en el movimiento del agua (55-57). La figura 3 muestra un ejemplo de difusión y CDA en las mediciones del tálamo derecho (las imágenes en RM se presentan invertidas, es decir, de frente al radiólogo) de un paciente con un tumor primario del sistema nervioso.

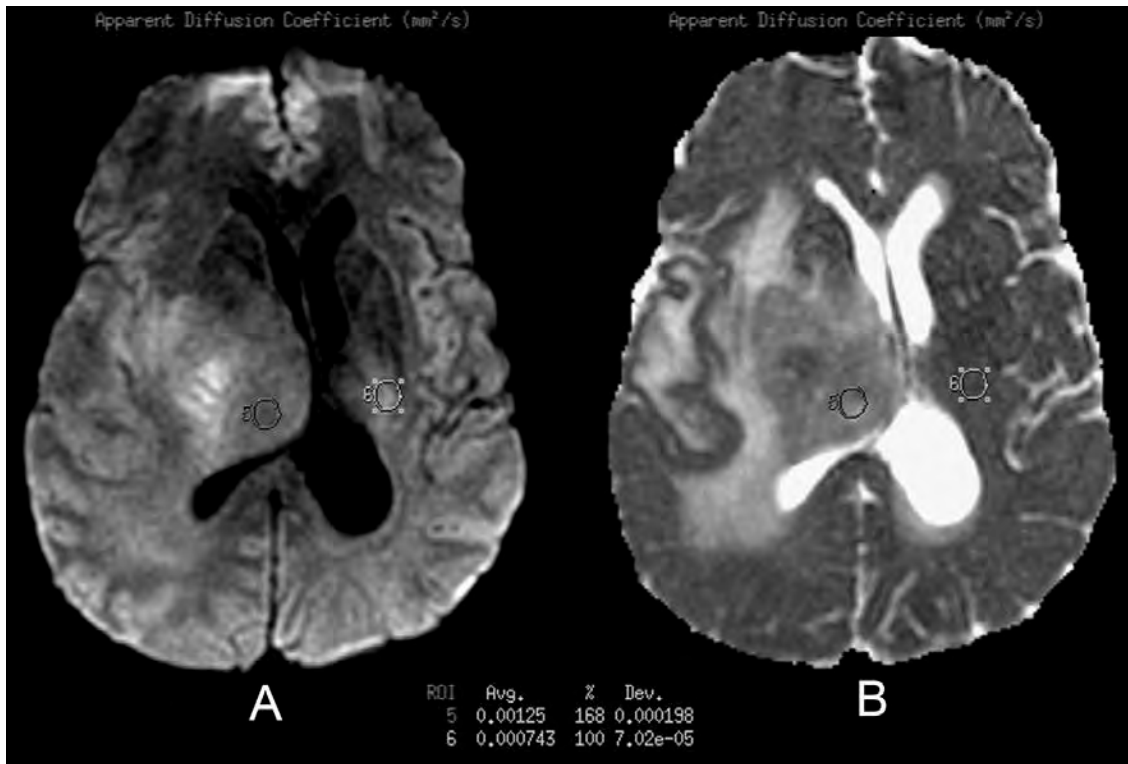


Fig. 3 – Mapas de difusión (A) y del coeficiente de difusión aparente (B) que muestra una lesión intraaxial con un efecto de masa significativo y que se encuentra además rodeada de edema. Se observan dos pequeños ROIs (regiones de interés) una colocada en el sitio del tumor y otra colocada en el sitio correspondiente del cerebro contralateral. El análisis cuantitativo mostro un CDA elevado en el sitio del tumor, lo que correspondió con un glioblastoma multiforme. (Imágenes procesadas en la Unidad de RM del hospital Médica Sur).

Hay una correlación negativa entre el CDA mínimo y la celularidad tumoral que ha sido verificado en histología en una amplia gama de tumors incluyendo a gliomas de alto y bajo grado, linfoma, meduloblastoma, meningioma y metástasis (57-61).

El valor promedio de CDA en sustancia blanca de tejido cerebral normal ha sido reportado en  $0.764 \pm 0.063$  ( $10^{-3}$ )  $\text{mm}^2/\text{s}$  (rango, 0.653– 0.855) y para el tejido tumoral en GBM en  $0.963 \pm 0.119$  ( $10^{-3}$ )  $\text{mm}^2/\text{s}$  (rango 0.768 –1.135).(62)

En los gliomas, se han reportado valores de CDA en por debajo de un rango de 1.7 a 2.5 para distinguir gliomas de alto y bajo grado (41, 63). Aunque el valor del CDA de gliomas de alto grado se ha demostrado por debajo de los de gliomas de bajo grado, hay un traslape sustancial (64); por lo tanto los mapas de CDA únicos, son insuficientes para predecir el tipo y grado de neoplasias gliales (65).

El CDA y la celularidad tumoral varían ampliamente dependiendo del grado del tumor (especialmente de alto grado) y por hallazgos relacionados (presencia en la lesión de necrosis, hemorragia y calcificaciones) (66). Esta heterogeneidad del CDA puede limitar la utilidad de la difusión como un

subrogado de la histopatología pero deja la posibilidad que el CDA pueda ayudar a sub estratificar los tumores dentro de los grados ya conocidos (40).

La difusión podría ser muy útil en el seguimiento de la respuesta al tratamiento y recurrencia subsecuente en pacientes individuales debido a que la radiación que es citotóxica, y la quimioterapia reducen ambas la celularidad tumoral y por lo tanto aumentan el CDA dentro de un área definida del tumor (67, 68).

### ***Anisotropía fraccional cuantificada con secuencia Tensor de Difusión***

La secuencia tensor difusión (DTI) permite la medición de la restricción de la difusión del agua en el tejido cerebral para producir imágenes de tractos nerviosos en lugar de utilizar los datos solamente para valorar el color o contraste de los píxeles de una imagen axial; esta secuencia permite la medición cuantitativa del movimiento de las moléculas en un espacio de 3 dimensiones.(69) Inicialmente un índice simple fue calculado de la imágenes ponderadas en difusión,(70) conocido como, este es ADC obtenido de una imagen con dirección perpendicular al movimiento del agua. El ADC desafortunadamente depende de la dirección escogida para realizar las mediciones.(71)

La anisotropía fraccional (FA) es aceptado como una medida de la direccionalidad de la difusión del agua (forma del tensor de difusión en cada voxel) del cerebro.(72) Esta FA puede apoyar a determinar el grado de infiltración de sustancia Blanca por el tumor, y provee evidencia de la degeneración de tractos distales a los sitios con tumor (degeneración Walleriana), esto cambia el pronóstico de un paciente que va a someterse a una resección extensa de un tumor, con lo que se produce un daño mínimo o nulo al paciente al observar que las fibras tienen ya un daño irreversible y no hay déficits adicionales que puedan surgir.(73)

La fracción de anisotropía se basa en la varianza normalizada de los valores centrales de los vectores principales de la difusión (correspondiente a los eigenvectores del tensor), su valor varía entre 0 (difusión isotrópica) y 1 (anisotropía infinita).(74) La difusión es anisotrópica en los tractos de sustancia blanca, debido a que las membranas axonales y las vainas de mielina representan barreras al movimiento d las moléculas de agua en direcciones no paralelas a su propia orientación. Una FA reducida (difusión del agua paralela a los tractos axonales) es indicativo de degeneración axonal y una difusión aumentada (movimiento del agua perpendicular a los tractos axonales) es asociado con cambios en el contenido de agua, en disrupción y rompimiento parcial de la citoarquitectura tisular, o bien de procesos de desmielinización.(75) Basados en reportes previos, valores de FA > 0.2 han sido considerados como indicativos de algún grado de orientación estructural dentro de los axones mielinizados.(76)

Utilizando los valores de FA del tensor de difusión y con un post procesamiento de imágenes, es posible obtener una reconstrucción tridimensional (3D) de los tractos cerebrales, un procedimiento llamado *tractografía*. Se han designado 3 colores básicos que pueden decir al observador cómo las fibras están

orientadas en un sistema de coordenadas 3D: esto se denomina "mapa anisotrópico". El software codifica los colores de esta manera: el rojo indica las direcciones en el eje X: de derecha a izquierda o de izquierda a derecha, el verde indica las direcciones en el eje Y: posterior a anterior o de anterior a posterior, azul indica las direcciones en el eje Z: dirección de pies a cabeza o viceversa, ver figura 4.

La tractografía es útil para proporcionar orientación en los procedimientos neuroquirúrgicos (77), tales como biopsias y tratamientos quirúrgicos, mediante la representación previa a la operación de tractos importantes de sustancia blanca, la visualización de la orientación de los tractos de fibras y su relación con el tumor puede reducir el riesgo de lesiones durante la realización de procedimientos quirúrgicos y biopsias.

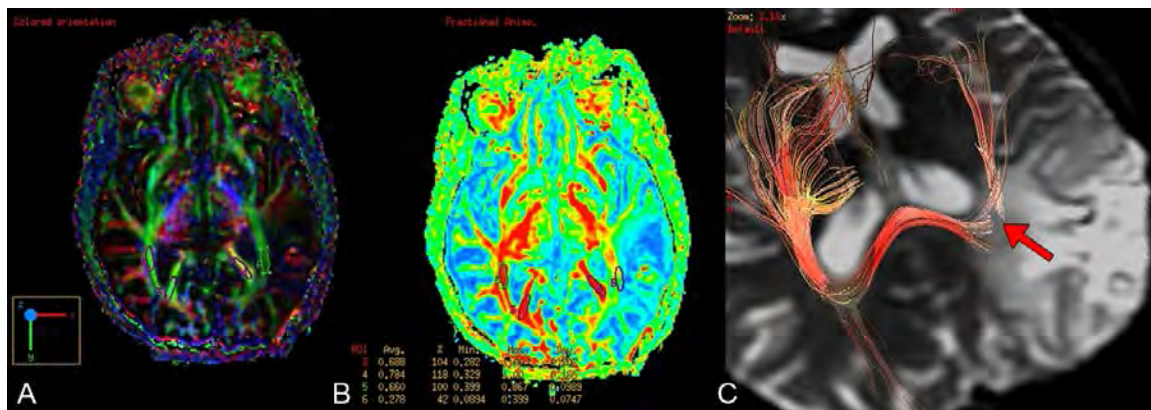


*Fig. 4 – Plano axial que muestra un mapa direccional de anisotropia (A) en un paciente con un glioma de bajo grado. El mapa de fracción de anisotropía muestra una reducción cuantitativa del trazo geniculocalcarino adyacente al ventrículo izquierdo (B). Se observa una tractografía (C) que muestra la disrupción de alguna fibras del tracto mencionado (flecha roja). (Imágenes procesadas en la Unidad de RM del hospital Médica Sur).*

Cuando un tumor esta presente y condiciona desplazamiento del tejido cerebral, edema peritumoral o infiltración, los tractos de sustancia Blanca pueden caracterizarse de la siguiente manera: desplazados, si mantienen su anisotropía normal relativa al tracto colateral correspondiente pero estan situados en una localización anormal con alteración en el mapa de color; edematoso, si mantiene su anisotropía normal y orientación pero demuestra alta señal en la secuencia T2; infiltrado si tienen anisotropía reducida pero pueden aun identificarse en el mapa; e interrumpidas, si la anisotropía esta marcadamente reducida asi que el tracto no puede ser identificado en su orientación (77).

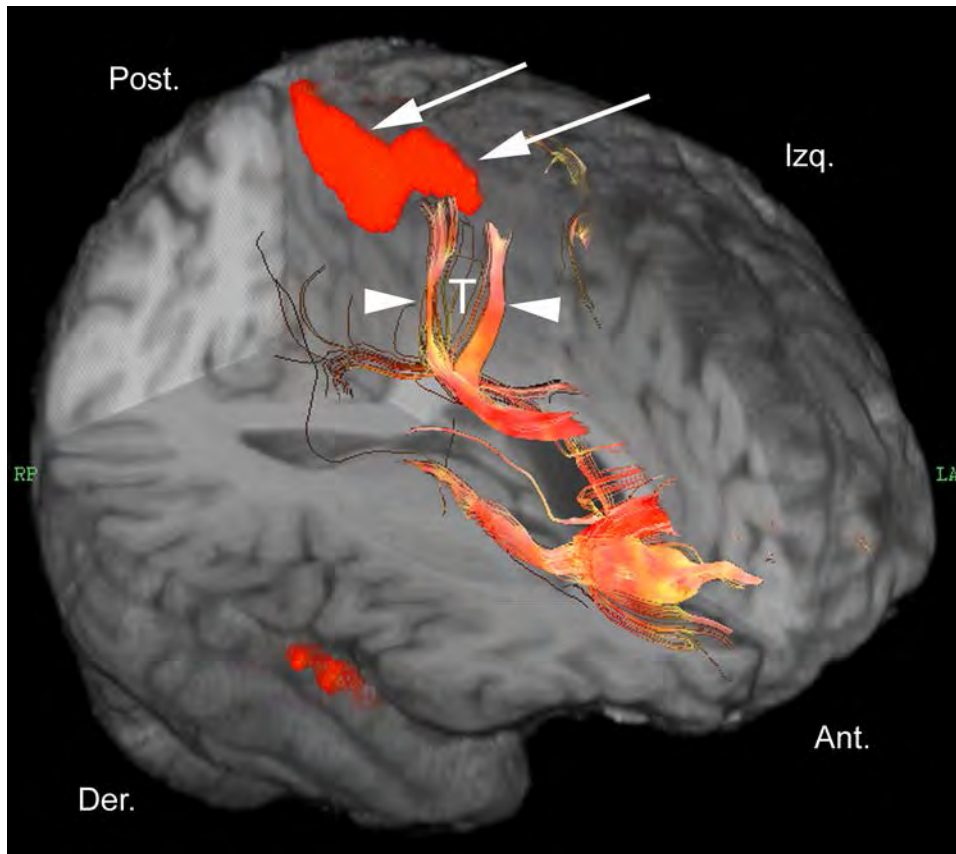


Figura 5. Ejemplo de tractografía fusionada con imágenes de RM funcional BOLD (imagen color naranja señalada por flechas). Se observa la activación de la zona motora correspondiente a la pierna derecha (origen en el hemisferio izquierdo) la cual se encuentra desplazada en sentido posterior y lateral debido a la presencia de un tumor (letra T), que también condiciona desplazamiento de la vía piramidal ipsilateral (cabecitas de flecha). Se visualizan en sentido anterior otros tractos correspondientes a la circunvolución del cíngulo y fascículo longitudinal inferior. (Imágenes procesadas en la Unidad de RM del hospital Médica Sur).

### **Volumen Cerebral Relativo en perfusión cerebral**

La perfusión cerebral con administración dinámica de contraste ofrece información hemodinámica cerebral que complementa la información anatómica del estudio convencional de RM (31). La perfusión cerebral de contraste explota los cambios de señal que acompañan al paso de un agente de contraste paramagnético a través del sistema vascular cerebral y puede usarse para obtener información del volumen y del flujo sanguíneo (78). Así, puede ser una técnica de investigación para evaluar lesiones tumorales intracraneales y poder correlacionar sus resultados con los de estudios histopatológicos.

El radiotrazador que se utiliza como contraste puede ser endógeno (agua arterial) o exógeno (gadolinio) y puede ser difusible o no. El gadolinio se usa más frecuentemente en imagen de perfusión porque se acorta el tiempo de obtención de imágenes (tiempo de relajación) y requiere herramientas del procesado de imágenes muy accesibles.

Para medir el flujo sanguíneo cerebral se adquieren múltiples imágenes de varios planos del parénquima cerebral en intervalos de aproximadamente 1s, antes, durante y después de la inyección del agente de contraste por vía endovenosa (79).

El cambio de señal en cada voxel se utiliza para calcular el volumen sanguíneo cerebral relativo (rCBV, por sus siglas en inglés) de ese voxel, que luego se puede mostrar como un mapa de colores o un gráfico de la variación de intensidad de la señal en una zona determinada en el tiempo (curva tiempo-intensidad), ver figura 4. Las imágenes potenciadas por perfusión permiten visualizar la angiogénesis, proceso esencial para el crecimiento neoplásico (40). En pacientes que reciben terapias anticancerosas, la perfusión RM puede ser un método no invasivo para ver cambios en el volumen sanguíneo cerebral relativo durante el tratamiento y puede usarse como monitorización de la eficacia terapéutica (80).

La angiogénesis inducida por un tumor resulta en alteración estructural de los vasos sanguíneos que tienden a ser mas permeables y por tanto tienen parámetros de permeabilidad aumentada en las imágenes de perfusión (40).

Las neoplasias primarias como los gliomas tienen un volumen tumoral relativo (rTBV) que tiende a aumentar con el grado histológico. Este grado, se correlaciona con el volumen sanguíneo (81, 82).

Se ha publicado un punto de corte para el rTBV de 1.75 sugerido como umbral para distinguir neoplasias de alto y bajo grado, donde el rTBV es el cociente del volumen sanguíneo máximo comparado con una región de interés en sustancia blanca del hemisferio contralateral.

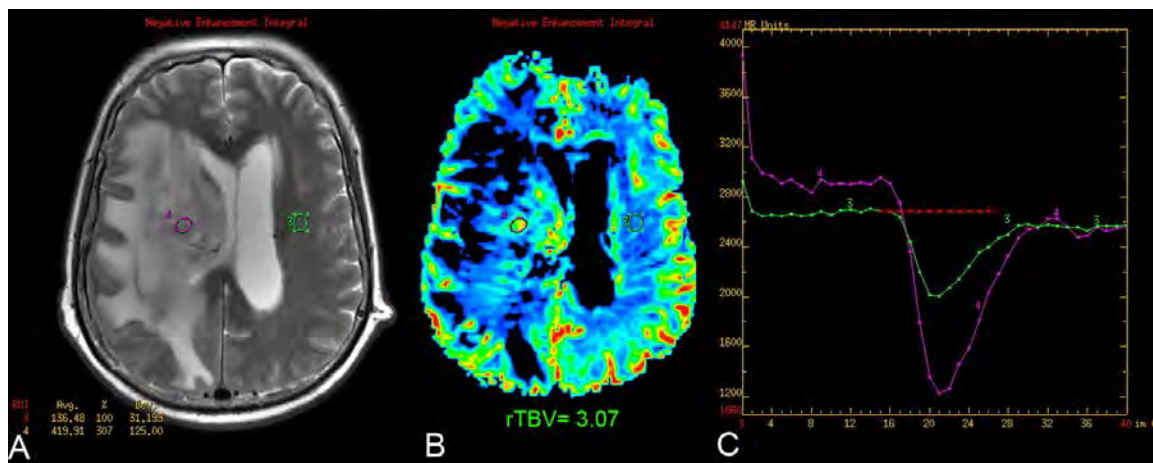


*Fig. 6. Perfusión cerebral en un paciente con un glioma de alto grado. A, imagen de referencia en T2 que muestra la localización de un ROI en el area sólida de un tumor. B, mapa de perfusión que muestra el rTBV elevado en 3.07, compatible con lesión glial de alto grado. C, Curva de perfusión que muestra la región de interés en color rosa, comparada con el tejido cerebral normal. El tumor carece de barrera hematoencefálica por lo que hay fuga de contraste durante la inyección del bolo de contraste. (Imágenes procesadas en la Unidad de RM del hospital Médica Sur).*

### **Evidencia del mejor biomarcador por RM**

Algunos estudios han comparado el desempeño diagnóstico de los biomarcadores de RM en la “gradación” de tumores cerebrales; estos resultados muestran cual método de RM permite una detección mas temprana, lo que puede utilizarse en la evaluación de la respuesta a radioterapia. De acuerdo a estas publicaciones, los biomarcadores de espectroscopia detectarían de forma mas temprana los tumores (83), seguidos por la perfusión cerebral (84) y la etapa final corresponde al realce con gadolinio (85). La Figura 7, muestra esta relación de biomarcadores avanzados de RM.

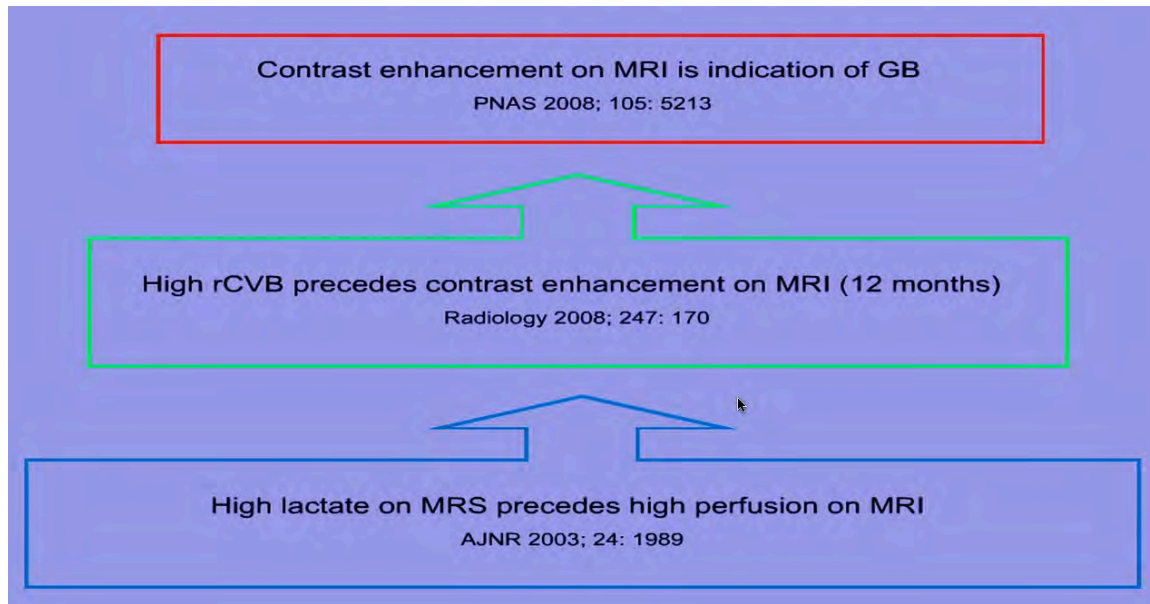


Fig. 7. Utilidad de las secuencias avanzadas de RM en el diagnóstico de tumores cerebrales.

### **Evolución clínica de los tumores gliales**

Los GBM, son los tumores cerebrales primarios más frecuentes y agresivos. Causan globalmente un 2% de las muertes por cáncer. Estos tumores poseen una alta tasa de recidiva local tras tratamiento quirúrgico, progresando localmente, lo que finalmente termina causando la muerte del paciente. Se diseminan principalmente a través de la sustancia blanca o por vía líquido cefalorraquídeo. A diferencia de otras neoplasias malignas avanzadas, éstas rara vez reportan metástasis a distancia.(86)

### **Sobrevida en GBM**

A pesar de terapias estándar como la cirugía, radioterapia y quimioterapia y a pesar del considerable esfuerzo que se realiza actualmente para optimizar estos tratamientos, la sobrevida de los pacientes con gliomas de alto grado tiene rangos de 8-9 meses a 2-3 años. Tradicionalmente se admitía que presentaba una supervivencia media, a los dos años, de aproximadamente 10 por ciento. El tratamiento con un abordaje multidisciplinario incluye cirugía, radioterapia y quimioterapia. Con uno de estos



protocolos de tratamiento, se ha alcanzado recientemente una supervivencia del 25% y aún más en los casos en los que se consiguió una excisión completa. Aunque el pronóstico es malo se han conseguido avances en los últimos años.(87) Lo ideal es que en el tratamiento participen especialistas en neurocirugía, neurología y oncología. El avance terapéutico que más reciente que ha impactado en el tratamiento de esta enfermedad sin duda es el uso de Temozolamida, un nuevo agente alquilante que proporciona una sobrevida media de hasta 14.83 meses comparado con 14.67 meses en el grupo que recibe radioterapia solamente o quimioterapia convencional.(88, 89)

### ***Tratamiento del GBM en el INNN***

El tratamiento de quimio/radioterapia utilizado en el INNN para pacientes con GBM esta protocolizado de la manera siguiente: Radioterapia estereotáctica fraccionada 60 Gy a la periferia, 30 sesiones de 2 Gy, delineando la enfermedad macroscópica en secuencia T1 con contraste, el edema perilesional en T2 y un márgen de 20 mm para conformar el PTV (planning Treatment Volume). Se les indica prednisona 50 mg iniciales y en reducción progresiva a lo largo de un mes, iniciándolo el día de fin de tratamiento. Quimioterapia: Temozolamida calculada a 75 mg/m<sup>2</sup>/d los días de radioterapia, y al terminar calculada a 150-200 mg/m<sup>2</sup>/d por 5 días por ciclos de 28 días. Cinco ciclos en total. En caso de que el paciente no pueda pagar el medicamento se les administra Carboplatino-Vincristina después de terminar la radioterapia.(90)

### ***Definición de Respuesta a Tratamiento***

Una respuesta positiva al tratamiento será asignada a aquellos pacientes que sobrepasen la media del análisis de sobrevida y cumplen con los criterios del análisis de partición recursiva (RPA) el cual en su ultima revisión, utiliza tres grupos pronósticos para GBM considerando: edad, estado de desempeño, extensión de la resección, y función neurológica.(91)

*La media del analisis de sobrevida que será de 14.2 meses para los pacientes del INNN tratados con temozolamida e incluidos en el estudio.(92)*

Adicionalmente, en el INNN, se valora la respuesta al tratamiento dada por la imagen, donde una buena respuesta es el no crecimiento del tumor en las variables que componen el índice de edema tumoral. (90)

## 2) PLANTEAMIENTO DEL PROBLEMA

### **Planteamiento del problema**

Aunque la evaluación con RM del GBM constituye la herramienta fundamental con la que el neurocirujano realiza la planeación de la resección quirúrgica, la planeación de la radioterapia y la

evaluación de la respuesta al tratamiento. *No existe un consenso internacional de cual es el biomarcador de RM que ofrece el mejor valor pronostico de respuesta al tratamiento.*

En el depto. de radioneurocirugía del INNN se utilizan 3 parámetros numéricos de la RM convencional para valorar la respuesta: volumen tumoral en T1, volumen tumoral en T2, y el índice de edema tumoral.

La literatura especializada de imágenes de RM sugiere que al menos 8 biomarcadores avanzados de RM podrían ser efectivos en el pronostico: índice de Colina/Naa, % de grasa en el tejido tumoral, índice de lactato/creatina, índice de mioinositol/creatina, índice de Naa/creatina, volumen sanguíneo cerebral relativo, coeficiente de difusión aparente y anisotropia fraccional.

*El contar con biomarcadores de sobrevida institucionales permitirá diseñar una mejor herramienta pronostica que permita una terapia personalizada a las necesidades del paciente.*

### **Pregunta de Investigación**

¿Cuál es el biomarcador de resonancia magnética con mejor valor pronóstico para el calculo de sobrevida en pacientes del INNN con glioblastoma multiforme?

### 3) HIPÓTESIS

#### **HIPÓTESIS**

*Ha: Hipótesis alterna.*

Las mediciones de espectroscopia muestran un mejor valor pronóstico para el calculo de sobrevida comparados con los de difusión, perfusión, y tensor de difusión en pacientes con glioblastoma multiforme.

*Ho: Hipótesis nula.*

No existe diferencia significativa en los valores de difusión, perfusión, espectroscopia y tensor de difusión para el calculo de la sobrevida de pacientes del INNN con glioblastoma multiforme.

#### **Hipótesis de trabajo**

Las mediciones de metabolitos de espectroscopia, presentar mejor valor pronostico para el calculo de sobrevida de pacientes con GBM, comparados con los de perfusión y tensor de difusión.

### 4) OBJETIVOS

#### **Objetivos**

##### **Objetivo General**

Identificar el biomarcador de RM que muestre el mejor valor pronóstico de sobrevida en pacientes con glioblastoma multiforme.

### **Objetivos Específicos**

- Identificar el grado de asociación (coeficiente de correlación) y realizar una evaluación completa de pruebas diagnósticas para cada uno de los biomarcadores de RM avanzada mas comúnmente reportados en la literatura: coeficiente de difusión aparente, volumen cerebral relativo, índice de colina/N-acetilaspártato y fracción de anisotropía.
- Evaluar otros biomarcadores adquiridos con las secuencias avanzadas de RM: volumetría 3D, lípidos, lactato, mioinositol, índice de infiltración tumoral;(72) y en las convencionales: volumen tumoral en secuencias T1 y T2 e índice de edema tumoral.
- Realizar análisis multivariado, de regresión múltiple y logística para definir modelos pronósticos con las variables disponibles.

### **Objetivos Secundarios**

- Determinar la correlación entre los diferentes biomarcadores y los parámetros de evaluación clínica (v.gr. escala de Karnofsky).

## 5) JUSTIFICACIÓN

### **Justificación**

#### *Magnitud del problema*

El GBM es el tumor que causa la mayor parte de las consultas y es el principal motivo de intervención quirúrgica en los pacientes derechohabientes del INNN.(93, 94) El GBM afecta no solamente a sujetos en la 5ª y 6ª década de la vida principalmente, en el INNN el 30% de los pacientes con GBM son menores de 45 años de edad lo que representa población económicamente activa.(93)

El tumor es rápidamente progresivo con una historia natural que lleva al fallecimiento del paciente al año del diagnóstico en el 90% de los casos. A pesar de los avances mundiales en investigación no se ha modificado significativamente la sobrevida tras 4 décadas de investigación.(93)

#### *Viabilidad*

La investigación es viable, evaluando pacientes del centro de referencia más grande del país para esta enfermedad; el INNN proporciona los requerimientos tecnológicos, la infraestructura física y personal capacitado para tratar a estos pacientes. El protocolo propone la colaboración de 5 departamentos del instituto: neuroradiología, neuroquímica, neuropatología, neurocirugía y neuroradiocirugía.

#### *Vulnerabilidad*

El protocolo no escapa a la posibilidad que eventualmente pudiera ser modificado en el flujograma de pacientes si el seguimiento clínico considera una evaluación menos estrecha de los pacientes.

### *Trascendencia*

Este sería el primer estudio de esta naturaleza en Mestizo-Mexicana, esta acotación es importante ya que la mayoría de estudios previos han sido desarrollados principalmente en población caucásica.(8)

Este es un protocolo de investigación propuesto por un radiólogo, alumno de doctorado en el INNN, y con la revisión del jefe del Depto. De Radioneurocirugía y del jefe de neuroradiología. Los resultados del proyecto podrán apoyar el seguimiento de pacientes del INNN y para evaluar la respuesta a la radioterapia.

### Revisión de PubMed sobre biomarcadores pronósticos en RM para Glioblastoma (hasta 2010)

Año	Autor	Titulo	Ptes.	Marcadores
2010	Senft C	1. Influence of imri-guidance on the extent of resection and survival of patients with glioblastoma multiforme	43	T1 post Gd y MRS
2010	Tugcu B	2. Efficacy of clinical prognostic factors on survival in patients with glioblastoma	50	Realce en T1 post Gd
2010	Allahdini F	3. Evaluating the prognostic factors effective on the outcome of patients with glioblastoma multiformis: Does maximal resection of the tumor lengthen the median survival?	35	Volumetria en T1 post Gd
2010	Yamasaki F	4. Glioblastoma treated with postoperative radio-chemotherapy: Prognostic value of apparent diffusion coefficient at MR imaging	33	ADC, apparent difussion coefficient
2009	Wang CH	5. Prognostic significance of growth kinetics in newly diagnosed glioblastomas revealed by combining serial imaging with a novel biomathematical model	32	Volumetria en T1 post Gd y edema en T2
2008	Hirai T	6. Prognostic value of perfusion mr imaging of high-grade astrocytomas: Long-term follow-up study	31	rCBV, volumen cerebral relativo
2007	Murakami R	7. Prognostic value of pretreatment quantitative diffusion-weighted MR imaging	79	ADC, apparent difussion coefficient
2006	Pallud J	8. Prognostic value of initial magnetic resonance imaging growth rates for world health organization grade ii gliomas	143	Volumetria en T1 post Gd
2005	Pope WB	9. MR imaging correlates of survival in patients with high-grade gliomas	110	Volumetria en T1 post Gd y edema en T2
2004	Kurimoto M	10. Impact of neuronavigation and image-guided extensive resection for adult patients with supratentorial malignant astrocytomas: A single-institution retrospective study	76	T1 con Gd en el postoperatorio temprano
2004	Li X	11. Identification of mri and 1h mrsi parameters that may predict survival for patients with malignant gliomas	39	T1 post Gd y MRS

Estos artículos muestran evidencia de la falta de evaluación conjunta de biomarcadores de RM, los cuales son de rápida adquisición y bajo costo.

## 6) METODOLOGÍA

### a) Diseño

Estudio prospectivo longitudinal de seguimiento de pacientes con diagnóstico de GBM.

### b) Población y muestra

#### *Población blanco*

Pacientes Mestizo-Mexicanos de cualquier género y edad con evidencia de GBM.

#### *Población elegible*

Pacientes portadores de GBM que ingresen para tratamiento al Instituto Nacional de Neurología y Neurocirugía de la ciudad de México.

#### *Población estudiada*

Pacientes con GBM, demostrado por biopsia, que cumplan con los criterios de inclusión y acepten firmar el consentimiento informado.

#### *Tamaño de la muestra*

El cálculo del tamaño de muestra se realizó utilizando el software G\*Power v3.1.3 (Franz Faul, Edgar Erdfelder, Albert-Georg Lang, and Axel Buchner, 2006, 2009).(95)

Se escogió el método de regresión lineal múltiple, y tomando en cuenta los 4 biomarcadores de básicos principales: coeficiente de difusión aparente, volumen cerebral relativo, índice de Cho/NAA y Fracción de anisotropía, se obtuvo el siguiente output:

*F tests - Linear multiple regression: Fixed model, R<sup>2</sup> deviation from zero*

<i>Analysis:</i>	<i>A priori: Compute required sample size</i>		
<i>Input:</i>	<i>Effect size f<sup>2</sup></i>	=	0.35
	<i>α err prob</i>	=	0.05
	<i>Power (1-β err prob)</i>	=	0.95
	<i>Number of predictors</i>	=	4
<i>Output:</i>	<i>Noncentrality parameter λ</i>	=	20.6500000
	<i>Critical F</i>	=	2.5429175
	<i>Numerator df</i>	=	4
	<i>Denominator df</i>	=	54
	<b>Total sample size</b>	=	<b>59</b>
	<i>Actual power</i>	=	0.9536733

El tamaño de la muestra obtenido es de 59 pacientes.

Criterios de selección del estudio

#### *Criterios de inclusión*

1. adultos mayores de 18 años,

2. de cualquier género,
3. con diagnóstico por biopsia esterotáxica de glioblastoma multiforme (astrocitoma IV de la OMS).
4. Consentimiento informado debidamente firmado por el paciente o familiar responsable.

*Criterios de exclusión*

1. Contraindicaciones para recibir radiocirugía o quimioterapia,
2. Haber recibido tratamiento anterior,
3. Pacientes con algún tipo de patología o tratamiento previo que implique algún tipo de inmunosupresión.
4. Cualquier contraindicación para un estudio de RM.

*Criterios de eliminación*

1. Presencia de tumor cerebral con otra estirpe histológica.
2. Rechazo del consentimiento informado
3. Registro de variables incompleto y

Estudio de RM no valorable por artificios durante la adquisición del estudio o el postproceso.

c) Variables

*Definición de variables y unidades de medición*

<b>Variable</b>	<b>Definición Conceptual (C) y Operacional (Op)</b>	<b>Instrumento</b>	<b>Tipo de variable</b>	<b>Codificación</b>
Edad	C: Tiempo transcurrido en años desde el nacimiento. Op: cálculo de los años. basados en acta de nacimiento.	Historia Clínica	Continua	Años
Género	C: aspecto masculino o femenino de la persona. Op: fenotipo de la persona correspondiente a masculino o femenino.	Historia Clínica	Categórica Nominal	0: masculino 1: femenino
Puntuacion Karnofsky	C: evalua el estado de desempeño. Op: califica del 100 a 0, donde 100 es perfecta salud y 0 es muerte.	Historia Clínica	Categórica Nominal	100 a 0
Grado de resección	C: presencia de tumor después de la cirugía. Op: califica el resultado postquirurgica de la reseccion tumoral.	Historia Clínica	Dicotomica	0: sin tumor 1: residual
Respuesta al tratamiento	C: control tumoral. Op: pacientes que sobrepasen la media de sobrevida para pacientes del INNN con GBM.	Historia clinica	Dicotomica	No. días
% de grasa tumoral	C: Concentracion de grasa en el tejido. Op: medición del porcentaje de	Espectroscopia	Continua	Porcentaje (%)

	grasa.			
Indice de Colina /creatina	C: medición indirecta del contenido de lípidos en membranas celulares, marcador de proliferación. Op: de dividir las concentraciones absolutas de colina entre creatina	Espectroscopia	Continua	adimensional
Indice de Lactato /creatina	C: medición indirecta del metabolismo anaerobio a nivel celular, marcador de hipoxia celular. Op: de dividir las concentraciones absolutas de lactato entre creatina	Espectroscopia	Continua	adimensional
Indice de Naa /creatina	C: medición indirecta del numero de neuronas en corteza cerebral, marcador de viabilidad neuronal. Op: de dividir las concentraciones absolutas de N-acetilaspártato entre creatina	Espectroscopia	Continua	adimensional
Indice de Mioinositol /Naa	C: medición indirecta de la actividad de fibroblastos en SN, marcador de gliosis. Op: de dividir las concentraciones absolutas de mioinositol entre Naa	Espectroscopia	Continua	adimensional
Coeficiente de Difusión Aparente	C: medición del movimiento de las moléculas de agua en la célula, marcador de edema citotóxico. Op: medición del área de desplazamiento de los protones en los átomos de hidrógeno de las moléculas de agua por unidad de tiempo.	Secuencia de Difusión	Continua	mm <sup>2</sup> /seg
Anisotropia Fraccional	C: medición de la direccional de las moléculas de agua en tractos cerebrales definidos. Op: medición del 0 al 1 (mínimo-máximo) de la direccionalidad específica de c/ tracto cerebral.	Secuencia tensor de difusión	Continua	adimensional
Volumen tumoral relativo	C: perfusión sanguínea tumoral por unidad de tiempo. Op: comparación relativa del volumen sanguíneo cerebral entre tejido cerebro sano y tejido sólido infiltrado con GBM.	Secuencia de perfusión	Continua	Porcentaje (%)
Volumen tumoral post gadolinio	C: volumen de tumor cerebral viable.	Secuencia T1/SPGR post gadolinio	Continua	mm <sup>3</sup>



	Op: medicion volumétrica del tejido tumoral que realza con contraste.			
Volumen de edema cerebral	C: volumen del edema cerebral tumoral. Op: medicion volumétrica del edema vasogénico por fuera del tejido viable (que realza con contraste), causado por el GBM.	Secuencia T2 sin gadolinio	Continua	mm <sup>3</sup>
Indice de edema tumoral	C: relación entre volumen tumoral versus el edema que causa un tumor cerebral. Op: cociente de dividir el volumen tumoral que realza con contraste entre el volumen tumoral con su edema vasogénico asociado.	T1 post gadolinio / T2	Continua	mm <sup>3</sup>

d) Análisis Estadístico

Todas las evaluaciones estadísticas se llevaran a cabo utilizando el software SPSS versión 17.0 (SPSS Inc., Chicago, IL). La significancia estadística se considerará con 1 valor de  $p < 0.05$  (2 colas). La presentación de los datos se realizará siguiendo las guías para publicaciones de la Asociación Psicológica Americana.(96, 97)

Comparación de medias aritméticas y tamaño del efecto

Los valores de serán evaluados para distribución normal con la prueba de Kolmogorov-Smirnov y con la prueba de Levene statistics para verificar la presencia de homogeneidad de varianzas. La demostración de una distribución normal en las variables permitirá la aplicación de pruebas paramétricas, en el caso contrario se aplicarán por lo tanto pruebas no para métricas en la evaluación.

Se realizará análisis para determinar las frecuencias de las variables de estudio, así como medidas de tendencia central y dispersión para determinar el comportamiento normal o sesgado de la población.

Se realizará análisis bivariado mediante la prueba de Chi 2 o exacta de Fisher para variables categóricas y prueba de t de *student* o Mann–Whitney para variables numéricas.

La medias aritméticas serán comparadas con pruebas t de Student para muestras independientes. Para calcular el tamaño del efecto de cada variable, los valores de t y los grados de libertad (df) serán utilizados para calcular el valor de la "d" de Cohen's *d* y el tamaño del efecto "r"; utilizaremos la definición de un tamaño de efecto pequeño con valores de ( $d = 0.2$ ), medio ( $d = 0.5$ ), y grande ( $d = 0.8$ ).(98)

Correlación.

El grado de asociación entre las variables será valorado por los coeficientes de correlación de Pearson o Spearman según corresponda. Los valores del coeficiente de correlación "r" cercanos o por arriba a 0.75 indicarán 1 correlación buena o excelente. Para esta prueba, se considerarán datos significativos cuando  $p < 0.05$  (una cola).

### Análisis de supervivencia.

Se realizará prueba de Cox para análisis de supervivencia y regresión logística para determinar la influencia de variables.

El análisis de regresión de Cox(99) será realizado para determinar un modelo matemático que permita identificar cuales son los mejores biomarcadores pronósticos. Antes de comenzar el análisis de regresión, en caso de obtenerse un resultado no paramétrico de alguna de las variables dependientes se aplicará transformación logarítmica a las variables con el propósito de lograr distribución normal, una vez más la significancia estadística para esta prueba será considerada en  $p < 0.05$ .

### Evaluación de Pruebas Diagnósticas con Curvas ROC

Se utilizarán curvas para características del operador receptor, con el propósito de evaluar el desempeño diagnóstico de los parámetros.(100) El área bajo cada una de las curvas ROC (AUROC, por sus siglas en inglés), serán interpretadas como el valor promedio de la sensibilidad para todos los valores posibles de especificidad, esta medida será considerada como el representante del desempeño global para cada variable;(101, 102) se obtendrán también los valores para error estándar, valor de  $p$  y los intervalos de confianza del 95% CI. La respuesta al tratamiento será considerado el estándar de oro para el análisis de las curvas ROC. Se realizará el cálculo de los "puntos de corte" para cada variable y representarán los puntos previos y subsecuentes que rodean el umbral óptimo para maximizar la sensibilidad y la especificidad.

La precisión de cada marcador se ha determinado utilizando sistema tradicional para clasificar la puntuación: 0.90–1 = excelente (A), 0.80–0.90 = buena (B), 0.70–0.80 = regular (C), 0.60–0.70 = pobre (D), y 0.50–0.60 = fallida (F) (103). Los valores de sensibilidad, especificidad, valor predictivo positivo, valor predictivo negativo, y razones de verosimilitud positivas y negativas así como la precisión, serán también calculadas en este análisis. La significancia estadística para este análisis de curvas ROC se considera con  $p < 0.05$  basado en la utilización de la prueba exacta de Fisher.

## 7) CONSIDERACIONES ÉTICAS

Esta investigación tiene un riesgo mayor al mínimo de la Ley General de Salud en Materia de Investigación para la Salud debido a que los sujetos serán expuestos a estudios de resonancia magnética funcional. El aspecto clínico del estudio se considera de investigación con riesgo mínimo tratándose de procedimientos comunes en exámenes físicos o psicológicos de diagnósticos o tratamiento rutinarios. Así mismo se apega a las pautas establecidas en la Declaración de Helsinki de 1983, en todos los casos los participantes del estudio firmarán un consentimiento informado.

El estudio garantiza los aspectos bioéticos inherentes a los estudios de investigación clínica como son confidencialidad de la información obtenida, principio de autonomía de los sujetos participantes, principio

de beneficencia y consentimiento informado, sin tener conflicto de intereses y permitiendo el acceso a documentos fuente en caso de ser solicitado por autoridades normativas.

A los pacientes se les comentará el tipo de estudio, la intención del mismo y se les solicitará autorización para ingresar al mismo, así como se especificaran detalles respecto al procedimiento de imagen y a la toma y el uso de muestras tanto de sangre periférica. Debido a que los pacientes con GBM pueden tener afección de las funciones mentales se explicara a detalle el protocolo al familiar responsable a fin de que no quede duda del objetivo, destino y uso de las muestras que se analizarán.

8) CONSIDERACIONES FINANCIERAS

Este protocolo no tiene implicaciones financieras adicionales.

Los análisis de la imagen representados por los post-procesos computacionales de la imagen, serán realizados sin costo adicional por el investigador principal Dr. Ernesto Roldan

Los pacientes incluidos, cubrirán el costo que corresponda a su tratamiento y consultas de acuerdo a su clasificación socioeconómica en el INNN.

a) Aporte Financiero

Sin aporte financiero.

b) Recursos con los que se cuenta

*Recursos Humanos*

1. Neurocirujano con Posgrado en radiocirugía, a cargo del ingreso y manejo de los pacientes en el departamento de radioneurocirugía en el INNN.
2. Técnico radiólogo, a cargo de realizar los ajustes al software y obtención de secuencias, en el INNN.
3. Radiólogo a cargo del post procesamiento del análisis avanzado de tumores (ciego a pacientes), *el alumno del doctorado en ciencias médicas INNN proponente del protocolo, Dr. Ernesto Roldan.*
4. Patólogo, cualquier patólogo asignado a los procedimientos de diagnóstico de las biopsias de cerebro, en INNN.
5. Neuroquímico, Dr. Camilo Ríos, para procesos de morfometría y cuantificación total de lípidos, en INNN.

*Personal a cargo de las evaluaciones*

<b>Técnica</b>	<b>Método</b>	<b>Lugar</b>	<b>Responsable</b>
1. Inclusión de pacientes y Tx Radiocirugía	Consulta	Departamento de Radioneurocirugía INNN	Personal Depto. Radioneurocirugía
2. Procesamiento de la biopsia	Tinción convencional con hematoxilina y eosina	Departamento de patología, INNN	Personal Depto. Patología
3. Cuantificación de grasa en laminillas	Morfometría	Departamento de Neuroquímica, INNN	Alumno del Doctorado en Ciencias Médicas
4. Cuantificación de grasa no invasiva	RM con espectroscopia	Depto. Neuroradiología del INNN	Alumno del Doctorado en Ciencias Médicas
5. Análisis avanzado de tumores	difusión, perfusión, espectroscopia, volumetría	Depto. Neuroradiología del INNN	Alumno del Doctorado en Ciencias Médicas

### *Materiales*

- Resonador 3T General Electric, modelo HDX Excite.
- Estación de trabajo para postproceso de espectroscopía, secuencias doble eco y secuencias T2 con saturación grasa.
- Computadora portátil
- Paquete estadístico SPSS v17.0
- Material y equipo del laboratorio para procesamiento de biopsia cerebral. Departamento de Patología, INNN.
- Cuantificación de la Grasa en las Biopsias Tenidas con Hematoxilina Eosina To Departamento de Neuroquímica, INNN.
- Software de GE para postproceso de imágenes medicas.

c) Recursos a solicitar  
Ninguno

d) Análisis del costo por paciente  
Sin costo adicional para el paciente.

9) CRONOGRAMA DE ACTIVIDADES

**Nuevo Programa de Doctorado en Ciencias Médicas UNAM  
(8 semestres 2011-2014)**

Actividades programadas de acuerdo a la duración del programa

Actividad	1	2	3	4	5	6	7	8
Redacción de protocolo y presentación a Comité de Ética	Yellow	Yellow	Yellow					
Inclusión de pacientes	Blue	Blue	Blue	Green	Green	Green		
Captura de datos	Light Green	Light Green	Light Green	Light Green	Light Green	Light Green		
Análisis			Dark Blue			Dark Blue		
Resultados			Red			Red		
Envío de Artículos a Publicación			Blue			Blue		
Carta del editor, resultados de la revisión				Orange			Orange	
Presentación final de resultados ante el Comité de Evaluación del Posgrado de la UNAM							Dark Purple	

## **Procedimientos**

### *Reclutamiento de pacientes*

Se invitara a los pacientes con diagnóstico de glioblastoma multiforme, que hayan ingresado para tratamiento a departamento de radioneurocirugía del INNN y que debido a su condición clínica sean candidatos a tratamiento. Los pacientes deberán cubrir los criterios de inclusión y firmar un consentimiento informado. La muestra se empezara, a reclutar en el período en cuento sea aprobado el protocolo (se espera el mes de septiembre de 2012) y hasta alcanza el numero planeado de pacientes.

### *Evaluación clínica*

Los pacientes a su ingreso contarán con una historia clínica completa que incluye los datos de identificación, y antecedentes familiares para enfermedades atópicas y alérgicas.

Durante la consulta de ingreso a radioneurocirugía se obtendrán *variables demográficas* consistentes en edad, sexo, peso, talla e índice de masa corporal (definido como peso/talla<sup>2</sup>).

Se realizará una historia clínica completa con exploración física general y neurológica, con documentación del uso de esteroides antiinflamatorios, tipo y dosis, enfermedades inmunosupresoras, antecedentes recientes de infección.

### *Escala de Karnofsky*

De manera ya protocolizada se evalua la KPSS (Karnofsky Performance Status Scale) a los pacientes en el periodo preoperatorio, postoperatorio inmediato dentro de las primeras 24 horas de la cirugía y al mes de realizada ésta, y posteriormente cada 3 meses de ser posible hasta el fallecimiento.

## **Postprocesamiento y analisis de las imágenes de RM**

Después de la evaluación clínica en el Departamento de Radiocirugía, el paciente será invitado a participar en el protocolo por el Dr. Sergio Moreno. La interpretación de las imágenes de Resonancia Magnética serán realizada por el departamento de neuroradiología del INNN con el reporte radiológico que corresponda a cada paciente, adicionalmente el Dr. Ernesto Roldan podrá realizar el post procesamiento de algunas secuencias con motivo del análisis cuantitativo de las secuencias propuestas en su protocolo de doctorado.

El Dr. Moreno explicara a los pacientes los hallazgos por imagen y las rutas del tratamiento multidisciplinario que se realizara en el INNN con el medico tratante que le haya sido asignado.

*Todos los pacientes deberán contar con RM preoperatoria con especial énfasis al T2 y al T1 con gadolinio.*

*La evaluación convencional de las imágenes incluye:*

- ✓ *Volumen tumoral en T1 post gadolinio.*
- ✓ *Volumen tumoral incluyendo el edema perilesional en T2.*
- ✓ *Índice de edema tumoral (volumen en T1 / volumen en T2)*

*El análisis avanzado del tumor, tratara de evaluar:*

- ✓ *Índices de Colina/Cr, Naa/Cr, Lactato/Cr y % de grasa tumoral con Espectroscopia.*
- ✓ *Volumen cerebral relativo (máximo) del tejido tumoral sólido con Perfusión (rCBV).*
- ✓ *Coefficiente de difusión aparente con secuencia de Difusión (ADC).*
- ✓ *Valor de anisotropía fraccional del tejido tumoral con secuencia tensor difusión (FA).*

La RM de cerebro se podrá realizar en los equipos de 1.5 y 3.0T HDxt GE Signa scanner (General Electric Healthcare, Milwaukee, WI) de la unidad de resonancia del INNN. Las imágenes serán adquiridas con una bobina para cráneo de 8 canales. Esta consideración es particularmente importante, considerando que existen periodos durante el año que alguno de los equipos se encuentra en mantenimiento (fuera de servicio), por lo que los pacientes podrán ser evaluados en el magneto disponible sin retrasar la programación de cirugía y tratamiento de los pacientes.

El protocolo de adquisición de las imágenes se encuentra detallado en el apéndice No. 2 para ambos magnetos.



### **Cronograma para seguimiento de los pacientes con RM**

Los pacientes serán evaluados cada 3 meses con el mismo protocolo de RM después de realizada la cirugía, y de forma previa a sus seguimientos en la consulta externa de radioneurocirugía de acuerdo al siguiente esquema.

Periodo	Basal	Citas en la consulta externa de radioneurocirugía después de la resección quirúrgica del tumor			
		3 meses	6 meses	9 meses	12 meses
VARIABLES EVALUADAS	<b>Para el tejido tumoral:</b> Vol. Tumoral, Vol. Edema y el Índice tumoral  <b>Para 3 ROIs diferentes en tumor, edema y tejido normal:</b> rCBV, ADC, FA, Cho/Naa, Naa/Cr, Lipidos, lactato.	La evaluación se realizara idealmente solo en 1 ROI de tejido normal.  Si el tumor NO pudo tener resección completa, se utilizaran 2 ROIs adicionales en zonas que muestren edema y tejido tumoral residual.			

#### **Grado de Resección Postoperatoria**

Después de la cirugía, misma que será realizada por el personal adscrito a Neurocirugía del INNN se procederá a determinar el grado de resección tumoral en el postoperatorio.

#### **Grado de resección tumoral documentada con imagen**

Se realiza mediante una TAC o RM postoperatoria con contraste dentro de las primeras 24 horas posteriores a la cirugía para clasificar la resección en 1 de 4 grados posibles:

1. GTR (Gross Total Resection) Resección macroscópica total.
2. NGTR (Near Gross Total Resection) Resección casi total, mínimo refuerzo con medio de contraste.
3. SGR (Subtotal Gross Resection) Resección subtotal, moderado remanente o descompresión.
4. BX (Biopsy) Biopsia o mínima resección tumoral sólo para diagnóstico.

#### **Exámenes de laboratorio en sangre o suero.**

Se obtendrán los exámenes de laboratorio preoperatorios según estipulan las guías de diagnóstico y tratamiento del INNN.

### *Manejo de la biopsia*

La biopsia se procesara por el departamento de patología del INNN con técnicas convencionales.(104) Una vez teñida y posterior a su diagnostico histológico, la biopsia será transportada al Departamento de Neuroquímica del INNN, donde se realizará evaluación morfométrica,(105, 106) para cuantificación del porcentaje de biopsia en la laminilla.

### *Egreso y vigilancia del paciente.*

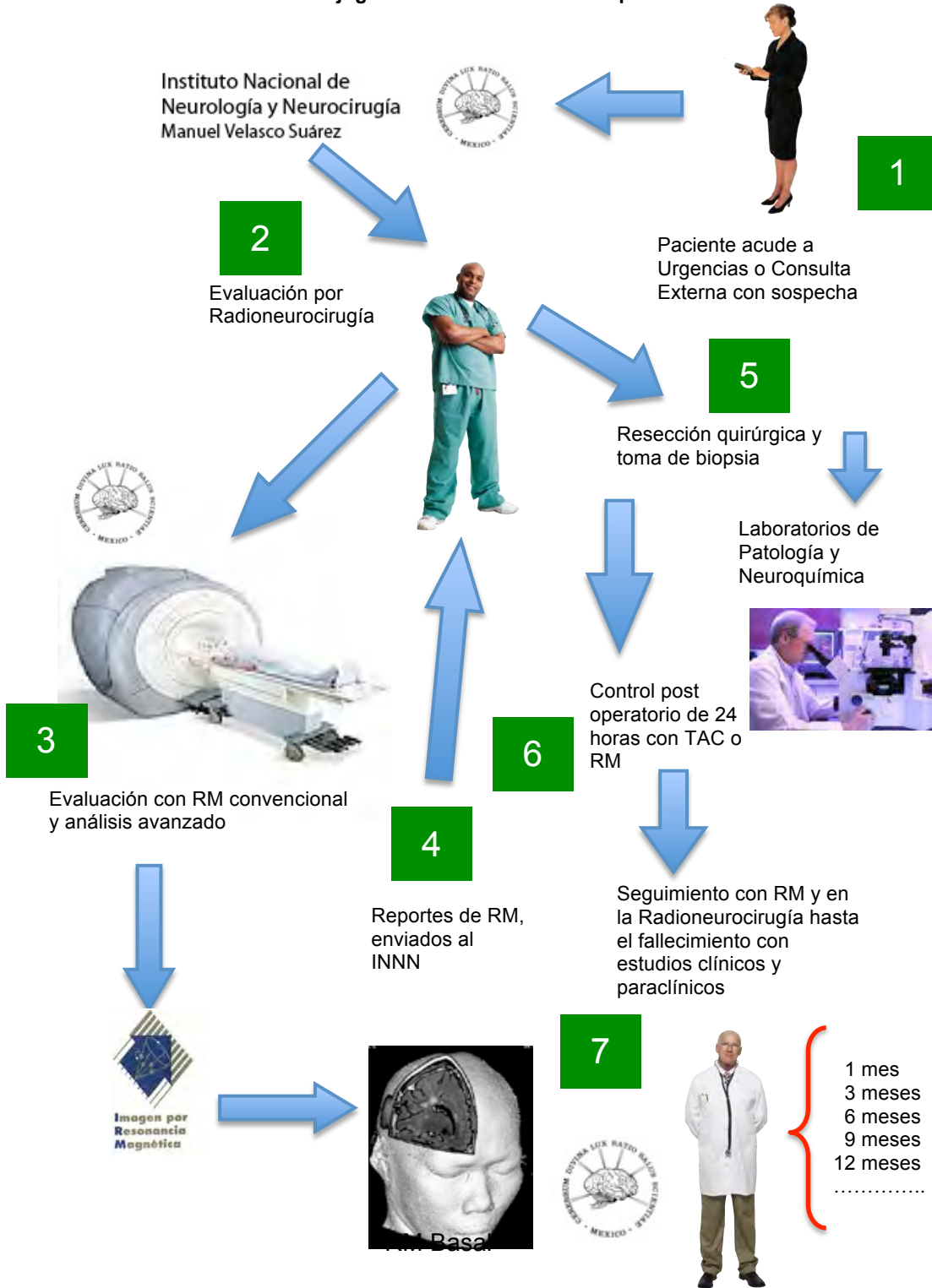
El manejo del pacientes seguirá los estándares del Departamento de Radioneurocirugía del INNN.

### *Tratamiento*

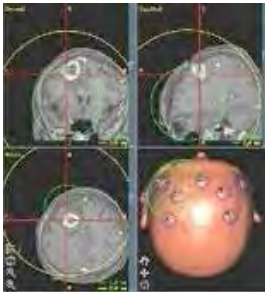
El tratamiento de quimio/radioterapia utilizado en el INNN para pacientes con GBM estará protocolizado de la manera siguiente:

Radioterapia estereotáctica fraccionada 60 Gy a la periferia, 30 sesiones de 2 Gy, delineando la enfermedad macroscópica en secuencia T1 con contraste, el edema perilesional en T2 y un margen de 20 mm para conformar el PTV (Planning Treatment Volume). Se les indica prednisona 50 mg iniciales y en reducción progresiva a lo largo de un mes, iniciándolo el día de fin de tratamiento. Quimioterapia: Temozolamida calculada a 75 mg/m<sup>2</sup>/d los días de radioterapia, y al terminar calculada a 150-200 mg/m<sup>2</sup>/d por 5 días por ciclos de 28 días. Cinco ciclos en total. En caso de que el paciente no pueda pagar el medicamento se les administrara Carboplatino-Vincristina después de terminar la radioterapia.(90)

### Flujograma de la evaluación del paciente



## Flujograma del analisis de datos



Respuesta a Radioterapia

- ✓ Correlación
- ✓ Regresión lineal múltiple
- ✓ Regresión de Cox

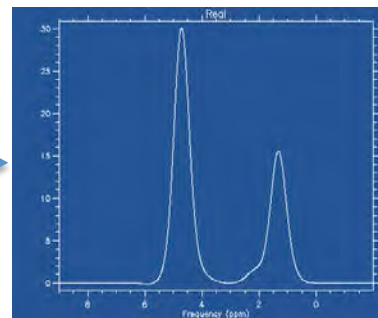


1. Coeficiente de difusión aparente,
2. Volumen tumoral relativo,
3. Anisotropia fraccional,
4. Volumetria en T1 y T2,
5. Indice de Colina/Naa,
6. Indice de Colina/Cr
7. Indice de Lactato/Cr
8. % de grasa con espectroscopia
9. % de Grasa con Morfometria,
10. Respuesta a tratamiento (sobrevida)
11. Edad
12. Sexo
13. Karnofsky



Morfometria en biopsia para cuantificación de grasa

- ✓ Correlación



Cuantificación de grasa tumoral en la espectroscopia cerebral

10) RESULTADOS QUE SE ESPERAN OBTENER Y SU POSIBLE IMPACTO EN LA INVESTIGACIÓN BIOMÉDICA (CONTRIBUCIÓN DE LA INVESTIGACIÓN EN EL AVANCE DEL CONOCIMIENTO CIENTÍFICO).

Conocer el valor pronostico de nuevos biomarcadores de resonancia magnética, obtenidos de las evaluaciones que se toman comúnmente a los pacientes pero que no se postprocesan:

- ✓ Coeficiente de difusión aparente,
- ✓ Volumen tumoral relativo
- ✓ Índice de colina/N-acetilaspártato
- ✓ Anisotropía fraccional

Con ello, es muy posible re-diseñar el estudio de Resonancia Magnética de Cerebro que se lleva a cabo para estos pacientes en el INNN. Así como apoyar la planeación de los tratamientos de Radioneurocirugía.

11) SATISFACCIÓN DE UNA NECESIDAD DE SALUD CON EL DESARROLLO DE ESTE TRABAJO.

La atención de tumores cerebrales malignos, principalmente el glioblastoma multiforme, es la principal causa de consulta, se invierten recursos humanos y materiales en la atención de pacientes con una sobrevida corta.

Este estudio pretende obtener evidencia cuantitativa para apoyar la planeación de tratamientos y conocer el pronostico de sobrevida, lo que impacta en los tiempos de tratamiento y seguimiento.

12) MENCIONE QUE APORTARÁ EL DESARROLLO DEL TRABAJO A LA COMPRESIÓN, PREVENCIÓN, DIAGNÓSTICO Y TRATAMIENTO A LAS AFECCIONES DEL SISTEMA NERVIOSO.

**Comprensión**

Ayudar a entender que las características por imagen del tumor pueden tener mayor valor para el pronostico y tratamiento que el resultado histológico inicial.

**Prevención**

Pacientes en quienes se midieran inicialmente, factores pronósticos pobres, ser mas agresivos en la planeación quirúrgica, de quimio y radioterapia.

**Diagnostico**

Utilizar los biomarcadores de imagen que recomienda la literatura internacional para una evaluación completa de tumores cerebrales.

**Tratamiento**

Tener una herramienta cuantitativa, que puede medir objetivamente la evolución de los pacientes, incluso antes que los datos clínicos (síntomas) sean reportados por el paciente (en el caso de recidiva tumoral).

13) REFERENCIAS

1. Stewart LA. Chemotherapy in adult high-grade glioma: a systematic review and meta-analysis of individual patient data from 12 randomised trials. *Lancet*. 2002;359(9311):1011-8. Epub 2002/04/09.
2. Ahsan H, Neugut AI, Bruce JN. Trends in incidence of primary malignant brain tumors in USA, 1981-1990. *Int J Epidemiol*. 1995;24(6):1078-85. Epub 1995/12/01.
3. Fleury A, Menegoz F, Grosclaude P, Daures JP, Henry-Amar M, Raverdy N, et al. Descriptive epidemiology of cerebral gliomas in France. *Cancer*. 1997;79(6):1195-202. Epub 1997/03/15.
4. Fathallah-Shaykh HM, McIntire DD. Brain tumors in the elderly: undefeated and gaining ground. *Arch Neurol*. 1998;55(7):905-6. Epub 1998/07/25.
5. Schmainda KM, Rand SD, Joseph AM, Lund R, Ward BD, Pathak AP, et al. Characterization of a first-pass gradient-echo spin-echo method to predict brain tumor grade and angiogenesis. *AJNR Am J Neuroradiol*. 2004;25(9):1524-32. Epub 2004/10/27.
6. George J, Banik NL, Ray SK. Combination of hTERT knockdown and IFN-gamma treatment inhibited angiogenesis and tumor progression in glioblastoma. *Clin Cancer Res*. 2009;15(23):7186-95. Epub 2009/11/26.
7. Guevara-Donde J. Incidencia de gliomas malignos en derechohabientes del IMSS residentes en el estado de Veracruz, México. *Arch Neurocienc*. 2004;9(2):80-4
8. Lopez-Gonzalez MA, Sotelo J. Brain tumors in Mexico: characteristics and prognosis of glioblastoma. *Surg Neurol*. 2000;53(2):157-62. Epub 2000/03/14.
9. Moreno S. Incidence of Glioblastoma Multiforme at the Mexican National Institute of Neurology and Neurosurgery. In: Roldan-Valadez E, editor. Mexico city, Mexico: Department of Radioneurosurgery; 2011. p. 1.
10. Iacob G, Dinca EB. Current data and strategy in glioblastoma multiforme. *J Med Life*. 2009;2(4):386-93. Epub 2010/01/30.
11. Pronin IN, McManus KA, Holodny AI, Peck KK, Kornienko VN. Quantification of dispersion of Gd-DTPA from the initial area of enhancement into the peritumoral zone of edema in brain tumors. *Journal of neuro-oncology*. 2009;94(3):399-408. Epub 2009/03/31.
12. Engelhorn T, Savaskan NE, Schwarz MA, Kreutzer J, Meyer EP, Hahnen E, et al. Cellular characterization of the peritumoral edema zone in malignant brain tumors. *Cancer Sci*. 2009;100(10):1856-62. Epub 2009/08/18.
13. Ge Y, Grossman RI, Babb JS, Rabin ML, Mannon LJ, Kolson DL. Age-related total gray matter and white matter changes in normal adult brain. Part I: volumetric MR imaging analysis. *AJNR Am J Neuroradiol*. 2002;23(8):1327-33. Epub 2002/09/12.
14. Fleisher AS, Sun S, Taylor C, Ward CP, Gamst AC, Petersen RC, et al. Volumetric MRI vs clinical predictors of Alzheimer disease in mild cognitive impairment. *Neurology*. 2008;70(3):191-9. Epub 2008/01/16.
15. Jacobsen LK, Giedd JN, Berquin PC, Krain AL, Hamburger SD, Kumra S, et al. Quantitative morphology of the cerebellum and fourth ventricle in childhood-onset schizophrenia. *Am J Psychiatry*. 1997;154(12):1663-9. Epub 1997/12/16.
16. Schlaepfer TE, Harris GJ, Tien AY, Peng LW, Lee S, Federman EB, et al. Decreased regional cortical gray matter volume in schizophrenia. *Am J Psychiatry*. 1994;151(6):842-8. Epub 1994/06/01.
17. Baumgardner TL, Singer HS, Denckla MB, Rubin MA, Abrams MT, Colli MJ, et al. Corpus callosum morphology in children with Tourette syndrome and attention deficit hyperactivity disorder. *Neurology*. 1996;47(2):477-82. Epub 1996/08/01.

18. Berquin PC, Giedd JN, Jacobsen LK, Hamburger SD, Krain AL, Rapoport JL, et al. Cerebellum in attention-deficit hyperactivity disorder: a morphometric MRI study. *Neurology*. 1998;50(4):1087-93. Epub 1998/05/05.
19. Hynd GW, Semrud-Clikeman M, Lorys AR, Novey ES, Eliopoulos D, Lyytinen H. Corpus callosum morphology in attention deficit-hyperactivity disorder: morphometric analysis of MRI. *J Learn Disabil*. 1991;24(3):141-6. Epub 1991/03/01.
20. Courchesne E, Yeung-Courchesne R, Press GA, Hesselink JR, Jernigan TL. Hypoplasia of cerebellar vermal lobules VI and VII in autism. *N Engl J Med*. 1988;318(21):1349-54. Epub 1988/05/26.
21. Courchesne E, Saitoh O, Yeung-Courchesne R, Press GA, Lincoln AJ, Haas RH, et al. Abnormality of cerebellar vermal lobules VI and VII in patients with infantile autism: identification of hypoplastic and hyperplastic subgroups with MR imaging. *AJR Am J Roentgenol*. 1994;162(1):123-30. Epub 1994/01/01.
22. Egaas B, Courchesne E, Saitoh O. Reduced size of corpus callosum in autism. *Arch Neurol*. 1995;52(8):794-801. Epub 1995/08/01.
23. Gosain AK, McCarthy JG, Glatt P, Staffenberg D, Hoffmann RG. A study of intracranial volume in Apert syndrome. *Plast Reconstr Surg*. 1995;95(2):284-95. Epub 1995/02/01.
24. Raz N, Torres IJ, Briggs SD, Spencer WD, Thornton AE, Loken WJ, et al. Selective neuroanatomic abnormalities in Down's syndrome and their cognitive correlates: evidence from MRI morphometry. *Neurology*. 1995;45(2):356-66. Epub 1995/02/01.
25. Reiss AL, Faruque F, Naidu S, Abrams M, Beaty T, Bryan RN, et al. Neuroanatomy of Rett syndrome: a volumetric imaging study. *Ann Neurol*. 1993;34(2):227-34. Epub 1993/08/01.
26. Toft PB, Leth H, Ring PB, Peitersen B, Lou HC, Henriksen O. Volumetric analysis of the normal infant brain and in intrauterine growth retardation. *Early Hum Dev*. 1995;43(1):15-29. Epub 1995/08/30.
27. Rumsey JM, Donohue BC, Brady DR, Nace K, Giedd JN, Andreason P. A magnetic resonance imaging study of planum temporale asymmetry in men with developmental dyslexia. *Arch Neurol*. 1997;54(12):1481-9. Epub 1997/12/24.
28. Galldiks N, Ullrich R, Schroeter M, Fink GR, Jacobs AH, Kracht LW. Volumetry of [(11)C]-methionine PET uptake and MRI contrast enhancement in patients with recurrent glioblastoma multiforme. *Eur J Nucl Med Mol Imaging*. 2010;37(1):84-92. Epub 2009/08/08.
29. Al-Okaili RN, Krejza J, Wang S, Woo JH, Melhem ER. Advanced MR imaging techniques in the diagnosis of intraaxial brain tumors in adults. *Radiographics*. 2006;26 Suppl 1:S173-89. Epub 2006/10/20.
30. Young GS. Advanced MRI of adult brain tumors. *Neurol Clin*. 2007;25(4):947-73, viii. Epub 2007/10/30.
31. Fayed-Miguel N, Morales-Ramos H, Modrego-Pardo PJ. [Magnetic resonance imaging with spectroscopy, perfusion and cerebral diffusion in the diagnosis of brain tumours]. *Rev Neurol*. 2006;42(12):735-42. Epub 2006/06/16. Resonancia magnetica con espectroscopia, perfusion y difusion cerebral en el diagnostico de los tumores cerebrales.
32. Maheshwari SR, Fatterpekar GM, Castillo M, Mukherji SK. Proton MR spectroscopy of the brain. *Semin Ultrasound CT MR*. 2000;21(6):434-51. Epub 2001/01/04.
33. Bonavita S, Di Salle F, Tedeschi G. Proton MRS in neurological disorders. *Eur J Radiol*. 1999;30(2):125-31. Epub 1999/07/13.
34. Brandao LA, Domingues RC. Main Metabolites and their significance in spectral analysis. In: Brandao LA, Domingues RC, editors. *MR Spectroscopy of the brain*. Philadelphia: Lippincott Williams & Wilkins; 2004. p. 11-2.
35. Castillo M, Kwock L, Mukherji SK. Clinical applications of proton MR spectroscopy. *AJNR Am J Neuroradiol*. 1996;17(1):1-15. Epub 1996/01/01.
36. Kingsley PB, Shah TC, Woldenberg R. Identification of diffuse and focal brain lesions by clinical magnetic resonance spectroscopy. *NMR Biomed*. 2006;19(4):435-62. Epub 2006/06/10.

37. Burtscher IM, Skagerberg G, Geijer B, Englund E, Stahlberg F, Holtas S. Proton MR spectroscopy and preoperative diagnostic accuracy: an evaluation of intracranial mass lesions characterized by stereotactic biopsy findings. *AJNR Am J Neuroradiol.* 2000;21(1):84-93. Epub 2000/02/11.
38. Majos C, Aguilera C, Alonso J, Julia-Sape M, Castaner S, Sanchez JJ, et al. Proton MR spectroscopy improves discrimination between tumor and pseudotumoral lesion in solid brain masses. *AJNR Am J Neuroradiol.* 2009;30(3):544-51. Epub 2008/12/20.
39. Al-Okaili RN, Krejza J, Wang S, Woo JH, Melhem ER. Advanced MR imaging techniques in the diagnosis of intraaxial brain tumors in adults. *Radiographics.* 2006;26 Suppl 1:S173-89. Epub 2006/10/20.
40. Young GS. Advanced MRI of adult brain tumors. *Neurol Clin.* 2007;25(4):947-73, viii. Epub 2007/10/30.
41. Catalaa I, Henry R, Dillon WP, Graves EE, McKnight TR, Lu Y, et al. Perfusion, diffusion and spectroscopy values in newly diagnosed cerebral gliomas. *NMR Biomed.* 2006;19(4):463-75. Epub 2006/06/10.
42. Remy C, Foulhe N, Barba I, Sam-Lai E, Lahrech H, Cucurella MG, et al. Evidence that mobile lipids detected in rat brain glioma by <sup>1</sup>H nuclear magnetic resonance correspond to lipid droplets. *Cancer Res.* 1997;57(3):407-14. Epub 1997/02/01.
43. Kuesel AC, Sutherland GR, Halliday W, Smith IC. <sup>1</sup>H MRS of high grade astrocytomas: mobile lipid accumulation in necrotic tissue. *NMR Biomed.* 1994;7(3):149-55. Epub 1994/05/01.
44. Li X, Vigneron DB, Cha S, Graves EE, Crawford F, Chang SM, et al. Relationship of MR-derived lactate, mobile lipids, and relative blood volume for gliomas in vivo. *AJNR Am J Neuroradiol.* 2005;26(4):760-9. Epub 2005/04/09.
45. Roldan-Valadez E, Favila R, Martinez-Lopez M, Uribe M, Rios C, Mendez-Sanchez N. In vivo <sup>3</sup>T spectroscopic quantification of liver fat content in nonalcoholic fatty liver disease: Correlation with biochemical method and morphometry. *J Hepatol.* 2010;53(4):732-7. Epub 2010/07/03.
46. Allen N. Oxidative metabolism of brain tumors. *Prog Exp Tumor Res.* 1972;17:192-209. Epub 1972/01/01.
47. Burger PC. Malignant astrocytic neoplasms: classification, pathologic anatomy, and response to treatment. *Semin Oncol.* 1986;13(1):16-26. Epub 1986/03/01.
48. Chan AS, Leung SY, Wong MP, Yuen ST, Cheung N, Fan YW, et al. Expression of vascular endothelial growth factor and its receptors in the anaplastic progression of astrocytoma, oligodendroglioma, and ependymoma. *Am J Surg Pathol.* 1998;22(7):816-26. Epub 1998/07/21.
49. Plate KH, Mennel HD. Vascular morphology and angiogenesis in glial tumors. *Exp Toxicol Pathol.* 1995;47(2-3):89-94. Epub 1995/05/01.
50. Semenza GL. Hypoxia, clonal selection, and the role of HIF-1 in tumor progression. *Crit Rev Biochem Mol Biol.* 2000;35(2):71-103. Epub 2000/05/23.
51. Zagzag D, Friedlander DR, Margolis B, Grumet M, Semenza GL, Zhong H, et al. Molecular events implicated in brain tumor angiogenesis and invasion. *Pediatr Neurosurg.* 2000;33(1):49-55. Epub 2000/10/12.
52. Cha S. Update on brain tumor imaging: from anatomy to physiology. *AJNR Am J Neuroradiol.* 2006;27(3):475-87. Epub 2006/03/23.
53. Moritani T, Shrier DA, Numaguchi Y, Takase Y, Takahashi C, Wang HZ, et al. Diffusion-weighted echo-planar MR imaging: clinical applications and pitfalls -- a pictorial essay. *Clin Imaging.* 2000;24(4):181-92. Epub 2001/03/29.
54. Schaefer PW, Grant PE, Gonzalez RG. Diffusion-weighted MR imaging of the brain. *Radiology.* 2000;217(2):331-45. Epub 2000/11/04.
55. Gupta RK, Sinha U, Cloughesy TF, Alger JR. Inverse correlation between choline magnetic resonance spectroscopy signal intensity and the apparent diffusion coefficient in human glioma. *Magn Reson Med.* 1999;41(1):2-7. Epub 1999/02/20.



56. Lai PH, Ho JT, Chen WL, Hsu SS, Wang JS, Pan HB, et al. Brain abscess and necrotic brain tumor: discrimination with proton MR spectroscopy and diffusion-weighted imaging. *AJNR Am J Neuroradiol.* 2002;23(8):1369-77. Epub 2002/09/12.
57. Chenevert TL, Stegman LD, Taylor JM, Robertson PL, Greenberg HS, Rehemtulla A, et al. Diffusion magnetic resonance imaging: an early surrogate marker of therapeutic efficacy in brain tumors. *J Natl Cancer Inst.* 2000;92(24):2029-36. Epub 2000/12/21.
58. Kotsenas AL, Roth TC, Manness WK, Faerber EN. Abnormal diffusion-weighted MRI in medulloblastoma: does it reflect small cell histology? *Pediatr Radiol.* 1999;29(7):524-6. Epub 1999/07/10.
59. Chenevert TL, McKeever PE, Ross BD. Monitoring early response of experimental brain tumors to therapy using diffusion magnetic resonance imaging. *Clin Cancer Res.* 1997;3(9):1457-66. Epub 1998/11/17.
60. Filippi CG, Edgar MA, Ulug AM, Prowda JC, Heier LA, Zimmerman RD. Appearance of meningiomas on diffusion-weighted images: correlating diffusion constants with histopathologic findings. *AJNR Am J Neuroradiol.* 2001;22(1):65-72. Epub 2001/02/13.
61. Hayashida Y, Hirai T, Morishita S, Kitajima M, Murakami R, Korogi Y, et al. Diffusion-weighted imaging of metastatic brain tumors: comparison with histologic type and tumor cellularity. *AJNR Am J Neuroradiol.* 2006;27(7):1419-25. Epub 2006/08/16.
62. Toh CH, Castillo M, Wong AM, Wei KC, Wong HF, Ng SH, et al. Primary cerebral lymphoma and glioblastoma multiforme: differences in diffusion characteristics evaluated with diffusion tensor imaging. *AJNR Am J Neuroradiol.* 2008;29(3):471-5. Epub 2007/12/11.
63. Sugahara T, Korogi Y, Kochi M, Ikushima I, Shigematu Y, Hirai T, et al. Usefulness of diffusion-weighted MRI with echo-planar technique in the evaluation of cellularity in gliomas. *J Magn Reson Imaging.* 1999;9(1):53-60. Epub 1999/02/25.
64. Yang D, Korogi Y, Sugahara T, Kitajima M, Shigematsu Y, Liang L, et al. Cerebral gliomas: prospective comparison of multivoxel 2D chemical-shift imaging proton MR spectroscopy, echoplanar perfusion and diffusion-weighted MRI. *Neuroradiology.* 2002;44(8):656-66. Epub 2002/08/20.
65. Lam WW, Poon WS, Metreweli C. Diffusion MR imaging in glioma: does it have any role in the pre-operation determination of grading of glioma? *Clin Radiol.* 2002;57(3):219-25. Epub 2002/04/16.
66. Castillo M, Smith JK, Kwock L, Wilber K. Apparent diffusion coefficients in the evaluation of high-grade cerebral gliomas. *AJNR Am J Neuroradiol.* 2001;22(1):60-4. Epub 2001/02/13.
67. Hein PA, Eskey CJ, Dunn JF, Hug EB. Diffusion-weighted imaging in the follow-up of treated high-grade gliomas: tumor recurrence versus radiation injury. *AJNR Am J Neuroradiol.* 2004;25(2):201-9. Epub 2004/02/19.
68. Chan YL, Yeung DK, Leung SF, Chan PN. Diffusion-weighted magnetic resonance imaging in radiation-induced cerebral necrosis. Apparent diffusion coefficient in lesion components. *J Comput Assist Tomogr.* 2003;27(5):674-80. Epub 2003/09/23.
69. Basser PJ, Pierpaoli C. Microstructural and physiological features of tissues elucidated by quantitative-diffusion-tensor MRI. *J Magn Reson B.* 1996;111(3):209-19. Epub 1996/06/01.
70. Moseley ME, Cohen Y, Kucharczyk J, Mintorovitch J, Asgari HS, Wendland MF, et al. Diffusion-weighted MR imaging of anisotropic water diffusion in cat central nervous system. *Radiology.* 1990;176(2):439-45. Epub 1990/08/01.
71. Le Bihan D, Mangin JF, Poupon C, Clark CA, Pappata S, Molko N, et al. Diffusion tensor imaging: concepts and applications. *J Magn Reson Imaging.* 2001;13(4):534-46. Epub 2001/03/29.
72. Lu S, Ahn D, Johnson G, Law M, Zagzag D, Grossman RI. Diffusion-tensor MR imaging of intracranial neoplasia and associated peritumoral edema: introduction of the tumor infiltration index. *Radiology.* 2004;232(1):221-8. Epub 2004/06/29.
73. Jellison BJ, Field AS, Medow J, Lazar M, Salamat MS, Alexander AL. Diffusion tensor imaging of cerebral white matter: a pictorial review of physics, fiber tract anatomy, and tumor imaging patterns. *AJNR Am J Neuroradiol.* 2004;25(3):356-69. Epub 2004/03/24.

74. Pierpaoli C, Basser PJ. Toward a quantitative assessment of diffusion anisotropy. *Magn Reson Med.* 1996;36(6):893-906. Epub 1996/12/01.
75. Neil J, Miller J, Mukherjee P, Huppi PS. Diffusion tensor imaging of normal and injured developing human brain - a technical review. *NMR Biomed.* 2002;15(7-8):543-52. Epub 2002/12/19.
76. Gupta RK, Hasan KM, Mishra AM, Jha D, Husain M, Prasad KN, et al. High fractional anisotropy in brain abscesses versus other cystic intracranial lesions. *AJNR Am J Neuroradiol.* 2005;26(5):1107-14. Epub 2005/05/14.
77. Witwer BP, Moftakhar R, Hasan KM, Deshmukh P, Haughton V, Field A, et al. Diffusion-tensor imaging of white matter tracts in patients with cerebral neoplasm. *J Neurosurg.* 2002;97(3):568-75. Epub 2002/09/26.
78. Petrella JR, Provenzale JM. MR perfusion imaging of the brain: techniques and applications. *AJR Am J Roentgenol.* 2000;175(1):207-19. Epub 2000/07/06.
79. Aksoy FG, Lev MH. Dynamic contrast-enhanced brain perfusion imaging: technique and clinical applications. *Semin Ultrasound CT MR.* 2000;21(6):462-77. Epub 2001/01/04.
80. Henry RG, Vigneron DB, Fischbein NJ, Grant PE, Day MR, Noworolski SM, et al. Comparison of relative cerebral blood volume and proton spectroscopy in patients with treated gliomas. *AJNR Am J Neuroradiol.* 2000;21(2):357-66. Epub 2000/03/01.
81. Aronen HJ, Pardo FS, Kennedy DN, Belliveau JW, Packard SD, Hsu DW, et al. High microvascular blood volume is associated with high glucose uptake and tumor angiogenesis in human gliomas. *Clin Cancer Res.* 2000;6(6):2189-200. Epub 2000/06/29.
82. Law M, Yang S, Wang H, Babb JS, Johnson G, Cha S, et al. Glioma grading: sensitivity, specificity, and predictive values of perfusion MR imaging and proton MR spectroscopic imaging compared with conventional MR imaging. *AJNR Am J Neuroradiol.* 2003;24(10):1989-98. Epub 2003/11/20.
83. Law M, Yang S, Wang H, Babb JS, Johnson G, Cha S, et al. Glioma grading: sensitivity, specificity, and predictive values of perfusion MR imaging and proton MR spectroscopic imaging compared with conventional MR imaging. *AJNR American journal of neuroradiology.* 2003;24(10):1989-98. Epub 2003/11/20.
84. Danchavijitr N, Waldman AD, Tozer DJ, Benton CE, Brasil Caseiras G, Tofts PS, et al. Low-grade gliomas: do changes in rCBV measurements at longitudinal perfusion-weighted MR imaging predict malignant transformation? *Radiology.* 2008;247(1):170-8. Epub 2008/03/29.
85. Diehn M, Nardini C, Wang DS, McGovern S, Jayaraman M, Liang Y, et al. Identification of noninvasive imaging surrogates for brain tumor gene-expression modules. *Proc Natl Acad Sci U S A.* 2008;105(13):5213-8. Epub 2008/03/26.
86. Fatooh A, Nanaszko MJ, Allen BB, Mok CL, Bukanova EN, Beyene R, et al. Understanding the role of tumor stem cells in glioblastoma multiforme: a review article. *J Neurooncol.* 2010. Epub 2010/09/21.
87. Adamson C, Kanu OO, Mehta AI, Di C, Lin N, Mattox AK, et al. Glioblastoma multiforme: a review of where we have been and where we are going. *Expert Opin Investig Drugs.* 2009;18(8):1061-83. Epub 2009/06/27.
88. Groves MD, Puduvalli VK, Gilbert MR, Levin VA, Conrad CA, Liu VH, et al. Two phase II trials of temozolomide with interferon-alpha2b (pegylated and non-pegylated) in patients with recurrent glioblastoma multiforme. *Br J Cancer.* 2009;101(4):615-20. Epub 2009/08/13.
89. Yaneva MP, Semerdjieva ML, Radev LR, Vlaikova MI. Postoperative chemo-radiotherapy with temodal in patients with glioblastoma multiforme--survival rates and prognostic factors. *Folia Med (Plovdiv).* 2010;52(1):26-33. Epub 2010/04/13.
90. Moreno S. Radio- and quimotherapy of Glioblastoma Multiforme at the Mexican National Institute of Neurology and Neurosurgery. In: Roldan-Valadez E, editor. Mexico city, Mexico: Department of Radioneurosurgery. Secretariath of Health.; 2011. p. 1.

91. Li J, Wang M, Won M, Shaw EG, Coughlin C, Curran WJ, Jr., et al. Validation and Simplification of the Radiation Therapy Oncology Group Recursive Partitioning Analysis Classification for Glioblastoma. *Int J Radiat Oncol Biol Phys*. 2010. Epub 2010/10/05.
92. Dresemann G. Temozolomide in malignant glioma. *OncoTargets and therapy*. 2010;3:139-46. Epub 2010/09/22.
93. Garcia-Lopez U. ASOCIACIÓN ENTRE LOS POLIMORFISMOS EN LOS GENES DE IL1, IL4, IL6, IL10, FNT $\alpha$  E INF $\gamma$  Y LA INTENSIDAD DE LA RESPUESTA INFLAMATORIA EN PACIENTES MEXICANOS CON GLIOBLASTOMA MULTIFORME. Mexico city, Mexico.: Department of Neurosurgery. Mexican National Institute of Neurology and Neurosurgery. Secretariath of Health. Mexico.
94. Gamiño-Sabag I. Fruencia de Glioblastomas tratados con cirugia gamma-knife en el Hospital Médica Sur. In: Roldan-Valadez E, editor. Mexico city, Mexico.2010.
95. Faul F, Erdfelder E, Lang AG, Buchner A. G\*Power 3: a flexible statistical power analysis program for the social, behavioral, and biomedical sciences. *Behavior research methods*. 2007;39(2):175-91. Epub 2007/08/19.
96. Wilkinson L. Statistical Methods in Psychology Journals. Task Force on Statistical Inference. APA Board of Scientific Affairs. *American Psychologist*. 1999;54(8):594-604.
97. Publication Manual of the American Psychological Association. American Psychological Association (APA). 6 ed. ed2009.
98. Cohen J. *Statistical Power Analysis for the Behavioral Sciences*. Hillsdale, NJ: Lawrence Erlbaum Associates; 1988. p. 21-5.
99. Cox DR, Oakes D. *Analysis of survival data*. London: Chapman and Hall; 1984.
100. Park SH, Goo JM, Jo CH. Receiver operating characteristic (ROC) curve: practical review for radiologists. *Korean J Radiol*. 2004;5(1):11-8. Epub 2004/04/06.
101. Hanley JA, McNeil BJ. The meaning and use of the area under a receiver operating characteristic (ROC) curve. *Radiology*. 1982;143(1):29-36. Epub 1982/04/01.
102. Obuchowski NA. Receiver operating characteristic curves and their use in radiology. *Radiology*. 2003;229(1):3-8. Epub 2003/10/02.
103. Metz CE. Basic principles of ROC analysis. *Semin Nucl Med*. 1978;8(4):283-98. Epub 1978/10/01.
104. Hernández-Salazar M, Lorenzana-Galicia RD, Ramírez-Castañeda VO, Zárate-Méndez A, Cervera-Maltos UI, Cevallos J. Utilidad de la biopsia estereotáctica en lesiones del tallo cerebral. *Arch Neurocién Mex* 2004;9(2):73-80.
105. Zaitoun AM, Al Mardini H, Awad S, Ukabam S, Makadisi S, Record CO. Quantitative assessment of fibrosis and steatosis in liver biopsies from patients with chronic hepatitis C. *J Clin Pathol*. 2001;54(6):461-5. Epub 2001/05/29.
106. Franzen LE, Ekstedt M, Kechagias S, Bodin L. Semiquantitative evaluation overestimates the degree of steatosis in liver biopsies: a comparison to stereological point counting. *Mod Pathol*. 2005;18(7):912-6. Epub 2005/05/28.

14) APÉDICE 1: CARTA DE CONSENTIMIENTO INFORMADO



INSTITUTO NACIONAL DE NEUROLOGÍA Y NEUROCIRUGÍA  
MANUEL VELASCO SUÁREZ  
DIRECCIÓN DE INVESTIGACIÓN

Insurgentes Sur 3877  
Col. La Fama, C.P. 14269  
Mexico, D.F., Tel. 55-28-80-36

**Consentimiento informado**

Fecha: \_\_\_\_\_

**PROTOCOLO DE INVESTIGACIÓN No.:** 84/11

El departamento de Radioneurocirugía dirigido por el Dr. Sergio Moreno Jimenéz lo invita a participar en el protocolo de investigación:

**Biomarcadores avanzados de resonancia magnética como factores pronósticos para la sobrevida de pacientes con glioblastoma multiforme.**

Se está invitando a participar en este proyecto a los pacientes como usted con diagnóstico de glioblastoma multiforme (cáncer cerebral).

**CONFIDENCIALIDAD**

Si acepta contribuir con este proyecto debe saber que la información relacionada con su enfermedad y datos personales son confidenciales y solo será usada con fines de investigación. Los pacientes que sean incluidos en el estudio serán identificados por números sin relación a su expediente clínico por lo que su nombre y demás datos de índole personal no serán revelados. Esta información no será compartida con otras personas sin su consentimiento.

Todas las personas involucradas están comprometidas a guardar la información de manera confidencial y velar por la seguridad física, moral y psicológica de los participantes en este estudio.

**OBJETIVO DEL ESTUDIO**

Este proyecto estudiará la relación entre los parametros avanzados de la resonancia magnetica (difusión, perfusión, espectroscopia y tractografía) que se realizara a su cerebro como parte del diagnostico y seguimiento de su evolución clínica en este instituto. El diagnostico y tratamiento de cada paciente no será verificado o afectado.

**PROCEDIMIENTOS**

Si usted acepta participar en este proyecto se le pedirá que tenga una entrevista con los médicos encargados del estudio.

Se le harán preguntas en relación a su enfermedad y se recabarán esta información en un formato con fines de recolección de datos. Usted será diagnosticado y tratado como cualquier otro paciente del Instituto con diagnóstico de cáncer cerebral si acepta participar en este estudio.

**BENEFICIOS PREVISTOS PARA LOS PACIENTES**

Mediante este estudio no obtendra beneficio economico y su condicion de salud no mejorara como resultado de su participacion en mismo.

**RIESGOS Y MOLESTIAS POSIBLES**

No hay riesgos ni molestias adicionales a las del estudio de resonancia magnetica que su médico solicitó.

**ALTERNATIVAS DE TRATAMIENTO**

El participar en este protocolo no influirá en las indicaciones medicas de su tratamiento.

**RECOMENDACIONES**

Solamente las indicadas por su medico tratante.

**OBLIGACIONES FINANCIERAS Y COMPENSACIÓN**

Su participación en este estudio no tiene costo alguno para usted, no recibirá remuneración económica alguna por su participación.

**ABANDONO DEL ESTUDIO**

Usted puede abandonar o revocar su autorización a participar en el estudio en el momento que así lo desee sin que esto interfiera con la atención médica recibida o que recibirá en este Instituto.

El médico responsable tiene la facultad de suspender su participación en el estudio con el fin de proteger su salud, si así lo considera necesario.

**IDENTIFICACIÓN DE LOS INVESTIGADORES**

Si tiene una pregunta o duda sobre cualquier asunto relacionado con este estudio por favor contacte a los médicos encargados del proyecto

Dr. Ernesto Roldan Valadez al telefono 5424-7230 o 5424-7231.

Dr. Sergio Moreno Jiménez al teléfono 56 06 38 22 extensión 4472 y 4473.

**CONSIDERACIONES ÉTICAS**

Este estudio se realizará bajo las recomendaciones de la Asociación Médica Mundial (conforme a la Declaración de Helsinki de 1964 y en apego a la Ley General de Salud, al Reglamento de la Ley General de Salud en Materia de Investigación para la Salud). Además los procedimientos de este estudio han sido revisados y aprobados por el Comité de Ética del Instituto Nacional de Neurología y Neurocirugía.

**FIRMA DE CONSENTIMIENTO INFORMADO**

Manifiesto haber leído y entendido completamente el objetivo del estudio, haber tenido la oportunidad de hacer preguntas adicionales y recibido respuestas satisfactorias. Entiendo la razón por la que se requiere recopilar la información de este estudio así como el manejo que se le dará a la misma, con lo cual estoy totalmente de acuerdo.

*Por este conducto, acepto participar en el presente protocolo de investigación titulado:*

**Biomarcadores avanzados de resonancia magnética como factores pronósticos para la sobrevida de pacientes con glioblastoma multiforme.**

_____ <b>Nombre del paciente</b> (Apellido paterno, materno y nombre(s))	_____ <b>Firma</b>
_____ <b>Teléfonos de contacto</b>	_____ <b>Fecha</b> (DD/MMM/AAAA)

_____ <b>Nombre del Testigo I</b> (Apellido paterno, materno y nombre(s))	_____ <b>Domicilio</b> (Calle, N°, Colonia, Código Postal)
_____ <b>Fecha</b> (DD/MMM/AAAA)	_____ <b>Firma</b>

\_\_\_\_\_  
**Nombre del Testigo II**  
(Apellido paterno, materno y nombre(s))

\_\_\_\_\_  
**Domicilio**  
(Calle, N°, Colonia, Código Postal)

\_\_\_\_\_  
**Fecha** (DD/MMM/AAAA)

\_\_\_\_\_  
**Firma**

\_\_\_\_\_  
**Parentesco**

Firma del Representante Legal (si aplica)

\_\_\_\_\_  
**Nombre del Representante Legal**  
(Apellido paterno, materno y nombre (s))

\_\_\_\_\_  
**Firma**

\_\_\_\_\_  
**Telefonos de contacto**

\_\_\_\_\_  
**Fecha** (DD/MMM/AAAA)

15) APÉNDICE 2: OTROS CRITERIOS DE ACUERDO AL TIPO DE ESTUDIO

INSTITUTO NACIONAL DE NEUROLOGÍA Y NEUROCIROLOGÍA

MANUEL VELASCO SUÁREZ  
DIRECCIÓN DE INVESTIGACIÓN



www.in

Insurgentes Sur 3877  
Col. La Fama, C.P. 14269  
Mexico, D.F., Tel. 55-28-80-36

**Secuencias de RM para el Protocolo:**

***Biomarcadores avanzados de resonancia magnética como factores pronósticos para la supervivencia de pacientes con glioblastoma multiforme.***

Fecha: Agosto 21 de 2012

**PROTOCOLO DE INVESTIGACIÓN No.: 84/11**

Objetivo: Este protocolo pretende estudiar los cambios por GBM en tejido tumoral, en edema y en tejido sano.

**Protocolo de Secuencias para el Resonador de 3.0T \***

Secuencias a realizar	Comentarios	Tiempo
Difusión	✓ Utilizar valor-b de 1000 s/mm <sup>2</sup> , FOV=25.6 cm, matriz 128x128, grosor=5 mm, espaciamento=1 mm, TE mínimo, TR suficiente para adquirir todos los cortes, NEX=3, ASSET.	~1:10
Secuencia T2 Cubo-sagital, isométrica	✓ FOV=25.6 cm, matriz=256x256, grosor=1 mm, TR=2500 ms, cortes suficientes para cubrir toda la cabeza, ajustar ETL para que el TE sea cercano a 120 ms, ARC.	~2:00
Secuencia FLAIR T2 Cubo-sagital	✓ FOV=25.6 cm, matriz=256x256, grosor=1 mm, TR=7000 ms, cortes suficientes para cubrir toda la cabeza, ajustar ETL para que el TE sea cercano a 120 ms, ARC.	~3:00
Tensor de Difusión (Tractografía)	✓ Utilizar valor-b de 700 s/mm <sup>2</sup> , 35 direcciones de difusión, FOV=25.6 cm, matriz 128x128, grosor=3 mm, espaciamento=0 mm, TE mínimo, cubrir todo el encéfalo y el cerebelo, TR suficiente para adquirir todos los cortes, NEX=1, ASSET.	~8:00
Perfusión	✓ EPI-GRE, FOV=25.6 cm, matriz 128x128, grosor=5 mm, espaciamento=1 mm, TE=50 ms, TR suficiente para adquirir todos los cortes, 40 fases por corte, Tiempo de duración aprox. 1:08 minutos para 20 cortes.	~1:10
Secuencia T1 3D isométrica axial pre y post gadolinio-axial	✓ Fast SPGR, FOV=25.6 cm, matriz=256x256, phase FOV=0.75, TE Min Full, T1=450 ms, FA=15°, grosor=1 mm, cortes suficientes para cubrir todo el encéfalo y el cerebelo.	~8:00
Espectroscopia 3D Multivoxel	✓ Incluye zona del tumor y edema perilesional, si es posible alguna zona de tejido sano. FOV=16 cm, matriz=8x8, TE=144 ms, TR=1000 ms, NEX=1.6 ó 2.	~8:30
1 Espectro univoxel para medición de grasa del tumor (zona sólida) y 1 espectro univoxel para medición de grasa en tejido sano (hemisferio cerebral contralateral).	✓ TE=30 ms, TR=1500 ms, voxel=2x2x2 cm, 128 scans.	~4:00
<b>Total Minutos</b>		<b>~36:00</b>

\* Las secuencias de RM fueron planeadas con apoyo del Especialista en Aplicaciones Avanzadas M. en C. Rafael Favila (GE Healthcare, México).





**Secuencias de RM para el Procotolo:**

***Biomarcadores avanzados de resonancia magnética como factores pronósticos para la sobrevivida de pacientes con glioblastoma multiforme.***

Fecha: Agosto 21 de 2012

**PROTOCOLO DE INVESTIGACIÓN No.:** 84/11

**IMPORTANTE:** En caso que el magneto de 3.0 T no este disponible, las secuencias pueden adquirirse en el magneto de 1.5T con los siguientes parametros:

**Protocolo de Secuencias para el Resonador de 1.5T \***

Secuencias a realizar	Comentarios	Tiempo
Difusión	✓ Utilizar valor-b de 1000 s/mm <sup>2</sup> , FOV=25.6 cm, matriz 128x128, grosor=5 mm, espaciamento=1 mm, TE mínimo, TR suficiente para adquirir todos los cortes, NEX=3, ASSET.	~1:05
Secuencia T2 Cubo-sagital, isométrica	✓ FOV=26.8 cm, matriz=224x224, grosor=1.2 mm, TR=2500 ms, cortes suficientes para cubrir toda la cabeza, ajustar ETL para que el TE sea cercano a 120 ms, ARC.	~1:55
Secuencia FLAIR T2 Cubo-sagital	✓ FOV=26.8 cm, matriz=224x224, grosor=1.2 mm, TR=7000 ms, cortes suficientes para cubrir toda la cabeza, ajustar ETL para que el TE sea cercano a 120 ms, ARC.	~2:55
Tensor de Difusión (Tractografía)	✓ Utilizar valor-b de 700 s/mm <sup>2</sup> , 35 direccionse de difusión, FOV=25.6 cm, matriz 128x128, grosor=3 mm, espaciamento=0 mm, TE mínimo, cubrir todo el encéfalo y el cerebelo, TR suficiente para adquirir todos los cortes, NEX=1, ASSET.	~7:55
Perfusión	✓ EPI-GRE, FOV=25.6 cm, matriz 128x128, grosor=5 mm, espaciamento=1 mm, TE=50 ms, TR suficiente para adquirir todos los cortes, 40 fases por corte, Tiempo de duracion aprox. 1:08 minutos para 20 cortes.	~1:05
Secuencia T1 3D isométrica axiala pre y post gadolinio-axial	✓ Fast SPGR, FOV=25.6 cm, matriz=256x256, phase FOV=0.75, TE Min Full, TI=450 ms, FA=15°, grosor=1 mm, cortes suficientes para cubrir todo el encéfalo y el cerebelo.	~7:55
Espectroscopia 3D Multivoxel	✓ Incluye zona del tumor y edema perilesional, si es posible alguna zona de tejido sano. FOV=16 cm, matriz=8x8, TE=144 ms, TR=1000 ms, NEX=1.6 ó 2.	~8:25
2 Espectro univoxel para medición de grasa: 1 en zona solida del y 2 en tejido sano (hemisferio contralateral).	✓ TE=30 ms, TR=1500 ms, vóxel=2x2x2 cm, 128 scans.	~3:55
<b>Total Minutos</b>		<b>~36:10</b>

\* Las secuencias de RM fueron planeadas con apoyo del Especialista en Aplicaciones Avanzadas M. en C. Rafael Favila (GE Healthcare, México).

Preguntas y comentarios:

Dr. Ernesto Roldan-Valadez, Radiólogo, Posgrado en RM. Alumno del Doctorado en Ciencias Medicas UNAM. Departamento de Neuroquímica, INNN.

Tel. 5606-3822, Ext. 2006. Celular. 04455-4390-4729.

Dr. Sergio Moreno Jimenez, Depto. de Radioneurocirugia.

Dr. Camilo Rios Catañeda, Depto. de Neuroquímica.

15) APÉNDICE 3: OTROS CRITERIOS DE ACUERDO AL TIPO DE ESTUDIO

**Formato de captura de datos**

**Biomarcadores avanzados de resonancia magnética como factores pronosticos para la sobrevida de pacientes con glioblastoma multiforme.**

Nombre del Paciente \_\_\_\_\_

Número del paciente en el protocolo \_\_\_\_\_

Fecha del Estudio \_\_\_\_\_

Médico Tratante \_\_\_\_\_ No. Expediente \_\_\_\_\_

Variable	Resultado
Edad	
Sexo	
Volumen tumoral en T1 post gadolinio	
Volumen en T2 (del edema perilesional)	
Coficiente de Difusión Aparente (ADC)	
Índice de Colina/Naa	
Índice de Naa/Cr	
Índice de Lactato/Cr	
Índice de mioinositol/Naa	
% de grasa en espectroscopia	
Volumen cerebral relativo	
Anisotropia Fraccional	
Grado de resección Qx.	
Respuesta al tratamiento (mediana de sobrevida)	

16) ETAPAS EN QUE PROGRAMA SU INVESTIGACION (NUMERO DE ETAPAS QUE USTED CONSIDERE INTERVIENEN EN SU PROYECTO):

1a.	<u>Diseño de protocolo y presentación a Comité Ética</u>	<u>20</u> %
2a.	<u>Inclusion de Pacientes</u>	<u>40</u> %
3a.	<u>Analisis de los Datos</u>	<u>20</u> %
4a.	<u>Publicación de los Resultados</u>	<u>20</u> %
5a.	_____	_____ %
6a.	_____	_____ %

100 %

FECHA DE INICIO PROGRAMADA:

Agosto  
MES

2011  
AÑO

FECHA DE INICIO REAL:

Julio  
MES

2014  
AÑO

FECHA DE TERMINACIÓN PROGRAMADA:

Julio  
MES

2014  
AÑO

FECHA DE TERMINACIÓN REAL:

Julio  
MES

2016  
AÑO

\_\_\_\_\_



INSTITUTO NACIONAL DE NEUROLOGÍA Y NEUROCIRUGÍA  
MANUEL VELASCO SUÁREZ

Insurgentes Sur 3877  
Col. La Fama, C. P. 14269  
México, D.F., Tel. 56-06-14-07  
<http://www.innn.salud.gob.mx>

México, D. F., a 21 de agosto de 2012

DR. DANIEL SAN JUAN ORTA,  
JEFE DEL DEPTO. DE INVESTIGACIÓN CLÍNICA,  
P R E S E N T E.

A fin de cumplir con lo que exige la Ley General de Salud de México, y el Reglamento para Investigación Clínica del Instituto Nacional de Neurología y Neurocirugía Manuel Velasco Suárez, envío a usted:

1. El protocolo titulado "**Biomarcadores avanzados de resonancia magnética como factores pronósticos para la sobrevida de pacientes con glioblastoma multiforme**", elaborado de acuerdo al formato oficial, firmado por todos los autores. Original y dos copias.
2. El formato de identificación del ámbito de estudio del protocolo.

Para su evaluación de acuerdo con los Principios Básicos Científicos aceptados en las Declaraciones sobre Investigación Biomédica en seres humanos, de Helsinki II en 1975, Venecia en 1983, Hong Kong en 1989, Sudáfrica 1996, Edimburgo 2000, que señalan textualmente "el protocolo se remitirá a un comité independiente del investigador y de la entidad patrocinadora, para consideración, comentarios y asesoramiento", en lo cual se basará la aprobación, en cuyo caso debe informar trimestralmente del avance del estudio.

A T E N T A M E N T E

Dr. Ernesto Roldán Valdez  
Nombre y firma del Investigador Principal

## FORMATO DE IDENTIFICACIÓN DEL ÁMBITO DE ESTUDIO DE LOS PROTOCOLOS DE INVESTIGACIÓN CLÍNICA

Título del proyecto:

1) Mencione cual es la vinculación de su proyecto de investigación con las líneas de avance médico actual y futuro:

El protocolo propone la utilización de las secuencias de resonancia magnética que marca la literatura medica actual como las ideales para el estudio de los tumores cerebrales, estas secuencias en la actualidad no se utilizan en el INNN.

2) Mencione el vínculo de su proyecto con las líneas de interés nacional:

Cada año se detectan 30 mil nuevos casos en promedio de cáncer cerebral, en México, de estos, los tumores gliales de alto grado (glioblastoma multiforme) representan el tipo más común de tumor cerebral maligno y representan el 40-50% de las neoplasias cerebrales primarias en adultos. A nivel nacional, es uno de los 3 tipos de tumores mas comunes junto con linfomas y leucemias. En las últimas tres décadas, se ha observado un incremento en su mortalidad, más evidente en los pacientes mayores de 60 años, en quienes la incidencia se incrementa 2.5% por año desde 1980.

3) Diga como se vincula su investigación con las líneas de interés para la Secretaría de Salud:

La atención a los tumores cerebrales es una de las líneas prioritarias de la Secretaria de Salud de México, este protocolo se alinea directamente con un interés nacional para atender esta patología.

4) Diga cómo se vincula su proyecto con las líneas de interés para el Instituto:

El Instituto Nacional de Neurología y Neurocirugía (INNN) de la Secretaría de Salud cuenta con el equipo tecnológico más moderno para la atención de tumores cerebrales benignos y malignos, lo que coloca a México como líder en Latinoamérica en la atención de esos problemas. En el año 2010 se atendieron aproximadamente 100 casos de glioblastoma multiforme, un promedio de 2 pacientes por semana.

5) Mencione cuales son las líneas de investigación de interés para usted mismo:

- ✓ Análisis avanzado con resonancia magnetica de tumores cerebrales.
- ✓ Evaluacion diagnostica del análisis difusión-perfusión en el infarto cerebral.
- ✓ Diagnostico temprano de Alzheimer con análisis cuantitativo de resonancia magnética.
- ✓ Caracterizacion de patología psiquiatrica con espectroscopia por resonancia magnética.

Fecha:

Firma del investigador:

Agosto 21 de 2012

Dr. Ernesto Roldán Valadez

## Avances del proyecto de tesis

- Se ha creado una línea de investigación original que previamente no existía en el Instituto Nacional de Neurología y en la Fundación Clínica Médica Sur, esta última lugar de trabajo del alumno.
- En las primeras etapas del proyecto se evaluó la capacidad pronostica para sobrevida de las secuencias de resonancia magnética conocidas como análisis avanzado en 28 pacientes con diagnóstico de glioblastoma multiforme y en 34 controles sanos. Se obtuvieron resultados preliminares de los mejores biomarcadores que dan respuesta a los objetivos planteados en el protocolo de investigación.
- Al termino del 3er año del doctorado, se completaron 5 artículos originales relacionados directamente con el protocolo de investigación, 3 de ellos han sido publicados, y los otros 2 se encuentran en proceso de revisión, todos enviados a revistas indexadas en el *Journal Citation Reports*.
- El alumno fue responsable de escribir cada uno de los 5 artículos terminados, incluyendo su análisis estadístico correspondiente; en todo los manuscritos el alumno figura como 1er autor y/o autor correspondiente. Los manuscritos fueron revisados y comentados con el tutor.
- Durante el desarrollo del doctorado, el alumno presento avances semestrales del protocolo de investigación a la Coordinación de Estudios de Posgrado de la Facultad de Medicina, durante la actividad denominada *Coloquios de investigación*. Al final de cada presentación un grupo de expertos designado por el Subcomité de Ciencias Médicas califico los avances semestrales del proyecto y emitió recomendaciones que fueron seguidas por el alumno.
- Hasta el momento de la presentación de esta tesis, se ha obtenido: la aprobación del Examen de Candidatura, el reconocimiento de 3 publicaciones por el Subcomité de Ciencias Médicas y la autorización para presentar el Examen de Grado en la *modalidad de producción científica*. Con la presentación de esta tesis, se finaliza la ultima etapa del proceso de titulación del programa Doctorado en Ciencias Médicas avalado por la División de Estudios de Posgrado de la Facultad de Medicina de la UNAM.

**Submission #256 version #1 submitted on January 6, 2014****Title**

Choline-to-N-acetylaspartate and lipids-lactate-to-creatine ratios together with age assemble a significant Cox's proportional-hazards regression mode

**Authors**

Dr. Ernesto Ernesto Roldan-Valadez Roldan-Valadez\* (Magnetic Resonance Unit, Medica Sur Clinic & Foundation. Mexico City, Mexico.)  
 Dr. Camilo Rios (Department of Neurochemistry, National Institute of Neurology and Neurosurgery. Mexico City, Mexico.)  
 Dr. Daniel Motola-Kuba (Oncology Unit, Medica Sur Clinic & Foundation. Mexico City, Mexico.)  
 Dr. Juan Matus-Santos (Oncology Unit, Medica Sur Clinic & Foundation. Mexico City, Mexico.)  
 Dr. Antonio Villa-Romero (Coordination of Research, Department of Public Health, National Autonomous University of Mexico. Mexico City, Mexico.)  
 Dr. Sergio Moreno-Jimenez (Radioneurosurgery Unit, National Institute of Neurology and Neurosurgery. Mexico City, Mexico.)






**Keywords**

Biological markers; Glioblastoma; Magnetic Resonance Imaging; Prognosis; Survival Analysis.

**Abstract**

**Introduction.** There has been a longstanding interest in the identification of prognostic biomarkers for high-grade gliomas (HGGs) using magnetic resonance (MR) imaging, but a consensus of which parameters assemble a significant survival model is still missing in the literature; we investigated the significant positive or negative contribution of several MR biomarkers in the prognosis of these tumors. **Materials and Methods.** A cohort of 28 patients with supratentorial HGGs (11 GBM and 17 anaplastic astrocytomas) was included (19 men and 9 women, mean age of 50.4 years, SD: 16.28; range: 13 – 85 y). Edema and viable tumor measurements were acquired using ROIs in T1-w, T2-w, Flair, apparent diffusion coefficient (ADC) and MR Spectroscopy. Kaplan-Meier and Cox's proportional hazards model were performed. **Results.** 17 patients died within the follow-up period (3 to 98 months). The median survival time was 1.73 years (range, 0.287-8.947 years). Only 3 out of 20 covariates (Choline-to-N-acetylaspartate and lipids-lactate-to-creatine ratios, and age) contribute significantly to explaining variability in the survival hazards model, score test:  $\chi^2(3) = 9.098, p = .028$ . **Conclusions.** For this data-set MR-spectroscopy metabolites overcome volumetric biomarkers (peritumoral edema and viable tumor) as well as tumor-regions ADC measurements. A consensus about which MR biomarkers should be included in the imaging follow-up is still in need for these tumors.

## Files list

File name	File size	File category	File upload date	File comment	View file
00000256_Manuscript-GBM Survival Jan-05-2014.docx	0.1 MB	manuscript	2014-01-06 02:10:04	Manuscript-blinded	
00000256_Cover letter-ANE Jan-05-2014.pdf	0.5 MB	cover letter	2014-01-06 02:15:24	Cover letter	
00000256_Figure 1 flatten.tif	1.8 MB	figures	2014-01-06 02:16:20	Figure 1. Conventional MRI sequences in a patient with GBM, axial-plane images in: A, T2-w; B, post gadolinium T1-w; C, Flair; D, gradient echo.	
00000256_Figure 2 BW.tif	0.1 MB	figures	2014-01-06 02:16:35	Figure 2. Survival curve of patients with high-grade gliomas.	
00000256_Figure 3A-C flatten.tif	1.2 MB	figures	2014-01-06 02:17:06	Figure 3. Schoenfeld residual plots for the selected covariates in the Cox regression model for survival in HGGs. A, Cho/Naa ratio and B, Lipids-lactate/Creatine ratio; in both plots the Lowess curve varies around the zero reference line in a nonsystematic way; after the 3rd-4th year the smooth line appear to demonstrate a trend over time with a negative slope and thus that it had a negative proportional hazard. C, plot of the Age (years); the fitted line appeared to have a positive line, suggesting that the hazard ratio for this covariate increases over time and thus it has a proportional hazard.	

[Back to submissions list](#)[Back to main menu](#)



**Choline-to-N-acetylaspartate and lipids-lactate-to-creatine ratios together with age assemble a significant Cox's proportional-hazards regression model for survival prediction in patients with high-grade gliomas.**

Ernesto Roldan-Valadez, M.D., M.Sc. <sup>1</sup>

Camilo Rios, Ph.D. <sup>2</sup>

Daniel Motola-Kuba, M.D. <sup>3</sup>

Juan Matus-Santos, M.D. <sup>3</sup>

Antonio Villa-Romero, M.D., Ph.D. <sup>4</sup>

Sergio Moreno-Jimenez, M.D., Ph.D. <sup>5</sup>

<sup>1</sup> Magnetic Resonance Unit, Medica Sur Clinic & Foundation. Mexico City, Mexico.

<sup>2</sup> Department of Neurochemistry. National Institute of Neurology and Neurosurgery. Mexico City, Mexico.

<sup>3</sup> Oncology Unit, Medica Sur Clinic & Foundation. Mexico City, Mexico.

<sup>3</sup> Coordination of Research, Department of Public Health. National Autonomous University of Mexico. Mexico City, Mexico.

<sup>5</sup> Radioneurosurgery Unit, National Institute of Neurology and Neurosurgery. Mexico City, Mexico.

**Address for correspondence:**

Ernesto Roldan-Valadez, M.D., M.Sc.  
Coordination of Research and Innovation in MRI.  
Magnetic Resonance Unit.  
Medica Sur Clinic & Foundation.  
Puente de Piedra # 150. Col. Toriello Guerra. Deleg. Tlalpan.  
CP 14050. Mexico City, Mexico.  
Phone: (+52-55) 5424-7230.  
Fax: (+52-55) 5424-4429.  
Email: [ernest.roldan@usa.net](mailto:ernest.roldan@usa.net)

**Running Title:** *MRI model for survival in GBM patients.*

**Choline-to-N-acetylaspartate and lipids-lactate-to-creatine ratios together with age, assemble a significant Cox's proportional-hazards regression model for survival prediction in patients with high-grade gliomas.**

### Abstract

**Introduction.** There has been a longstanding interest in the identification of prognostic biomarkers for high-grade gliomas (HGGs) using magnetic resonance (MR) imaging, but a consensus of which parameters assemble a significant survival model is still missing in the literature; we investigated the significant positive or negative contribution of several MR biomarkers in the prognosis of these tumors.

**Materials and Methods.** A cohort of 28 patients with supratentorial HGGs (11 GBM and 17 anaplastic astrocytomas) was included (19 men and 9 women, mean age of 50.4 years, SD: 16.28; range: 13 – 85 y). Edema and viable tumor measurements were acquired using ROIs in T1-w, T2-w, Flair, apparent diffusion coefficient (ADC) and MR Spectroscopy. Kaplan-Meier and Cox's proportional hazards model were performed.

**Results.** 17 patients died within the follow-up period (3 to 98 months). The median survival time was 1.73 years (range, 0.287-8.947 years). Only 3 out of 20 covariates (Choline-to-N-acetylaspartate and lipids-lactate-to-creatine ratios, and age) contribute significantly to explaining variability in the survival hazards model, score test:  $\chi^2(3) = 9.098$ ,  $p = .028$ .

**Conclusions.** For this data-set MR-spectroscopy metabolites overcome volumetric biomarkers (peritumoral edema and viable tumor) as well as tumor-regions ADC measurements. A consensus about which MR biomarkers should be included in the imaging follow-up is still in need for these tumors.

**Key words:** Biological markers; Glioblastoma; Magnetic Resonance Imaging; Prognosis; Survival Analysis.

## Introduction

There has been a longstanding interest in the identification of prognostic markers for gliomas;(1) supported by the fact they constitute the most common primary brain tumors with a frequency of approximately 38%.(2) Most of them being glioblastoma multiforme (GBM) grade IV, as classified by the World Health Organization (WHO). It has been considered that conventional imaging reveals only the “tip of the iceberg” of each glioma, with a significant portion of the glioma cells already invading peripheral tissue.(3) The biological behavior of gliomas produces microscopic invasion to surrounding tissues, especially white matter (WM) tracts,(4) from the obvious area of disease;(5) as results there is normal appearance white matter (NAWM), where infiltration is not able to be detected using conventional imaging protocols of MR.(6) With this regard, areas of extensive edema surrounding the tumor on T<sub>2</sub>-weighted imaging (T<sub>2</sub>-w) are often assumed to contain tumor cells that have infiltrated into the brain tissue.(7) These factors may affect the survival rate of patients, because even when all radiologically visible portions of a tumor have been excised, the surgical margins may not be "clean," and further neoplastic growth can occur in the adjacent brain, leading from microscopic residual to gross recurrence.(8)

GBM shows a mean patient survival of still only 14 months, despite recent advances in surgery and radiochemotherapy.(9) The mean life expectancy for patients with anaplastic astrocytoma (WHO grade III) is slightly longer, at 41 months.(10) A complete surgical excision of high-grade gliomas (HGGs) (WHO grades III and IV) without tumor recurrence is impossible, due to their biological behavior. Thus, the interdisciplinary therapeutic concept today combines microsurgery followed by fractionated external beam radiation and chemotherapy.(11)

Several studies for predicting the outcome in HGGs patients have been described considering clinical factors as Karnofsky performance scale, tumor localization, tumor size, histopathologic subgroups, extent of resection, radiotherapy and reoperation, molecular and genetic factors; however, many of them have shown conflicting results.(1) Even given the same pathological diagnosis and equivalent treatments, some patients have a relatively favorable outcome, while others have a very poor prognosis.(12) Conventional MR examination for diagnosis of gliomas around the world is usually limited to identify edema boundaries and regional tumor infiltration to those patterns observed in the T<sub>2</sub>-w pre-contrast and T<sub>1</sub>-w post-contrast images;(13, 14) recent studies have proved predictive value of the apparent diffusion coefficient (ADC),(15) the measurement of choline-to-N-acetylaspartate ratio (Cho/NAA) using MR spectroscopy (MRS),(16) and the presence of immediate (<1 cm) and distant edema (>1 cm),(14) in the survival analysis of patients with GBM.

Despite the growing evidence of studies exploring the prognostic ability of magnetic resonance (MR) biomarkers in patients with HGGs, a consensus of the best survival biomarkers is still missing in the literature; we considered necessary to investigate additional evidence of the quantitative MR biomarkers contribution's towards a positive or negative effect on survival in these

group of patients. In this study, we specifically investigated the role of basic demographics of a small group of patients together with conventional MR volumetric measurements, diffusion weighted imaging and MRS as biomarkers able to predict overall survival in patients with HGGs.

## **Material and Methods**

### *Patients*

A cohort of 28 patients with supratentorial HGGs underwent follow-up from December 1999 to January 2012. The group consisted of 19 men and 9 women, with a mean age of 50.4 years (SD: 16.28; range: 13 – 85 y). The patients' postoperative survival times (in years) were retrospectively obtained according to the Oncology Unit tumor register database. Pathologic findings included 11 GBM and 17 anaplastic gliomas. Exclusion criteria were any surgery, radiation therapy, or chemotherapy of a brain tumor before inclusion in the study as well as lack of histopathologic diagnoses, missing imaging data or presence of artifacts. Treatment was not used to exclude patients. Most of the patients were treated under the same protocol; after resection, they received chemotherapy including Temozolomide (Temodal, Schering-Plough, NJ, USA), and radiation therapy (60 Gy), the Stupp protocol. All patients underwent biopsy or surgical resection of the tumor with histopathologic diagnosis based on WHO criteria. A radiologist interpreted the MR images blinded to the patient's history. MRI examinations with other structural abnormalities were excluded. The local Institutional Review Board approved the study (reference number 2011.044).

### *Brain image and data acquisition*

MR was performed by using a 3T unit (Signa HDxt, GE Healthcare, Waukesha, WI, USA) with a high-resolution eight-channel head coil (Invivo, Gainesville, FL, USA). MR sequences included conventional axial T<sub>2</sub>-w, axial Fluid-Attenuated Inversion Recovery (Flair), axial Spoiled Gradient Echo (SPGR), diffusion-weighted imaging (DWI) and axial T<sub>1</sub>-w, using 0.1 mmol/kg of body weight of gadopentetate dimeglumine (Magnevist; Schering, Berlin, Germany). DWI was performed using a single-shot SE EPI sequence with b-values of 1000 s/mm<sup>2</sup> and an image without diffusion weighting with b-value of 0 s/mm<sup>2</sup>. Figure 1 shows the appearance of conventional MRI sequences in a patient with GBM.

Multi-voxel spectroscopic imaging (MV-MRS) was performed using a point-resolved spectroscopic sequence technique (PRESS), the volume of interest (VOI) size was specifically adjusted positioning the voxel over the lesion and trying to minimize partial-volume effects resulting from other neighboring tissues including bones and cerebral spinal fluid (CSF) of the ventricles. Proton spectra were recorded in the axial plane with T<sub>1</sub>-w post-contrast images via TR; 1500 ms, TE; 26 and 144 ms, FOV; 24 × 24 cm, 1-1.5 cm section thickness, 256 × 256 matrix and 24 × 24 phase encoding.

### *Image postprocessing and data analysis*

One radiologist, blind to the clinical history of each patient, manually traced the boundaries of the tumor regions; volumetric calculations were included in the analysis: the T<sub>1</sub>-w post-contrast volume, the T<sub>2</sub>-w pre-contrast volume, the T<sub>1</sub>-w/T<sub>2</sub>-w ratio, the Flair pre-contrast volume, and the Flair/T<sub>1</sub>-w ratio.

For the DWI sequence, the ADC was measured at five tumor regions: viable tumor region (area of enhanced rim at T<sub>1</sub>-w post-contrast); necrosis (considered the cystic cavity); an immediate zone of edema (arbitrarily chosen as a 10-mm-wide band); a distant zone of edema (area adjacent to the immediate zone of edema, chosen also as a 10-mm-wide band) and an area of normal-appearing white matter (NAWM), drawn in the patient's contralateral hemisphere.

For the MRS data, metabolite signal peaks were analyzed and centered within a range of 0-4.35 ppm as follows: methyl protons of N-acetylaspartate (NAA) at 2.0 ppm, N-trimethyl protons of choline-containing metabolites at 3.2 ppm (Cho), creatine (Cr) at 3-3.1 ppm, a compound peak containing lipids and lactate (LL) at 0.8-1.4 ppm, and a compound peak of the protons of myo-inositol (mI) at 3.56 and 4.06 ppm.<sup>(17)</sup> Automatic shimming of the linear x, y, z channels was used to optimize field homogeneity, water resonance and water suppression pulses were optimized. All volumetric and MRS imaging data were analyzed in a GE Advantage Workstation with the software FuncTool 9.4.04b (GE Medical Systems, Milwaukee, WI, USA).

#### *Definition of Survival Time*

For the purpose of this study, the preoperative images acquired at the time of the first operation were considered as the baseline and were used to monitor the evolution of the disease. Overall survival was evaluated from the baseline to death or, for cases that were not followed until death (eg, living patients), from the baseline to the time of last available follow-up.

#### *Statistical analysis*

According to the aims of the study, only 20 variables related with basic demographics and MRI biomarkers were included in the analyses: three related to clinical findings (gender, age, tumor grade); two obtained from the visual inspection of conventional MR imaging (affected side and tumor location), 3 variables from the post-processing of volumetric measurements (T<sub>1</sub>-w post-contrast volume, T<sub>2</sub>-w pre-contrast volume, T<sub>1</sub>-w/T<sub>2</sub>-w ratio, Flair pre-contrast volume, Flair/T<sub>1</sub>-w ratio); 5 variables from ADC measurements at five tumor regions (viable tumor region, necrosis, immediate zone of edema, a distant zone of edema, normal-appearing white matter), and 5 variables from MRS metabolites quantification (NAA/Cr, Cho/Cr, LL/Cr, Cho/Naa, and mI/Cr). Univariate analysis using the Kaplan-Meier method was used for the calculation of median survival time.<sup>(18)</sup> Multivariate analysis was performed using a Cox's proportional hazards model.<sup>(19)</sup> Hazard ratios (HRs) and their adjusted 95% confidence intervals (CIs) were calculated. For all analysis, statistical significance was indicated by a *p-value* < 0.05.

*Software.* All analyses were carried out using the IBM® SPSS® Statistics software (version 22.0.0.0 IBM Corporation; Armonk, NY, USA). *Presentation of data.* General presentation of the manuscript followed the guidelines set by the International Committee of Medical Journal Editors.(20)

## Results

### *General data*

The postoperative follow-up period range was from 3 to 98 months, 17 patients died within the follow-up period. The median survival time was 1.73 years (range, 0.287-8.947 years). The descriptive statistics of the selected variables are summarized in Table I, the survival curve for this cohort is depicted in figure 2.

### *Survival analysis*

We performed a Cox proportional hazards regression analysis to fit a null model containing only an intercept parameter (residual  $\chi^2$  (13) = 22.647,  $p = .046$ ); which allowed us to identify the significant independent prognostic factors of survival time; only three out of 20 available covariates were selected: Cho/Naa ratio ( $p = .017$ ), age ( $p = .072$ ) and lipids-lactate/creatinine ( $p = .109$ ).

A second Cox regression analysis using only the three selected covariates and the complete method (Method = Enter) of regression for age (years) and Cho/Naa and lipids-lactate/creatinine ratios; provided an “Omnibus Test of Model Coefficients” that simultaneously assessed the effects of the parameters in the model. We found that our three covariates contribute significantly to explaining variability in the survival hazards, score test:  $\chi^2$  (3) = 9.098,  $p = .028$ . For this new model, the -2 x Log Likelihood relative to the null model also indicated a significant improvement in the model fit after adding the covariates, LR test:  $\chi^2$  (3) = 14.591,  $p = .002$ . The Wald’s tests calculated the effects of the variables in the model after adjusting for the effects of the remaining ones. At the 5% test level, the three covariates significantly affected the hazard function, table 2.

Cho/Naa ratio was the strongest survival predictor with a log-hazard function of 2.672. This value indicated that, for every additional unit increase in the Cho/Naa ratio, patients increased 2.672 times the hazard function to report a death stage than those who did not have an increase, controlling for all other factors in the model.

The LL/Cr ratio depicted a log-hazard function of 0.584; considering the negative sign of its beta value, this hazard value can be interpreted as a 41.6% reduction in the risk to report a death stage. The age has a positive value with a log-hazard function of 1.062, indicating a 6.2% increase in the risk to report death for every additional year in the patient’s age.

We completed our Cox’s analysis by plotting the *Schoenfeld residuals* to check for proportional hazards;(21) they contain values for subjects with uncensored survival times. For the first two covariates (Cho/Naa and LL/Cr), the Lowess curve varies

around the zero reference line in a nonsystematic way, figures 3 A and B; although after the 3<sup>rd</sup>-4<sup>th</sup> year the smooth line appear to demonstrate a trend over time with a negative slope and thus it had a negative proportional hazard; for both variables, the plots are only based in few events and it is seen; it is largely influenced by the residuals at the first time points. For the covariate age, the fitted line appeared to have a positive line, suggesting that the hazard ratio for this covariate increases over time and thus it has a proportional hazard; figure 3 C.

## Discussion

Survival time for GBM is still approximately 1 year despite all the treatment modalities including surgical resection, radiotherapy and chemotherapy.(1) The median survival time of 1.73 years in this study is explained by the combined analysis of grade III and IV tumors. However, until recently, a 3 year life period for glioblastoma was indicated in 3% of patients and a 5 years life period was indicated in 0%; nowadays, there are documentations of patients surviving 10 years with GBM.(22, 23) To date, the usually selected variables for predicting prognostic subgroups of patients with HGGs patients include age, Karnofsky performance score, tumor localization, tumor size, histopathologic subgroups, extend of resection, adjuvant therapy and reoperation; recent studies tend to evaluate molecular genetics or molecular biology excluding in most cases an integrative assessment of quantitative MR biomarkers in the prognosis such as those from spectroscopy.(24)

Among all the factors studied in our Cox analysis, the Cho/Naa was confirmed as the most significant factor influencing the survival time ( $P < 0.028$ ) through the hazard function; a recent work demonstrated that the signal intensity ratio of Cho to the metabolic marker for neuronal integrity N-acetyl-aspartate (NAA) changed upon antiangiogenic treatment and that these changes may predict the outcome of therapy;(25) our data support a similar study using the same index almost a decade ago but that manuscript did no report on the influence of lipids-lactate-to-creatine ratio;(16) a previous study has reported that MRS findings may precede the perfusion abnormalities and contrast enhancement features in HHGs.(26) It is interesting for our group that, despite the evidence supporting the use of these MR biomarkers there is still not international consensus whether the quantification of MRS metabolites should be mandatory in the imaging evaluation of brain tumors performed at most tertiary-care hospitals; the reality is that spectroscopy, perfusion and diffusion techniques are not used to anticipate tumor progression in a day-to-day basis,(11) then classic T1 and T2 imaging features remain as the criterion standard.(27)

Recent studies has proved a significant association of ADC in subgroups stratification,(15) and in the methylation status of the MGMT promoter in patients with GBM,(24) however these studies missed to complement their analyses including a Cox's regression model; our data showed that the simultaneous assessment of ADC values from several tumor regions were not considered as significant biomarkers using a Cox's regression method.



The association between low levels of lactate and hypoxia in tumor tissue was reported four decades ago,(28) this evidence is relevant because under hypoxic conditions an hypoxia inducible factor, up-regulates genes encoding vascular endothelial growth factor that participates in infiltration of tumor cells and angiogenesis.(29) In patients with HGGs, it has been observed a higher lipid and lactate levels measured by MRS associated with significantly worse overall survival.(30) Then, our finding that low levels of lipids-lactate/Cr ratio represents up to a 41.6% reduction in the risk of death is a reverse statement that increased levels of tumor hypoxia have been associated with worse clinical outcomes.(31)

The age at the time of diagnosis has been considered one of the most important prognostic factors.(32) Survival time is significantly longer in younger patients,(33) with a clear correlation between increasing age and decreasing overall survival; our findings supported this knowledge with a 6% increase in the risk of death per year of age.

Although the gender was not significant, we found a male dominance (67.8%), which is in agreement with most of the studies about incidence for glial malign tumors in the literature.(34)

The assessment of quantitative MR imaging biomarkers is becoming standard in tumor patients, but a real understanding of the significant effects of the several MR modalities is still in its early days. Several reports have reported that localization of tumor may effect patient's survival time,(34, 35) other multivariate analyses found that the location of the tumor may have better prognosis but its effect size is not enough to define this feature as an independent factor;(1, 36) in our analysis there was no significant effect between the location of the tumor and the survival.

We evaluated the effect of peritumoral edema through measurements of 3D volumes in T<sub>2</sub>-w and Flair sequences; although an association has been observed with a significantly shorter survival time in many studies,(36) we did not find significant influence for our data set.

Some limitations in this study need to be addressed: the data were obtained and analyzed retrospectively, so a control group was not available, although the study answers the questions posed at the introduction (which MRI biomarkers has a significant association with the survival in patients with HGGs), several clinical and surgical variables were intentionally out of the scope of this study (extent of resection, radiation dose and adjuvant chemotherapy), as we want to report the significance of MR biomarkers without the influence of other clinical/surgical/radiotherapy variables. The metabolism of phospholipid cell membrane turnover is associated to several metabolites such as glycerophosphocholine, phosphocholine, and phosphoethanolamine each one playing major roles as indicators for tumor growth; its discrimination however, can not be performed using the conventional (1) H MRS, it requires specialized hardware with (31) P MRS.(37) Then, the research on MR biomarkers still needs further investigation with larger patient population to determine the robustness of the selected variables in predicting survival and to increase understanding of the morphologic and functional characteristics of brain tumors, also to

promote generalizability of the results.

In conclusion for these data, a higher preoperative Cho/Naa ratio, a lower Lipids-lactate/Creatine ratio and the years of age, are significant predictors of survival that overcome the classic T<sub>2</sub>-w and T<sub>1</sub>-w post gadolinium volumetric standards (representatives of peritumoral edema and viable tumor respectively) and the ADC measurements (diffusibility of water). Considering MRS is able to detect the conversion of normal tissue to tumor infiltration before conventional MR sequences show conspicuous findings, and its acquisition do not require contrast; MRI units around the world might adapt the post-processing methods of MRS to their own contexts in order to validate data about implementation and outcomes that can be generalisable beyond one setting. Due to the large number of variables (qualitative and quantitative) to which a radiologist is exposed during an advanced imaging evaluation of brain tumors, the use of multivariate assessment combined not only with Kaplan-Meir but also with Cox's regression methods is a strong consideration in the diagnosis and follow-up of these patients.

**Acknowledgments**

This article was supported in part by Medica Sur Clinic & Foundation. The authors thank Dr. Sebastian Castillo-Rodriguez, Department of Radiology at Medica Sur Clinic & Foundation, for imaging postprocessing support.

## References

1. Tugcu B, Postalci LS, Gunaldi O, Tanriverdi O, Akdemir H. Efficacy of clinical prognostic factors on survival in patients with glioblastoma. *Turkish neurosurgery*. 2010 Apr;20(2):117-25. PubMed PMID: 20401838.
2. Kleihues P, Louis DN, Scheithauer BW, Rorke LB, Reifenberger G, Burger PC, et al. The WHO classification of tumors of the nervous system. *Journal of neuropathology and experimental neurology*. 2002 Mar;61(3):215-25; discussion 26-9. PubMed PMID: 11895036.
3. Wang CH, Rockhill JK, Mrugala M, Peacock DL, Lai A, Jusenius K, et al. Prognostic significance of growth kinetics in newly diagnosed glioblastomas revealed by combining serial imaging with a novel biomathematical model. *Cancer research*. 2009 Dec 1;69(23):9133-40. PubMed PMID: 19934335. Pubmed Central PMCID: 3467150.
4. Johnson PC, Hunt SJ, Drayer BP. Human cerebral gliomas: correlation of postmortem MR imaging and neuropathologic findings. *Radiology*. 1989 Jan;170(1 Pt 1):211-7. PubMed PMID: 2535765. Epub 1989/01/01. eng.
5. DeAngelis LM. Brain tumors. *The New England journal of medicine*. 2001 Jan 11;344(2):114-23. PubMed PMID: 11150363. Epub 2001/01/11. eng.
6. Watanabe M, Tanaka R, Takeda N. Magnetic resonance imaging and histopathology of cerebral gliomas. *Neuroradiology*. 1992;34(6):463-9. PubMed PMID: 1436452. Epub 1992/01/01. eng.
7. Kelly PJ, Dumas-Duport C, Kispert DB, Kall BA, Scheithauer BW, Illig JJ. Imaging-based stereotaxic serial biopsies in untreated intracranial glial neoplasms. *Journal of neurosurgery*. 1987 Jun;66(6):865-74. PubMed PMID: 3033172. Epub 1987/06/01. eng.
8. Zimmerman RA. Imaging of adult central nervous system primary malignant gliomas. Staging and follow-up. *Cancer*. 1991 Feb 15;67(4 Suppl):1278-83. PubMed PMID: 1991289. Epub 1991/02/15. eng.
9. Yaneva MP, Semerdjieva ML, Radev LR, Vlaikova MI. Postoperative chemo-radiotherapy with temodal in patients with glioblastoma multiforme--survival rates and prognostic factors. *Folia Med (Plovdiv)*. 2010 Jan-Mar;52(1):26-33. PubMed PMID: 20380284. Epub 2010/04/13. eng.
10. Keles GE, Chang EF, Lamborn KR, Tihan T, Chang CJ, Chang SM, et al. Volumetric extent of resection and residual contrast enhancement on initial surgery as predictors of outcome in adult patients with hemispheric anaplastic astrocytoma. *Journal of neurosurgery*. 2006 Jul;105(1):34-40. PubMed PMID: 16871879.

11. Kuhnt D, Becker A, Ganslandt O, Bauer M, Buchfelder M, Nimsky C. Correlation of the extent of tumor volume resection and patient survival in surgery of glioblastoma multiforme with high-field intraoperative MRI guidance. *Neuro-oncology*. 2011 Dec;13(12):1339-48. PubMed PMID: 21914639. Pubmed Central PMCID: 3223093.
12. Ron IG, Gal O, Vishne TH, Kovner F. Long-term follow-up in managing anaplastic astrocytoma by multimodality approach with surgery followed by postoperative radiotherapy and PCV-chemotherapy: phase II trial. *American journal of clinical oncology*. 2002 Jun;25(3):296-302. PubMed PMID: 12040293.
13. Seidel C, Dorner N, Osswald M, Wick A, Platten M, Bendszus M, et al. Does age matter? - A MRI study on peritumoral edema in newly diagnosed primary glioblastoma. *BMC cancer*. 2011;11:127. PubMed PMID: 21481277. Pubmed Central PMCID: 3094323. Epub 2011/04/13. eng.
14. Schoenegger K, Oberndorfer S, Wuschitz B, Struhal W, Hainfellner J, Prayer D, et al. Peritumoral edema on MRI at initial diagnosis: an independent prognostic factor for glioblastoma? *European journal of neurology : the official journal of the European Federation of Neurological Societies*. 2009 Jul;16(7):874-8. PubMed PMID: 19473360. Epub 2009/05/29. eng.
15. Ellingson BM, Cloughesy TF, Lai A, Mischel PS, Nghiemphu PL, Lalezari S, et al. Graded functional diffusion map-defined characteristics of apparent diffusion coefficients predict overall survival in recurrent glioblastoma treated with bevacizumab. *Neuro-oncology*. 2011 Oct;13(10):1151-61. PubMed PMID: 21856685. Pubmed Central PMCID: 3177656.
16. Oh J, Henry RG, Pirzkall A, Lu Y, Li X, Catalaa I, et al. Survival analysis in patients with glioblastoma multiforme: predictive value of choline-to-N-acetylaspartate index, apparent diffusion coefficient, and relative cerebral blood volume. *Journal of magnetic resonance imaging : JMRI*. 2004 May;19(5):546-54. PubMed PMID: 15112303.
17. Brandao LA, Domingues RC. Brain metabolites and their significance in spectral analysis. In: Brandao LA, Domingues RC, editors. *MR Spectroscopy of the Brain*. Philadelphia, PA: Lippincott Williams & Wilkins; 2004. p. 11-2.
18. Stel VS, Dekker FW, Tripepi G, Zoccali C, Jager KJ. Survival analysis I: the Kaplan-Meier method. *Nephron Clinical practice*. 2011;119(1):c83-8. PubMed PMID: 21677442.
19. Stel VS, Dekker FW, Tripepi G, Zoccali C, Jager KJ. Survival analysis II: Cox regression. *Nephron Clinical practice*. 2011;119(3):c255-60. PubMed PMID: 21921637.
20. Uniform requirements for manuscripts submitted to biomedical journals: Writing and editing for biomedical publication. *Journal of pharmacology & pharmacotherapeutics*. 2010 Jan;1(1):42-58. PubMed PMID: 21808590. Pubmed Central PMCID: 3142758.
21. Schoenfeld DA. Partial residuals for the proportional hazards regression model. *Biometrika*. 1982;39:499-503.

22. Shinojima N, Kochi M, Hamada J, Nakamura H, Yano S, Makino K, et al. The influence of sex and the presence of giant cells on postoperative long-term survival in adult patients with supratentorial glioblastoma multiforme. *Journal of neurosurgery*. 2004 Aug;101(2):219-26. PubMed PMID: 15309911.
23. Salvati M, Cervoni L, Artico M, Caruso R, Gagliardi FM. Long-term survival in patients with supratentorial glioblastoma. *Journal of neuro-oncology*. 1998 Jan;36(1):61-4. PubMed PMID: 9525826.
24. Romano A, Calabria LF, Tavanti F, Minniti G, Rossi-Espagnet MC, Coppola V, et al. Apparent diffusion coefficient obtained by magnetic resonance imaging as a prognostic marker in glioblastomas: correlation with MGMT promoter methylation status. *European radiology*. 2013 Feb;23(2):513-20. PubMed PMID: 22875158.
25. Kim H, Catana C, Ratai EM, Andronesi OC, Jennings DL, Batchelor TT, et al. Serial magnetic resonance spectroscopy reveals a direct metabolic effect of cediranib in glioblastoma. *Cancer research*. 2011 Jun 1;71(11):3745-52. PubMed PMID: 21507932. Pubmed Central PMCID: 3107375.
26. Law M, Yang S, Wang H, Babb JS, Johnson G, Cha S, et al. Glioma grading: sensitivity, specificity, and predictive values of perfusion MR imaging and proton MR spectroscopic imaging compared with conventional MR imaging. *AJNR American journal of neuroradiology*. 2003 Nov-Dec;24(10):1989-98. PubMed PMID: 14625221. Epub 2003/11/20. eng.
27. Leimgruber A, Ostermann S, Yeon EJ, Buff E, Maeder PP, Stupp R, et al. Perfusion and diffusion MRI of glioblastoma progression in a four-year prospective temozolomide clinical trial. *International journal of radiation oncology, biology, physics*. 2006 Mar 1;64(3):869-75. PubMed PMID: 16226399.
28. Allen N. Oxidative metabolism of brain tumors. *Progress in experimental tumor research*. 1972;17:192-209. PubMed PMID: 4344743.
29. Zagzag D, Friedlander DR, Margolis B, Grumet M, Semenza GL, Zhong H, et al. Molecular events implicated in brain tumor angiogenesis and invasion. *Pediatric neurosurgery*. 2000 Jul;33(1):49-55. PubMed PMID: 11025423.
30. Li Y, Lupo JM, Parvataneni R, Lamborn KR, Cha S, Chang SM, et al. Survival analysis in patients with newly diagnosed glioblastoma using pre- and postradiotherapy MR spectroscopic imaging. *Neuro-oncology*. 2013 May;15(5):607-17. PubMed PMID: 23393206. Pubmed Central PMCID: 3635514.
31. Lim KS, Lim KJ, Price AC, Orr BA, Eberhart CG, Bar EE. Inhibition of monocarboxylate transporter-4 depletes stem-like glioblastoma cells and inhibits HIF transcriptional response in a lactate-independent manner. *Oncogene*. 2013 Sep 30. PubMed PMID: 24077291.

32. Jeremic B, Milicic B, Grujicic D, Dagovic A, Aleksandrovic J, Nikolic N. Clinical prognostic factors in patients with malignant glioma treated with combined modality approach. *American journal of clinical oncology*. 2004 Apr;27(2):195-204. PubMed PMID: 15057161.
33. Teo M, Martin S, Owusu-Agyemang K, Nowicki S, Clark B, Mackinnon M, et al. A survival analysis of GBM patients in the West of Scotland pre- and post-introduction of the Stupp regime. *British journal of neurosurgery*. 2013 Oct 10. PubMed PMID: 24111708.
34. Gorlia T, van den Bent MJ, Hegi ME, Mirimanoff RO, Weller M, Cairncross JG, et al. Nomograms for predicting survival of patients with newly diagnosed glioblastoma: prognostic factor analysis of EORTC and NCIC trial 26981-22981/CE.3. *The lancet oncology*. 2008 Jan;9(1):29-38. PubMed PMID: 18082451.
35. Lamborn KR, Chang SM, Prados MD. Prognostic factors for survival of patients with glioblastoma: recursive partitioning analysis. *Neuro-oncology*. 2004 Jul;6(3):227-35. PubMed PMID: 15279715. Pubmed Central PMCID: 1871999.
36. Lacroix M, Abi-Said D, Fourney DR, Gokaslan ZL, Shi W, DeMonte F, et al. A multivariate analysis of 416 patients with glioblastoma multiforme: prognosis, extent of resection, and survival. *Journal of neurosurgery*. 2001 Aug;95(2):190-8. PubMed PMID: 11780887.
37. Hattingen E, Bahr O, Rieger J, Blasel S, Steinbach J, Pilatus U. Phospholipid metabolites in recurrent glioblastoma: in vivo markers detect different tumor phenotypes before and under antiangiogenic therapy. *PloS one*. 2013;8(3):e56439. PubMed PMID: 23520454. Pubmed Central PMCID: 3592858.

## Tables

Table 1. Descriptive statistics of the selected variables.

Categorical variables	Number	Percent
Gender		
Male	19	67.9%
Female	9	32.1%
Tumor Grade		
III	11	39.3%
IV	17	60.7%
Cerebral Hemisphere		
Left	13	52%
Right	8	32%
Both	4	16%
Tumor location		
Zone I	10	35.7%
Zone II	3	10.7%
Zone III	12	42.9%
Zone IV	3	10.7%
Continuous variables	Mean	Std. Deviation
Age (years)	50.54	16.283
ADC Tumor (mm <sup>2</sup> /s)	.001310	.000391
ADC Necrosis (mm <sup>2</sup> /s)	.002290	.000927
ADC Proximal Edema (mm <sup>2</sup> /s)	.001294	.000460
ADC Distal Edema (mm <sup>2</sup> /s)	.001323	.000283
ADC Normal Tissue (mm <sup>2</sup> /s)	.000885	.000200
Naa/Cr	.874	.637
Cho/Cr	2.353	1.190
Lipids-Lactate/Cr	3.806	3.204



mI/Cr	1.572	1.272
Cho/Naa	3.613	2.033
Post-contrast T1 volume (cm <sup>3</sup> )	24.047	29.551
Pre-contrast T2 volume (cm <sup>3</sup> )	74.948	46.699
T1/T2 volume ratio	.337	.316
Flair volume (cm <sup>3</sup> )	79.031	44.647
T1/Flair volume ratio	.298	.270

---

Table 2. Wald's tests assessing the covariates effects on the hazard function.

	B	SE	$\chi^2$ (Wald test)	df	p-value	Log-hazard functions	95.0% CI	
							Lower	Upper
Cho/Naa ratio	.983	.448	4.821	1	.028	2.672	1.111	6.423
LL/Cr ratio	-.538	.268	4.039	1	.044	.584	.345	.987
Age (years)	.060	.034	3.059	1	.080	1.062	.993	1.136

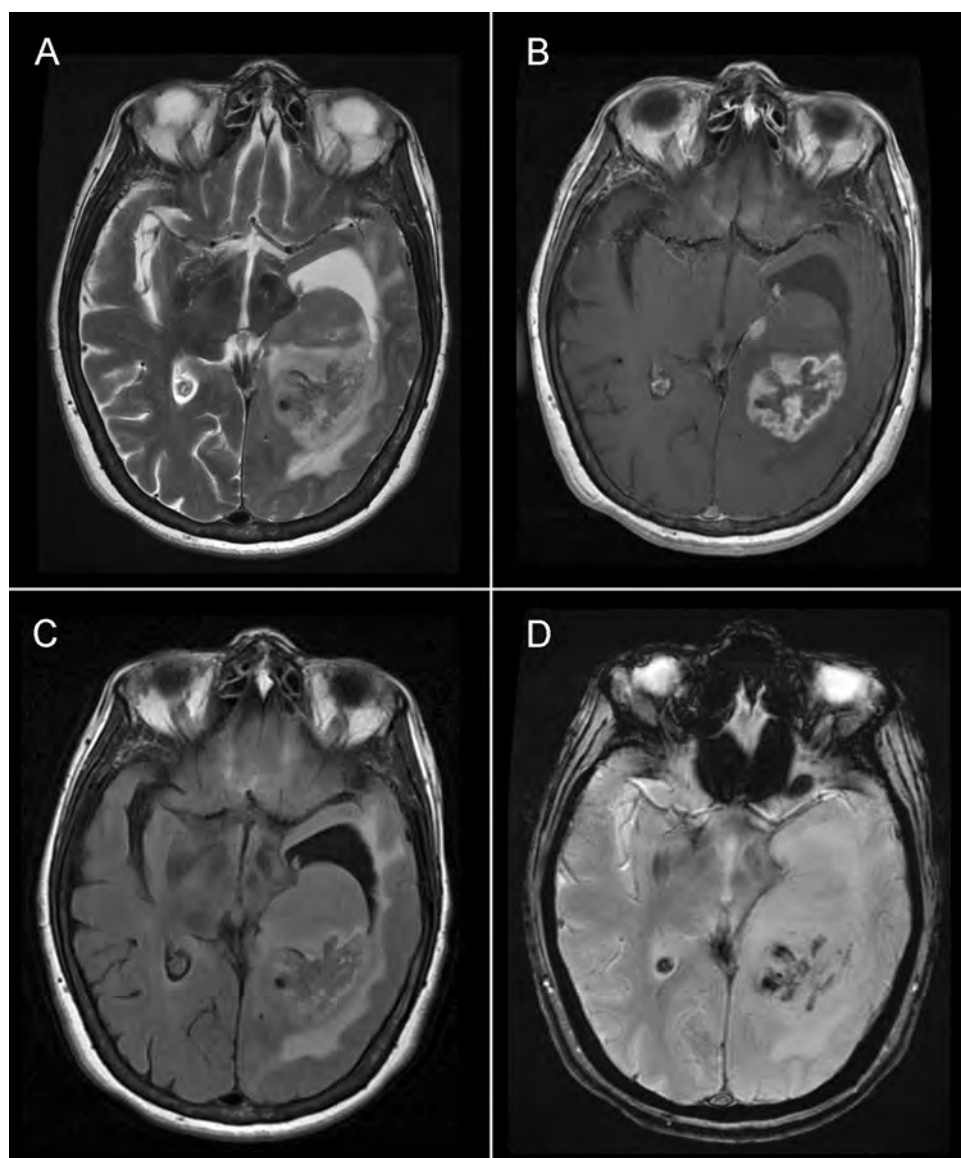
**Figure legends**

Figure 1. Conventional MRI sequences in a patient with GBM, axial-plane images in: A, T<sub>2</sub>-w; B, post gadolinium T<sub>1</sub>-w; C, Flair; D, gradient echo.

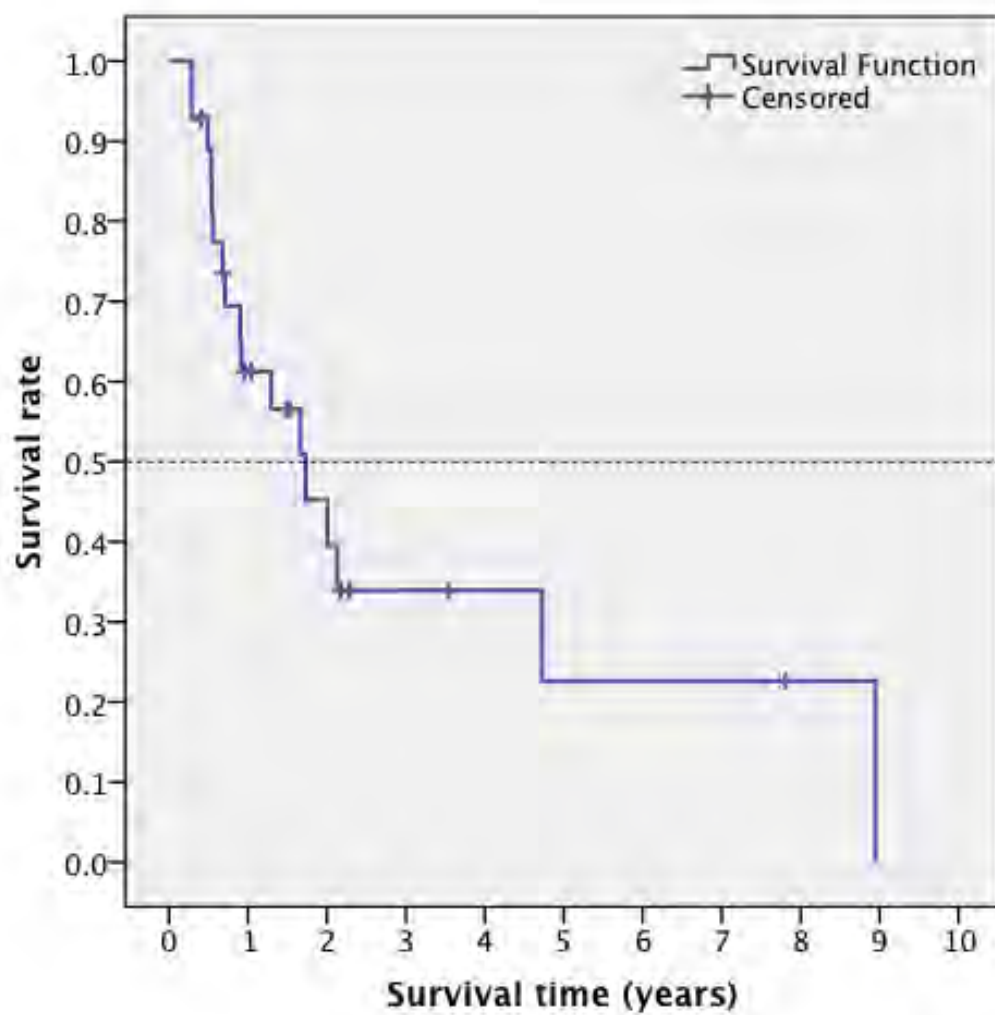


Figure 2. Survival curve of patients with high-grade gliomas.

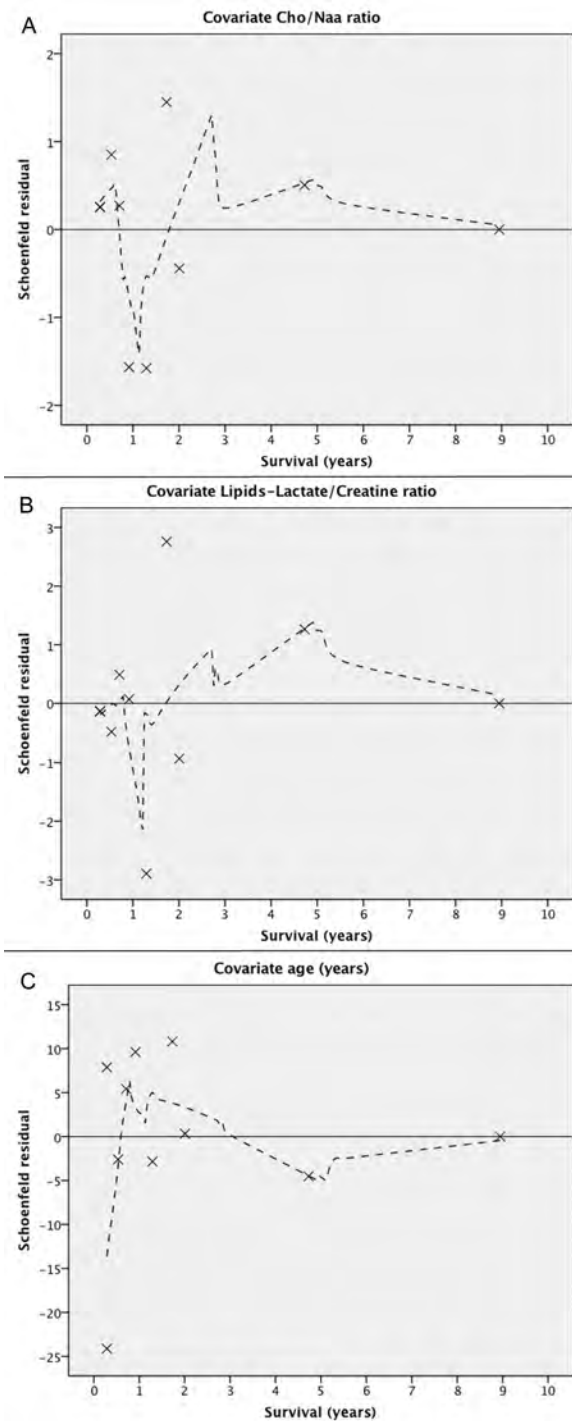


Figure 3. Schoenfeld residual plots for the selected covariates in the Cox regression model for survival in HGGs. A, Cho/Naa ratio and B, Lipids-lactate/Creatine ratio; in both plots the Lowess curve varies around the zero reference line in a nonsystematic way; after the 3<sup>rd</sup>-4<sup>th</sup> year the smooth line appear to demonstrate a trend over time with a negative slope and thus that it had a negative proportional hazard. C, plot of the Age (years); the fitted line appeared to have a positive line, suggesting that the hazard ratio for this covariate increases over time and thus it has a proportional hazard.

Elsevier Editorial System(tm) for Magnetic Resonance Imaging  
Manuscript Draft

Manuscript Number: MRI-D-13-00227

Title: Correlates and interactions among global DTI-derived metrics, gender and age: a pilot study in healthy and glioblastoma multiforme brains.

Article Type: Original Contribution

Keywords: Brain neoplasms; Diffusion Tensor Imaging; Magnetic Resonance Imaging; Statistics as Topic; Software Tools.

Corresponding Author: Dr. Ernesto Roldan-Valadez, M.D., M.Sc.

Corresponding Author's Institution: Medica Sur Clinic & Foundation

First Author: Ernesto Roldan-Valadez, M.D., M.Sc.

Order of Authors: Ernesto Roldan-Valadez, M.D., M.Sc.; Camilo Rios, Ph.D.; David Cortez-Conradis, M.Sc.; Sergio Moreno-Jimenez, M.D., Ph.D.

## Abstract

**Purpose.** Although some relationships among DTI-derived tensor metrics in healthy brains and brains with GBM (glioblastoma multiforme) have been reported in the last decade, they are still not completely understood.

**Subjects and methods.** Case-control study performed on brain MRI data by using DTI sequence with 25 directions. Image postprocessing using the FSL software allowed the calculation of eleven tensor metrics: mean diffusivity, fractional anisotropy, pure isotropic diffusion, pure anisotropic diffusion, the total magnitude of the diffusion tensor, linear tensor, planar tensor, spherical tensor, relative anisotropy axial and radial diffusivity. Partial correlation analyses and multivariate Mancova controlling the effect of age and gender were performed.

**Results.** 27 patients with GBM (mean, SD;  $48.41 \pm 15.18$  years; range, 18–78 years) and 34 controls (Mean, 41.47; SD,  $\pm 21.94$  years; range, 21-80 years) were included. From 56 comparisons among bivariate correlations, only seven were significantly different between groups. There was a main effect of diagnosis: F-value (11, 23) = 11.842,  $p = < .001$ , with a large effect size (partial eta squared = .850); a similar result was obtained for age.

**Conclusion.** DTI-derived metrics depict significant differences between healthy brains and brains with GBM, with specific magnitudes and correlations. This study makes a contribution to decrease the underlying empiricism about these novel biomarkers of brain impairment.

**Key words:** Brain neoplasms; Diffusion Tensor Imaging; Magnetic Resonance Imaging; Statistics as Topic; Software Tools.

## Introduction

Quantitative magnetic resonance (MR) techniques assessing the impairment of intraaxial brain tumors have been accepted in the diagnosis and follow-up, as it may complement the management of the surgical neuro-oncology team aimed to conserve vital cerebral tissue while maximizing tumor resection.(1, 2) A caveat should be raised in the pathologic and regional MR imaging evaluations of astrocytomas grades II to IV, as evidence suggest these tumors would benefit from the use of a *global* measurement of brain impairment: they frequently contains multiple areas of variable histologic features, conditioning that sampling error in a biopsy may mean that the degree of malignancy seen by the neuropathologist may not reflect the degree of malignancy present elsewhere in the tumor, which may result in significant undergrading of some lesions.(3)

The rising interest in the imaging evaluation of brain tumors using of diffusion tensor imaging (DTI)-derived metrics measurements has showed their clinical applicability in a tumor-region assessment (cystic cavity, enhancing rim, edema, normal-appearing white matter).(4-6) Almost a dozen of combinations of the terms of the diagonalized diffusion tensor, that is, the eigenvalues  $\lambda_1$ ,  $\lambda_2$ , and  $\lambda_3$ , have been reported with several scalar measures of diffusion, such as mean diffusivity (MD), fractional anisotropy (FA), pure isotropic diffusion (p), pure anisotropic diffusion (q), the total magnitude of the diffusion tensor (L), linear tensor (Cl), planar tensor (Cp), spherical tensor (Cs), relative anisotropy (RA); and axial (AD) and radial diffusivity (RD).(4, 5, 7-9) However, to best of our knowledge, there is currently neither a clear understanding of the expected measurements among these variables in each tissue, nor consensus about which tensor metrics might be useful in the evaluation of brain tumors.

In this study we aimed to (1) determine the normal limits (magnitudes) of previously reported DTI-derived tensor metrics in healthy brains and brains of patients with glioblastoma multiforme (GBM) by using a *global* approach, that is, a single measure of the whole brain for each metric; (2) evince the



statistical significance of the mean differences between these groups of subjects; and (3) to analyze the DTI-metrics correlates considering the influence of clinical diagnosis.

## **Materials and methods**

### *Subjects*

Case-control study design; inclusion criteria considered preoperative brain MR examinations between January 2010 and September 2012 of patients with at first (suspected) diagnosis and later pathology confirmation of astrocytoma grade IV, GBM according to the WHO. Exclusion criteria applied to corticosteroid or antibiotic treatment, lesions with areas related to calcification and/or haemorrhage and previous brain surgery. A control group included young and elderly healthy volunteers recruited among the enrolled interns and medical residents of the hospital as well as elderly subjects from our Geriatric unit. All volunteers received detailed health examinations; exclusion criteria considered major neurological, psychiatric, or cardiovascular diseases. A radiologist interpreted the MR images blinded to the patient's history. MR examinations with other structural abnormalities were excluded. The local Institutional Review Boards approved the study (Project #2011.044).

### *Brain image acquisition*

MR sequences included conventional axial T2-weighted imaging, axial Fluid-Attenuated Inversion Recovery (FLAIR), axial Spoiled Gradient Echo (SPGR), DWI and axial T1-weighted imaging, using 0.1 mmol/kg of body weight of gadopentetate dimeglumine (Magnevist; Schering, Berlin, Germany); healthy volunteers did not received endogenous contrast. DTI was performed using a single-shot SE EPI sequence. Diffusion gradients were applied in 25 directions with b-values of 1000 s/mm<sup>2</sup> and an image without diffusion weighting with b-value of 0 s/mm<sup>2</sup>. DTI sequences were acquired in the axial plane with 44 contiguous sections, 2.4 mm section thickness, no intersection gap, TR/TE of 17,000/80 ms, with parallel imaging to reduce off-resonance artifacts (PI factor was 2); 25 x 25 cm FOV, and 128 x 128

matrix size. MR was performed on a single occasion by using a 3T unit (Signa HDxt, GE Healthcare, Waukesha, WI, USA); and a high-resolution eight-channel head coil (Invivo, Gainesville, FL, USA).

#### *Image postprocessing and data analysis*

We use the software *dcm2nii* (10) and the FMRIB Software Library (FSL) v. 4.1.9;(11) extraction of DTI images used the *Brain Extraction Tool (BET)* v. 2.1.(12) Eddy currents were corrected using the *FMRIB's Diffusion Toolbox v. 2.0*; the *Reconstruct Diffusion Tensor (DTIFIT)* and the *fslmaths tool* generated the eigenvector and eigenvalue maps for each tensor metric. The *fslstats tool* calculated the scalar measures (mean values) of each whole-brain biomarker. By using the major ( $\lambda_1$ ), intermediate ( $\lambda_2$ ), and minor ( $\lambda_3$ ) eigenvalues it is possible to calculate a single global measure for each selected tensor metrics;(13), table 1 shows the tensor-metric formulas.

#### *Statistical analysis*

*Sample size.* The adequacy of the sample size to expect validity from our results was based on two considerations: First, we defined the phase of our research, as a Phase I, “exploratory phase”, according to Zhou et al;(14) in which new method is first evaluated in a clinical setting to determine whether the test discriminates between diseased from nondiseased patients. Second, by matching this phase with the summarized list of computed sample sizes needed for an exploratory retrospective study reported by Obuchowski et al.,(15) at least 10 diseased patients and 10 control patients are required to keep statistical validation considering the type I error rate is set at 0.05 and type II error rate is  $\leq 0.10$ , and power  $\geq 0.90$ . Additionally, our sample size allowed us to run a Manova analysis to investigate whether any mean differences between the healthy brains and brains of patients with GBM on the combination of dependent variables were likely to have occurred by chance. According to Pallant,(16) the absolute minimum of cases to have in each cell must equal at least the number of dependent variables, in our study, we had twenty-two cells (two levels of our independent variable: healthy brains/brains with GBM, and eleven dependent variables for each). The study was run in 34 controls and 27 patients; this size also follow the

recommendation of Tabachnik and Fidell,(17) for whom a sample size of at least 20 in each cell should ensure „robustness“ in the results. Assumptions testing assessed the normality of the distribution of the DTI-derived scores by using the Kolmogorov–Smirnov’s and Shapiro-Wilk normality tests;(18) outliers; multivariate normality; linearity; multicollinearity and singularity and the homogeneity of variance-covariance matrices.(16)

*Partial correlation analysis*, the Pearson’s correlation coefficient described the degree of linear relationship between each pair of variables. Considering the age range and the gender of the subjects in our study, we wanted to determine the correlations among tensor metrics *without the effect of age and gender*, so, a *partial correlation analysis* controlling these variables was carried out for each group (healthy brains and brains with GBM). The strength of the linear relationship corresponding to each correlation coefficient value was interpreted as *Very strong* (at least of 0.8), *Moderately strong* (0.6 up to 0.8), *Fair* (0.3 up to 0.6) and *Poor* (less than 0.3). Squaring r-values represented the *coefficient of determination*, the proportion of variance that each two compared variables had in common.(19) The statistical significance of the difference between r coefficients from both groups was tested converting each pair of r values into a standard z scores, then using the formula proposed by Pallant and colleagues (20):

$$Z_{obs} = \frac{Z_1 - Z_2}{\sqrt{\frac{1}{N_1 - 3} + \frac{1}{N_2 - 3}}}$$

Observed Z value  $\leq -1.96$  or  $\geq 1.96$  were considered statistically significantly different.

A two-way between-groups *multivariate analysis of covariance* (Mancova) was performed to investigate diagnosis and gender differences in tensor metrics measurements.(21) The eleven tensor-metrics represented the dependent variables used; independent variables were the diagnosis and gender; age was used as a covariate to control for individual differences. The *effect size* was obtained using the Eta squared

value.(22) It considered .01 as a small effect, .06 as a medium effect and .14 as a large effect.(23) Statistical significance was indicated by a *p-value* < 0.05.

*Software.* All analyses were carried out using the IBM® SPSS® Statistics software (version 21.0.0.0 IBM Corporation; Armonk, NY). General presentation of the manuscript followed the guidelines set by the International Committee of Medical Journal Editors.(24)

## **Results**

### *Demographic data and quantitative DTI tensor maps*

The study was conducted in 61 subjects; 27 patients: 13 females (mean age  $50.0 \pm 15.4$  years, range 31-73 years) and 14 males (mean age  $46.93 \pm 15.4$  years, range 18-78 years); and 34 controls: 26 females (mean age  $41.04 \pm 22.3$  years, range 21-80 years) and 8 males (mean age  $42.88 \pm 21.89$  years, range 24-72 years). All tensor maps could be generated using the FSL software, which added up 671 tensor-metrics measurements included in the analysis. Figure 1 shows an example of some of the MR sequences and tensor-metric maps used in the data analyses.

### *Normality tests, magnitudes of means and SD*

There was a normal distribution for all metrics (requisite for the Pearson's correlation analyses). We counted the number of decimal places to the right of the decimal point (to understand the corresponding magnitudes of each DTI biomarker); five tensor metrics reported mean values within the tenths place: Cs, FA, RA, Cp and Cl; none tensor measurement fell in the hundredths place; five tensors values fell in the thousandths place: L, p, AD, MD and RD; and one tensor metrics had values in the ten thousandths place: q. Table 2 shows the means and SD ordered by descending means.

### *Partial correlation analyses*

A scatterplot for each group showed no serious violation of the assumptions of linearity, homoscedasticity, and outliers (Fig 2). In healthy brains, significant very strong bivariate correlations

were observed for:  $Cs \leftrightarrow RA$  (-),  $Cs \leftrightarrow Cp$  (-),  $Cs \leftrightarrow L$  (-),  $RA \leftrightarrow Cp$  (+),  $RA \leftrightarrow Cl$  (+),  $Cp \leftrightarrow Cl$  (+),  $L \leftrightarrow p$  (+),  $L \leftrightarrow AD$  (+),  $L \leftrightarrow MD$  (+),  $L \leftrightarrow RD$  (+),  $p \leftrightarrow MD$  (+),  $p \leftrightarrow RD$  (+) and  $MD \leftrightarrow RD$  (+); and moderately strong significant correlations were calculated for:  $FA \leftrightarrow q$  (+),  $p \leftrightarrow AD$  (+),  $AD \leftrightarrow MD$  (+) and  $AD \leftrightarrow RD$  (+).

In brains with GBM, the corresponding significant very strong bivariate correlations included:  $Cs \leftrightarrow RA$  (-),  $Cs \leftrightarrow Cp$  (-),  $Cs \leftrightarrow L$  (-),  $FA \leftrightarrow Cl$  (+),  $FA \leftrightarrow q$  (+),  $RA \leftrightarrow Cp$  (+),  $RA \leftrightarrow Cl$  (+),  $Cp \leftrightarrow Cl$  (+),  $L \leftrightarrow p$  (+),  $L \leftrightarrow AD$  (+),  $L \leftrightarrow MD$  (+),  $p \leftrightarrow AD$  (+),  $p \leftrightarrow MD$  (+),  $p \leftrightarrow RD$  (+),  $AD \leftrightarrow MD$  (+), and  $MD \leftrightarrow RD$  (+); the moderately strong significant correlations were observed in:  $Cl \leftrightarrow q$  (+),  $AD \leftrightarrow RD$  (+) and  $AD \leftrightarrow q$  (+). Tables 2 and 3 present the means, SD, and correlations among the global tensor-metrics (controlled for the effect of age and gender).

From the 55 pairs of bivariate correlations in each a group, statistical significances of the difference between  $r$  coefficients were observed in only seven pairs of variables:  $Cs \leftrightarrow Cp$ ,  $FA \leftrightarrow Cl$ ,  $FA \leftrightarrow q$ ,  $RA \leftrightarrow q$ ,  $Cl \leftrightarrow q$ ,  $L \leftrightarrow p$  and  $L \leftrightarrow MD$ .

#### *Mancova analysis*

After adjusting for age, there was not interaction effect between the gender and clinical diagnosis  $F(11, 23) = 1.115$ ,  $p = .394$ . There was not main affect of gender  $F(11, 23) = 2.060$ ,  $p = .069$ ; however, the main effect of diagnosis was statistically significant  $F(11, 23) = 11.842$ ,  $p < .001$ , with a large effect size (partial eta squared = .850). The age also had a significant influence as a covariate  $F(11, 23) = 10.523$ ,  $p < .001$ , with a large effect size (partial eta squared = .834). Table 4 and figure 3 depict the estimated marginal means; the age was controlled at the value of 43.92 years.

## **Discussion**

DTI uses three eigenvectors and three eigenvalues to represent the main diffusion directions and magnitudes, respectively, of the molecular motion of water in a three dimensional space;(25) with this information, DTI produces neural tract images instead of using this data solely for the purpose of

assigning contrast or colors to pixels in a cross sectional image. The principal eigenvector is assumed to correspond to the main axis of diffusion and, therefore, the axis of the white matter tract.(26) Although early publications on this topic, used to measure only two DTI metrics, FA and MD as accepted biomarkers of brain impairment, recent protocols have included almost a dozen of DTI- metrics in their analyses;(6) the caveat of using several biomarkers to characterize brain pathology in clinical applications is that, it is still not completely understood a priori which are the magnitudes and associations among these measurements to quantify pathological changes in brain tissue.(7) MD is understood as a synonym of the coefficient of diffusion in different space guidelines.(27) FA measures the directionality of molecular motion in the brain,(28) it is a quantitative index for diffusion anisotropy that correlates with microstructural integrity of myelinated fiber tracts.(29)

We believe the clinical relevance of this study has several components: first, the importance to understand these metrics is supported by several studies in the MR-DTI literature: Cs, Cp, Cl, FA and MD, have been related with brain abscesses, GBM and brain metastasis;(4) p, q and L measurements have been previously applied to the evaluation of GBM and brain metastasis;(5, 30) AD has been reported in encephalomyelitis of the spinal cord,(31) AD and RD have been correlated with brain development,(32) infantile spasm,(33) amyotrophic lateral sclerosis,(34) schizophrenia,(35) and brain tumors;(36) with only one recent study integrating a tumor-region diagnostic evaluation of 11 DTI-metrics.(6) Interestingly, the way researchers report their findings in most of these studies, is by presenting the correlates among these metrics, that is, the increase/decrease in values of one variable, compared with those of others; more complex multivariate evaluation like Mancova analysis is missing in medical literature.

Second, our study intended to make a small contribution toward answering a clinically-relevant question in MR DTI: which are the relationships among the most recently published tensor metrics in the medical literature that help to characterize damage to brain tissue? We share our findings about the observed global magnitudes of these metrics in each group of subjects (useful data for detecting errors in software

calculations during the image postprocessing), the significant associations and direction (direct or inverse) for each bivariate correlation, and present a reference of estimated means after a multivariate analysis. We believe our data represent useful information for radiologist and/or bio imaging experts to explain the relationships between tensor metrics to clinicians (neurologists, neurosurgeons, psychiatrist, pediatricians, etc.) as well as in the preparation of prospective studies with clinical application.

Third, our study tested that a global approach is able to detect significant differences between healthy and diseased brains; we also got evidence that the gender neither had interaction nor main effect in the observed measurements of DTI metrics, however the age did, so multivariate analysis controlling this statistic effects should be included in future studies. We evaluated 56 different bivariate correlations for each studied group, with only 7 of them showing a significant difference between healthy brains and brains with GBM, none of these results have been previously reported. It will be interesting to know the data analyses from other research groups that help validate and support the clinical significance of the results presented in this study.

Fourth, despite that most of our results could not be compared with previous studies, some interesting associations are worthy to be noted: for example, the precise value of MD and FA in a clinical setting is still controversial;(5) Traditionally, MD and FA have showed negative correlation with increased MD and decreased FA in the peritumoral signal-intensity abnormality when compared with normal-appearing white matter;(37) we observed a poor-negative non-significant correlation when controlling the effect of age and gender. One explanation might be that, in contrast to MD that measures the magnitude of molecular motion of water and does not depend directly on the integrity of myelinated fiber tracts, FA depends on the restriction of water proton movement along myelinated fiber tracts, it is the weighted average of the anisotropic diffusion.(8) The absence of partial correlation analyses in previous reports could explain some conflicts in the values of MD and FA in characterizing tumor type.(5, 38)

For MD, the highest-significant correlation ( $r = 1$ ) was observed with  $p$  and RD, a positive correlation between RD and MD have been previously observed in human brains.(39) We found an inverse relationship between MD with  $C_p$ , which seems opposite to previously suggested direction measuring MD, FA and the shape tensor metrics ( $C_p$ ,  $C_s$ ,  $C_l$ ) between tumoral brain tissue, metastasis and abscesses.(4) A high correlation (more than 0.8) observed between some pairs of variables, is a warning for those investigators willing to conduct multivariate assessments (Anova, Mancova, Regression) as the presence of multicollinearity suggest the removal of some variables before the analysis.(40)

For most of the tensor metrics correlates, we observed a decrease in the strength of the linear relationship after controlling the effect of age and gender (unpublished data). A poor correlation between a pair of metrics should be interpreted cautiously; in clinical settings these measurements might have the physiological implication to represent independent biological biomarkers.

FA's mechanisms of decreasing its value in brain tumors are still unclear: they could be related to an increase in extracellular space secondary to neuronal and fiber tract destruction;(38) or a decrease in extracellular space secondary to tumor infiltration (observing a negative relationship between FA and tumor cellularity).(41) The FA-value can change by virtue of its definition as a ratio between  $q$  and  $L$ ;(7) the inclusion of the parameter  $q$  may be able to provide a more complete picture of the diffusion profile of a brain tumor, in our study this parameter showed the highest-significant strength of correlation with FA ( $r = .928$ ) in brains with GBM, it would seem an expected finding from its formula (ratio of  $q/L$ ); however, our findings differ from other authors who observed, when comparing measurements in metastasis, that the  $q$  value did not change significantly, suggesting that the variation in FA may be due to changes in the magnitude of the total diffusion ( $L$ ) rather than the anisotropy ( $q$ ). The inverse correlation between FA and RD observed in our study had been reported,(39) although there are not statements of the expected magnitudes among these correlations.



Several limitations in our study and factors that influence the clinical application of DTI-metrics need to be addressed: our decision to evaluate a single, *global* approach among tensor-metric relationships came up from reports depicting a non-significant difference in FA between the enhancing and non-enhancing peritumoral *regions*;(42) no difference in MD and FA values in peritumoral areas with T2 signal-intensity change,(43) and findings of high variance of FA values between several brain regions,(5) making all them a patent lack of agreement between investigators. Also, some studies have evaluated only small regions of interest within the tumors, which may miss much of the tumor or the peritumoral abnormalities, and those that have used regions of interest that cover the entire tumor, have not always studied the region closest to the tumor, which should contain the most infiltrated white matter tracts.(5)

Nowadays, there is still scarce evidence regarding the potential of these DTI biomarkers, for example, besides the clinical acceptance of FA; some studies have showed a marked increase in p (mean 68%) with marked reduction in q (mean 42%) in disrupted white matter.(44) Also, some proved biomarkers, for example, the increase of RD as a marker of demyelination and axonal loss has not had generalization in its use.(39) These facts reflect the limited acceptance of DTI by the medical community; it does not reach yet the anatomic validity of the myeloarchitectonic studies and currently cannot differentiate individual axons or synaptic connections.(45) The intricacies of DTI-derived tensor metrics to characterize the brain tissue in health and disease might be affected among other variables by the ratio of extracellular to intracellular space, vascularity, edema, microcysts, and extracellular matrix.(46)

We must acknowledge that a deep physics explanation of the several relationships presented in this research is beyond not only from the scope of the article but also from our knowledge as clinical investigators. Some readers might prefer more complex multivariate analyses such as anova and linear regression, we considered them, but they would require additional analyses and explanations. Our study is part of a research line trying to understand the role of tensor metrics in characterizing brain impairment

due to brain tumors; we are aware that, the clinical value of our findings has yet to be determined, and the biological impact of the different metrics should be explained in more detail in clinical journals.

In conclusion, our study make a contribution toward the understanding of the fundamentals of the tensor-metric's relationships; the presented data that will help to know *a priori* which relationships can be expected in a prospective analysis decreasing the underlying empiricism in this area. A comprehensive understanding of the currently available DTI-derived tensor metrics will allow them to be considered as imaging biomarkers in the diagnosis and treatment planning of brain tumors. Readers should be aware that, it is still not completely understood the different relationships of the brain structure with each tensor metric, it is possible they answer different questions; also, variations in DTI measures are not specific of one histologic type of tumor, which broaden the application of these biomarkers to a wider variety of intracranial pathologies. Given the increased availability of open source software in MRI units around the world, it is anticipated that DTI-derived tensor metrics may become a low-cost and common used approach. A standardized package of selected DTI processing tools might be included as an imaging protocol to be routinely performed in clinical settings, however this approach still needs further work and histologic examination to assess the depth and extent of its application and finally obtain objective and reproducible results.

**Conflict of interest**

**Acknowledgments**

## References

1. Al-Okaili RN, Krejza J, Wang S, Woo JH, Melhem ER. Advanced MR imaging techniques in the diagnosis of intraaxial brain tumors in adults. *Radiographics : a review publication of the Radiological Society of North America, Inc.* 2006 Oct;26 Suppl 1:S173-89. PubMed PMID: 17050514. Epub 2006/10/20. eng.
2. Witwer BP, Moftakhar R, Hasan KM, Deshmukh P, Haughton V, Field A, et al. Diffusion-tensor imaging of white matter tracts in patients with cerebral neoplasm. *Journal of neurosurgery.* 2002 Sep;97(3):568-75. PubMed PMID: 12296640. Epub 2002/09/26. eng.
3. Rees JH, Smirniotopoulos JG, Jones RV, Wong K. Glioblastoma multiforme: radiologic-pathologic correlation. *Radiographics : a review publication of the Radiological Society of North America, Inc.* 1996 Nov;16(6):1413-38; quiz 62-3. PubMed PMID: 8946545. Epub 1996/11/01. eng.
4. Toh CH, Wei KC, Ng SH, Wan YL, Lin CP, Castillo M. Differentiation of brain abscesses from necrotic glioblastomas and cystic metastatic brain tumors with diffusion tensor imaging. *AJNR American journal of neuroradiology.* 2011 Oct;32(9):1646-51. PubMed PMID: 21835939. Epub 2011/08/13. eng.
5. Wang W, Steward CE, Desmond PM. Diffusion tensor imaging in glioblastoma multiforme and brain metastases: the role of p, q, L, and fractional anisotropy. *AJNR American journal of neuroradiology.* 2009 Jan;30(1):203-8. PubMed PMID: 18842762. Epub 2008/10/10. eng.
6. Cortez-Conradis D, Favila R, Isaac-Olive K, Martinez-Lopez M, Rios C, Roldan-Valadez E. Diagnostic performance of regional DTI-derived tensor metrics in glioblastoma multiforme: simultaneous evaluation of p, q, L, Cl, Cp, Cs, RA, RD, AD, mean diffusivity and fractional anisotropy. *European radiology [Internet].* 2012 Oct 21:[DOI 10.1007/s00330-012-2688-7 pp.]. Available from: <http://www.ncbi.nlm.nih.gov/pubmed/23085868>.
7. Pena A, Green HA, Carpenter TA, Price SJ, Pickard JD, Gillard JH. Enhanced visualization and quantification of magnetic resonance diffusion tensor imaging using the p:q tensor decomposition. *The British journal of radiology.* 2006 Feb;79(938):101-9. PubMed PMID: 16489190. Epub 2006/02/21. eng.
8. Le Bihan D, Mangin JF, Poupon C, Clark CA, Pappata S, Molko N, et al. Diffusion tensor imaging: concepts and applications. *Journal of magnetic resonance imaging : JMRI.* 2001 Apr;13(4):534-46. PubMed PMID: 11276097. Epub 2001/03/29. eng.
9. Koch K, Wagner G, Schachtzabel C, Schultz CC, Gullmar D, Reichenbach JR, et al. Neural activation and radial diffusivity in schizophrenia: combined fMRI and diffusion tensor imaging study. *The British journal of psychiatry : the journal of mental science.* 2011 Mar;198(3):223-9. PubMed PMID: 21357881. Epub 2011/03/02. eng.

10. Rorden C, Karnath HO, Bonilha L. MRICron dicom to nifti converter. Neuroimaging Informatics Tools and Resources Clearinghouse (NITRC). <http://www.mccauslandcenter.sc.edu/mricro/mricron/dcm2nii.html> Accessed June 07, 2012.
11. Smith SM, Jenkinson M, Woolrich MW, Beckmann CF, Behrens TE, Johansen-Berg H, et al. Advances in functional and structural MR image analysis and implementation as FSL. *Neuroimage*. 2004;23 Suppl 1:S208-19. PubMed PMID: 15501092.
12. Smith SM. Fast robust automated brain extraction. *Hum Brain Mapp*. 2002 Nov;17(3):143-55. PubMed PMID: 12391568. Epub 2002/10/23. eng.
13. Cortez-Conradis D, Favila R, Isaac-Olive K, Martinez-Lopez M, Rios C, Roldan-Valadez E. Diagnostic performance of regional DTI-derived tensor metrics in glioblastoma multiforme: simultaneous evaluation of p, q, L, Cl, Cp, Cs, RA, RD, AD, mean diffusivity and fractional anisotropy. *European radiology* [Internet]. 2012 Oct 21:[DOI 10.1007/s00330-012-2688-7. pp.]. Available from: <http://www.ncbi.nlm.nih.gov/pubmed/23085868>.
14. Zhou XH, Obuchowski NA, McClish DK. *Statistical methods in diagnostic medicine*. Zhou XH, Obuchowski NA, McClish DK, editors. New York: Wiley & Sons Interscience; 2002.
15. Obuchowski NA, McClish DK. Sample size determination for diagnostic accuracy studies involving binormal ROC curve indices. *Statistics in medicine*. 1997 Jul 15;16(13):1529-42. PubMed PMID: 9249923. Epub 1997/07/15. eng.
16. Pallant J. Multivariate analysis of variance. In: Pallant J, editor. *SPSS Survival Manual*. 4th ed. Crows Nest, NSW, Australia: Allen & Unwin; 2011. p. 283-96.
17. Tabachnick BG, Fidell LS. Multivariate Normality. In: Tabachnick BG, Fidell LS, editors. *Using Multivariate Statistics*. 5th ed 2007. p. 251.
18. Pallant J. Assessing Normality. In: Pallant J, editor. *SPSS Survival Manual*. 4th ed. Crows Nest, NSW, Australia: Allen & Unwin; 2011. p. 59-64.
19. Chan YH. Biostatistics 104: correlational analysis. *Singapore Med J*. 2003 Dec;44(12):614-9. PubMed PMID: 14770254. Epub 2004/02/11. eng.
20. Pallant J. Testing the statistical significance of the difference between correlation coefficients. In: Pallant J, editor. *SPSS Survival Manual*. 4th ed. Crows Nest, NSW, Australia: Allen & Unwin; 2011. p. 139-41.
21. Pallant J. Analysis of covariance. In: Pallant J, editor. *SPSS Survival Manual*. 4th ed. Crows Nest, NSW, Australia: Allen & Unwin; 2011. p. 297-318.
22. Pallant J. Calculating effect size. In: Pallant J, editor. *SPSS Survival Manual*. 4 ed. Crows Nest, Australia: Allen & Unwin; 2011. p. 254-255.
23. Cohen JW. *Statistical power analysis for the behavioral sciences*. 2nd ed. Hillsdale, NJ: Lawrence Erlbaum Associates; 1988.

24. Uniform requirements for manuscripts submitted to biomedical journals: Writing and editing for biomedical publication. *Journal of pharmacology & pharmacotherapeutics*. 2010 Jan;1(1):42-58. PubMed PMID: 21808590. Pubmed Central PMCID: 3142758.
25. Basser PJ, Pierpaoli C. Microstructural and physiological features of tissues elucidated by quantitative-diffusion-tensor MRI. *J Magn Reson B*. 1996 Jun;111(3):209-19. PubMed PMID: 8661285. Epub 1996/06/01. eng.
26. Basser PJ, Mattiello J, LeBihan D. MR diffusion tensor spectroscopy and imaging. *Biophys J*. 1994 Jan;66(1):259-67. PubMed PMID: 8130344. Pubmed Central PMCID: 1275686. Epub 1994/01/01. eng.
27. Mori S, Barker PB. Diffusion magnetic resonance imaging: its principle and applications. *Anat Rec*. 1999 Jun 15;257(3):102-9. PubMed PMID: 10397783. Epub 1999/07/09. eng.
28. Lu S, Ahn D, Johnson G, Law M, Zagzag D, Grossman RI. Diffusion-tensor MR imaging of intracranial neoplasia and associated peritumoral edema: introduction of the tumor infiltration index. *Radiology*. 2004 Jul;232(1):221-8. PubMed PMID: 15220505. Epub 2004/06/29. eng.
29. Chenevert TL, Brunberg JA, Pipe JG. Anisotropic diffusion in human white matter: demonstration with MR techniques in vivo. *Radiology*. 1990 Nov;177(2):401-5. PubMed PMID: 2217776. Epub 1990/11/01. eng.
30. Price SJ, Jena R, Burnet NG, Hutchinson PJ, Dean AF, Pena A, et al. Improved delineation of glioma margins and regions of infiltration with the use of diffusion tensor imaging: an image-guided biopsy study. *AJNR American journal of neuroradiology*. 2006 Oct;27(9):1969-74. PubMed PMID: 17032877.
31. Budde MD, Xie M, Cross AH, Song SK. Axial diffusivity is the primary correlate of axonal injury in the experimental autoimmune encephalomyelitis spinal cord: a quantitative pixelwise analysis. *The Journal of neuroscience : the official journal of the Society for Neuroscience*. 2009 Mar 4;29(9):2805-13. PubMed PMID: 19261876. Pubmed Central PMCID: 2673458.
32. Kumar R, Nguyen HD, Macey PM, Woo MA, Harper RM. Regional brain axial and radial diffusivity changes during development. *Journal of neuroscience research*. 2012 Feb;90(2):346-55. PubMed PMID: 21938736. Pubmed Central PMCID: 3237749.
33. Simao GN, Zarei Mahmoodabadi S, Snead OC, Go C, Widjaja E. Abnormal axial diffusivity in the deep gray nuclei and dorsal brain stem in infantile spasm treated with vigabatrin. *AJNR American journal of neuroradiology*. 2011 Jan;32(1):199-203. PubMed PMID: 20801762.
34. Metwalli NS, Benatar M, Nair G, Usher S, Hu X, Carew JD. Utility of axial and radial diffusivity from diffusion tensor MRI as markers of neurodegeneration in amyotrophic lateral sclerosis. *Brain research*. 2010 Aug 12;1348:156-64. PubMed PMID: 20513367.
35. Seal ML, Yucel M, Fornito A, Wood SJ, Harrison BJ, Walterfang M, et al. Abnormal white matter microstructure in schizophrenia: a voxelwise analysis of axial and radial diffusivity. *Schizophrenia research*. 2008 Apr;101(1-3):106-10. PubMed PMID: 18262770.

36. Chen F, Zhang X, Li M, Wang R, Wang HT, Zhu F, et al. Axial diffusivity and tensor shape as early markers to assess cerebral white matter damage caused by brain tumors using quantitative diffusion tensor tractography. *CNS neuroscience & therapeutics*. 2012 Aug;18(8):667-73. PubMed PMID: 22712656.
37. Lu S, Ahn D, Johnson G, Cha S. Peritumoral diffusion tensor imaging of high-grade gliomas and metastatic brain tumors. *AJNR American journal of neuroradiology*. 2003 May;24(5):937-41. PubMed PMID: 12748097. Epub 2003/05/16. eng.
38. Wieshmann UC, Clark CA, Symms MR, Franconi F, Barker GJ, Shorvon SD. Reduced anisotropy of water diffusion in structural cerebral abnormalities demonstrated with diffusion tensor imaging. *Magnetic resonance imaging*. 1999 Nov;17(9):1269-74. PubMed PMID: 10576712. Epub 1999/11/27. eng.
39. Schmierer K, Wheeler-Kingshott CA, Boulby PA, Scaravilli F, Altmann DR, Barker GJ, et al. Diffusion tensor imaging of post mortem multiple sclerosis brain. *NeuroImage*. 2007 Apr 1;35(2):467-77. PubMed PMID: 17258908. Pubmed Central PMCID: 1892244. Epub 2007/01/30. eng.
40. Tabachnik BG, Fidell SL. Multicollinearity and Singularity. In: Tabachnik BG, Fidell SL, editors. *Using Multivariate Statistics*. 5th ed. Boston, MA: Pearson Education. Inc.; 2007. p. 88-91.
41. Stadlbauer A, Ganslandt O, Buslei R, Hammen T, Gruber S, Moser E, et al. Gliomas: histopathologic evaluation of changes in directionality and magnitude of water diffusion at diffusion-tensor MR imaging. *Radiology*. 2006 Sep;240(3):803-10. PubMed PMID: 16926329. Epub 2006/08/24. eng.
42. Tsuchiya K, Fujikawa A, Nakajima M, Honya K. Differentiation between solitary brain metastasis and high-grade glioma by diffusion tensor imaging. *The British journal of radiology*. 2005 Jun;78(930):533-7. PubMed PMID: 15900059. Epub 2005/05/19. eng.
43. van Westen D, Latt J, Englund E, Brockstedt S, Larsson EM. Tumor extension in high-grade gliomas assessed with diffusion magnetic resonance imaging: values and lesion-to-brain ratios of apparent diffusion coefficient and fractional anisotropy. *Acta Radiol*. 2006 Apr;47(3):311-9. PubMed PMID: 16613314. Epub 2006/04/15. eng.
44. Price SJ, Pena A, Burnet NG, Jena R, Green HA, Carpenter TA, et al. Tissue signature characterisation of diffusion tensor abnormalities in cerebral gliomas. *European radiology*. 2004 Oct;14(10):1909-17. PubMed PMID: 15221264. Epub 2004/06/29. eng.
45. Jones DK. Studying connections in the living human brain with diffusion MRI. *Cortex; a journal devoted to the study of the nervous system and behavior*. 2008 Sep;44(8):936-52. PubMed PMID: 18635164. Epub 2008/07/19. eng.
46. Brunberg JA, Chenevert TL, McKeever PE, Ross DA, Junck LR, Muraszko KM, et al. In vivo MR determination of water diffusion coefficients and diffusion anisotropy: correlation with structural alteration in gliomas of the cerebral hemispheres. *AJNR American journal of neuroradiology*. 1995 Feb;16(2):361-71. PubMed PMID: 7726086. Epub 1995/02/01. eng.





## Tables

Table 1. DTI-derived tensor metric formulas.

<p><i>Mean Diffusivity (MD)</i></p> $MD = D = \frac{\lambda_1 + \lambda_2 + \lambda_3}{3}$
<p><i>Fractional Anisotropy (FA)</i></p> $FA = \frac{\sqrt{3}q}{\sqrt{2}L} = \frac{\sqrt{3}}{\sqrt{2}} \frac{\sqrt{(\lambda_1 - D)^2 + (\lambda_2 - D)^2 + (\lambda_3 - D)^2}}{\sqrt{\lambda_1^2 + \lambda_2^2 + \lambda_3^2}}$
<p><i>Relative Anisotropy (RA)</i></p> $RA = \frac{q}{p} = \frac{\sqrt{(\lambda_1 - D)^2 + (\lambda_2 - D)^2 + (\lambda_3 - D)^2}}{\sqrt{3}D}$
<p><i>Radial Diffusivity (RD)</i></p> $RD = \frac{\lambda_2 + \lambda_3}{2}$
<p><i>Axial Diffusivity (AD)</i></p> $AD = \lambda_1$
<p><i>Spherical Tensor (Cs)</i></p> $Cs = \frac{3\lambda_3}{\lambda_1 + \lambda_2 + \lambda_3}$
<p><i>Pure Isotropic Diffusion (p)</i></p> $p = \sqrt{3}D = \frac{\lambda_1 + \lambda_2 + \lambda_3}{\sqrt{3}}$
<p><i>Pure Anisotropic Diffusion (q)</i></p> $q = \sqrt{(\lambda_1 - D)^2 + (\lambda_2 - D)^2 + (\lambda_3 - D)^2}$
<p><i>Total Magnitude of the Diffusion Tensor (L)</i></p> $L = \sqrt{p^2 + q^2} = \sqrt{\lambda_1^2 + \lambda_2^2 + \lambda_3^2}$

*Linear Tensor (Cl)*

$$C_l = \frac{\lambda_1 - \lambda_2}{\lambda_1 + \lambda_2 + \lambda_3}$$

*Planar Tensor (Cp)*

$$C_p = \frac{2(\lambda_2 - \lambda_3)}{\lambda_1 + \lambda_2 + \lambda_3}$$

Table 2. Means, SD and correlations (*controlled* for the effect of age and gender) in healthy brains.

Tensor Metric											Mean	SD			
Cs											.756690	.032259			
FA	Pearson's R	-.456									.284317	.018917			
	p-value	.029													
RA	Pearson's R	-.992	.434								.224873	.029523			
	p-value	.000	.039												
Cp	Pearson's R	-.979	.460	.938						.133346	.017086				
	p-value	.000	.031	.000											
CI	Pearson's R	-.946	.442	.978	.855					.111574	.016583				
	p-value	.000	.024	.000	.000										
L	Pearson's R	.372	-.115	-.416	-.317	-.186					.002275	.000100			
	p-value	.117	.578	.076	.200	.408									
P	Pearson's R	.179	-.095	-.214	-.020	-.014	.945				.002096	.000087			
	p-value	.477	.652	.395	.938	.953	.000								
AD	Pearson's R	.322	-.012	-.348	-.287	.019	.804	.761			.001553	.000056			
	p-value	.179	.952	.144	.249	.933	.000	.000							
MD	Pearson's R	.181	-.096	-.215	-.022	-.014	.945	1.000	.762			.001210	.000050		
	p-value	.473	.649	.391	.934	.953	.000	.000	.000						
RD	Pearson's R	.053	-.297	-.119	.426	-.131	.877	.954	.628	.954			.001046	.000072	
	p-value	.821	.132	.606	.054	.542	.000	.000	.001	.000					
q	Pearson's R	-.077	.698	.019	.257	.138	.138	.153	.393	.152	.406			.000445	.000055
	p-value	.721	.000	.929	.225	.492	.502	.466	.047	.467	.029				

Table 3. Means, SD and correlations (*controlled* for the effect of age and gender) in brains with GBM.

Tensor Metric											Mean	SD			
Cs											.771562	.066812			
FA	Pearson's R	-.570	FA								.253531	.028425			
	p-value	.003													
RA	Pearson's R	-1.000	.592	RA							.201778	.053287			
	p-value	.000	.002												
Cp	Pearson's R	-.936	.576	.901	Cp					.133265	.043503				
	p-value	.000	.003	.000											
CI	Pearson's R	-.904	.819	.969	.803	CI				.098462	.011929				
	p-value	.000	.000	.000	.000										
L	Pearson's R	.096	.151	.009	-.159	.182	L			.002111	.000140				
	p-value	.648	.472	.967	.446	.469									
P	Pearson's R	.156	-.129	-.094	-.216	-.177	.834	P		.001961	.000123				
	p-value	.456	.540	.664	.299	.482	.000								
AD	Pearson's R	-.111	.343	.191	.053	.173	.871	.881	AD		.001397	.000080			
	p-value	.596	.094	.372	.803	.492	.000	.000							
MD	Pearson's R	.154	-.125	-.090	-.215	-.173	.837	1.000	.883	MD		.001132	.000071		
	p-value	.462	.550	.675	.303	.491	.000	.000	.000						
RD	Pearson's R	.305	-.411	-.260	-.360	-.395	.706	.954	.699	.953	RD		.000999	.000073	
	p-value	.139	.041	.219	.077	.105	.000	.000	.000	.000					
q	Pearson's R	-.484	.928	.539	.466	.736	.430	.187	.629	.191	-.114	q		.000363	.000048
	p-value	.014	.000	.007	.019	.001	.032	.371	.001	.361	.588				

Tables 4. Estimated marginal means SE and CI of DTI-derived tensor metrics (the effect of age was controlled at the value of 43.92 yr).

Tensor metric	Healthy brains				Brains with GBM			
	Mean	Std. Error	95% CI		Mean	Std. Error	95% CI	
			Lower	Upper			Lower	Upper
<b>Cs</b>	.739511	.009798	.719577	.759446	.766043	.007824	.750126	.781960
<b>FA</b>	.290160	.005721	.278520	.301799	.255660	.004568	.246366	.264954
<b>RA</b>	.241025	.008008	.224734	.257317	.211498	.006394	.198490	.224506
<b>Cp</b>	.141366	.007941	.125210	.157522	.137961	.006341	.125061	.150860
<b>CI</b>	.119041	.003243	.112443	.125638	.099495	.002589	.094227	.104763
<b>L</b>	.002287	.000029	.002227	.002347	.002103	.000024	.002055	.002151
<b>p</b>	.002122	.000027	.002068	.002177	.001946	.000021	.001903	.001990
<b>AD</b>	.001558	.000020	.001518	.001598	.001395	.000016	.001363	.001426
<b>MD</b>	.001225	.000015	.001194	.001257	.001124	.000012	.001099	.001149
<b>RD</b>	.001059	.000015	.001029	.001089	.000988	.000012	.000964	.001012
<b>q</b>	.000454	.000011	.000432	.000476	.000371	.000009	.000354	.000389

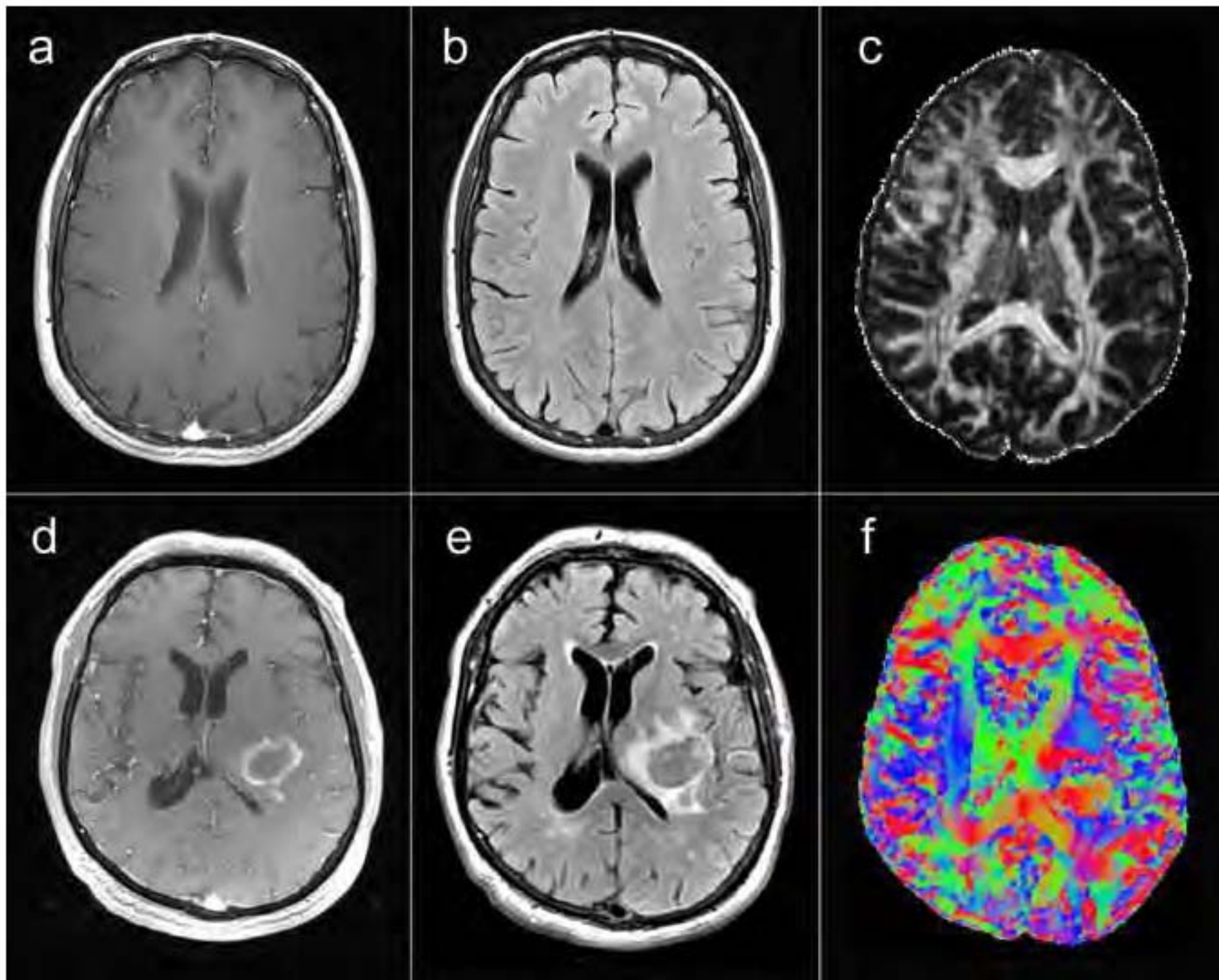
## Figure Legends

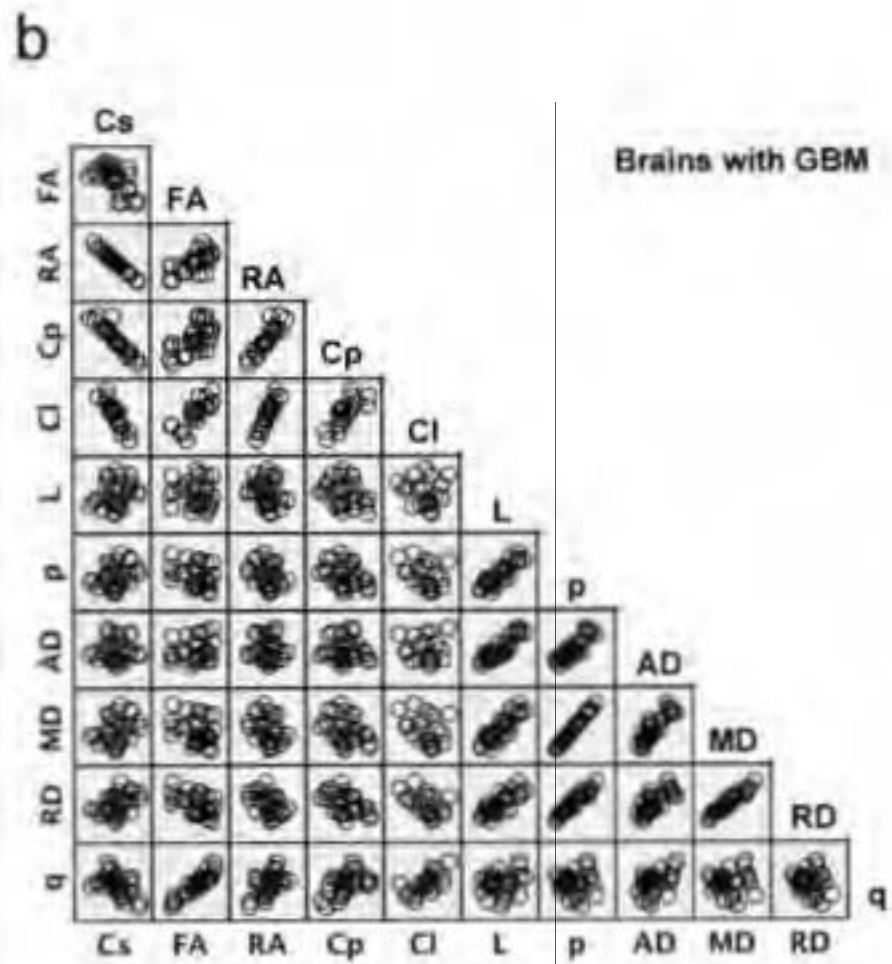
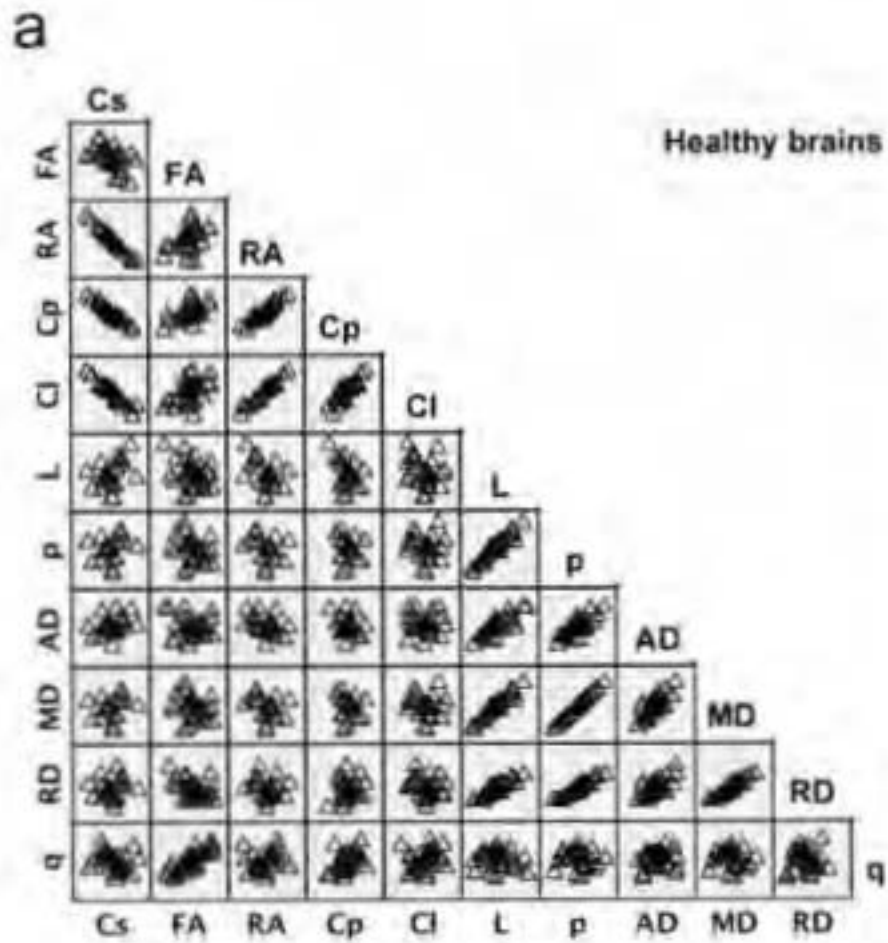
Fig. 1. Example of some sequences and DTI maps from healthy brains (upper row) and brains with GBM (lower row): a and d, T1-postgadolinium images; b and e, Flair sequence; c, pure isotropic diffusion; f, color map of the V1-vector.

Fig. 2. Scatter matrix of the variable's data grouped by diagnosis.

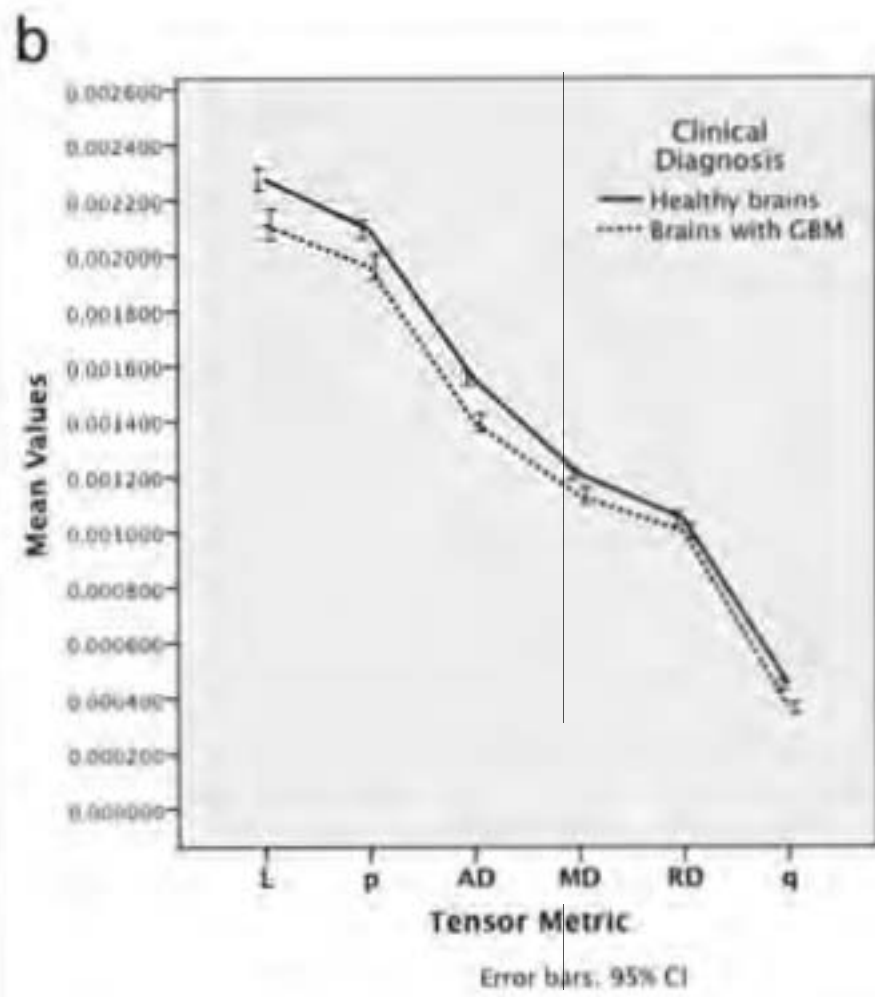
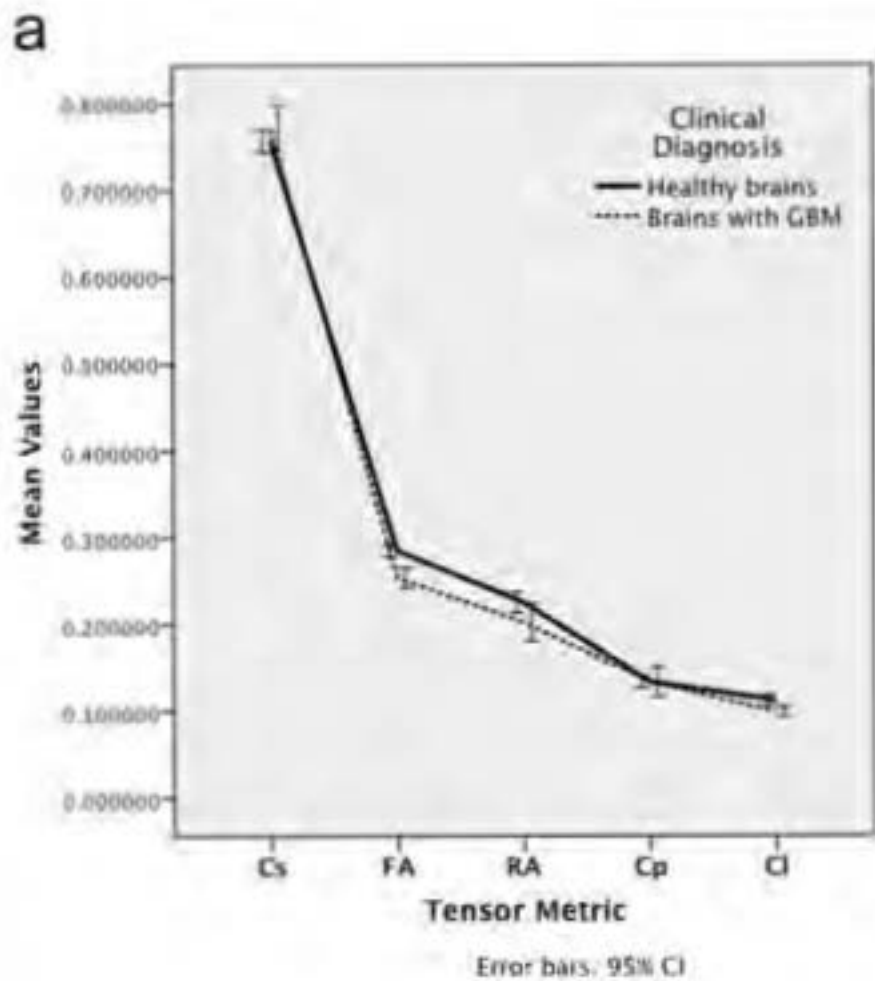
Fig. 3. Graphs of the estimated marginal means for each tensor metric, the influence of age was controlled at the value of 43.92 years.

Figure  
[Click here to download high resolution image](#)









## Original article

# Diffusion tensor imaging-derived measures of fractional anisotropy across the pyramidal tract are influenced by the cerebral hemisphere but not by gender in young healthy volunteers: a split-plot factorial analysis of variance

Ernesto Roldan-Valadez, Edgar Rios-Piedra, Rafael Favila, Sarael Alcauter and Camilo Rios

**Keywords:** anisotropy; diffusion tensor imaging; magnetic resonance imaging; multivariate analysis; analysis of variance

**Background** Diffusion tensor imaging (DTI) permits quantitative examination within the pyramidal tract (PT) by measuring fractional anisotropy (FA). To the best of our knowledge, the inter-variability measures of FA along the PT remain unexplained. A clear understanding of these reference values would help radiologists and neuroscientists to understand normality as well as to detect early pathophysiologic changes of brain diseases. The aim of our study was to calculate the variability of the FA at eleven anatomical landmarks along the PT and the influences of gender and cerebral hemisphere in these measurements in a sample of young, healthy volunteers.

**Methods** A retrospective, cross-sectional study was performed in twenty-three right-handed healthy volunteers who underwent magnetic resonance evaluation of the brain. Mean FA values from eleven anatomical landmarks across the PT (at centrum semiovale, corona radiata, posterior limb of internal capsule (PLIC), mesencephalon, pons, and medulla oblongata) were evaluated using split-plot factorial analysis of variance (ANOVA).

**Results** We found a significant interaction effect between anatomical landmark and cerebral hemisphere ( $F(10, 32)=4.516, P=0.001$ ; Wilks' Lambda 0.415, with a large effect size (partial  $\eta^2=0.585$ )). The influence of gender and age was non-significant. On average, the midbrain and PLIC FA values were higher than pons and medulla oblongata values; centrum semiovale measurements were higher than those of the corona radiata but lower than PLIC.

**Conclusions** There is a normal variability of FA measurements along PT in healthy individuals, which is influenced by regions of interest location (anatomical landmarks) and cerebral hemisphere. FA measurements should be reported for comparing same-side and same-landmark PT to help avoid comparisons with the contralateral PT; ideally, normative values should exist for a clinically significant age group. A standardized package of selected DTI processing tools would allow DTI processing to be routinely performed in clinical settings.

Chin Med J 2012;125(12):2180-2187

The evaluation of the integrity of motor fibers within the pyramidal tract (PT) as the main descending fiber bundle,<sup>1,2</sup> plays an important role in measuring the degree of motor impairment; this impairment can be measured with standardized, reliable, and valid clinical assessments.<sup>3,4</sup> An advanced magnetic resonance (MR) assessment of the PT can confirm lesion location, but this finding may not sufficiently demonstrate the extent to which motor fibers remain intact.<sup>5</sup> For accurate MR assessment, additional variables should also be considered in the investigation of motor impairment, specifically: lesion size,<sup>6,7</sup> the amount of previous lesion burden, and other factors such as patient age and comorbidities.<sup>8,9</sup>

Damage to major axonal pathways can now be studied noninvasively using diffusion tensor imaging (DTI), which permits the imaging and quantitative examination of major axonal pathways of the living brain and provides information about tissue microstructure by measuring fractional anisotropy (FA);<sup>10,11</sup> this permits the topographic relation of lesion location and corticospinal

fibers to be evaluated.<sup>12,13</sup> FA is an index of the diffusion characteristics of water molecules preferentially directed along the axis of major axonal pathways.<sup>10</sup>

Reduced FA has been interpreted as evidence of nerve degeneration and axonal loss.<sup>14,15</sup> Despite numerous studies that have reported FA altered values at a variety of

---

DOI: 10.3760/cma.j.issn.0366-6999.2012.12.018  
Magnetic Resonance Unit, Medica Sur Clinic & Foundation, Mexico City, Mexico (Roldan-Valadez E)  
Tecnologico de Monterrey, Health Sciences Division, México City Campus, México (Rios-Piedra E)  
GE Healthcare, Mexico City, Mexico (Favila R)  
Imágenes Cerebrales, Instituto Nacional de Psiquiatría Ramón de la Fuente Ciudad de México, México (Alcauter S)  
Department of Neurochemistry, National Institute of Neurology and Neurosurgery, Mexico City, Mexico (Rios C)  
Correspondence to: Dr. Ernesto Roldan-Valadez, Coordination of Research and Innovation in MRI, Magnetic Resonance Unit, Medica Sur Clinic & Foundation, Puente de Piedra # 150. Col. Toriello Guerra. Deleg. Tlalpan, CP 14050, Mexico City, Mexico (Tel: 52-55-5424-7230. Email: ernest.roldan@usa.net)  
This study was supported in part by Medica Sur Clinic & Foundation.

clinical entities (e.g., within stroke lesions), significant decreases in FA have been demonstrated as early as 7 to 14 hours poststroke.<sup>16</sup> In addition, secondary degeneration of the PT-altered FA has been recorded over a 12-week period,<sup>17</sup> yet at present little is known about specific changes in FA along the entire tract based on anatomical landmarks, gender, or cerebral hemispheres.<sup>18,19</sup>

To the best of our knowledge, there do not exist any published findings describing the normative values of FA as it relates to the regions along the PT; that is, the inter-variability measures of FA along the PT remain unexplained. Establishment of these reference values would help radiologists and neuroscientists to understand normality as well as early pathophysiologic changes associated with a variety of brain diseases.

The aim of our study was to know the variability of the FA at eleven anatomical landmarks along the PT, and to demonstrate the possible influences of gender and/or the cerebral hemisphere in these measures in a sample of young, healthy volunteers. We sought to evaluate these influences in order to obtain DTI-derived reference-biomarker values of motor tract integrity, which we expect could be compared to patterns of motor tract damage in future studies.

## METHODS

### Subjects

A retrospective, cross-sectional study was performed in twenty-three right-handed healthy volunteers (medical students at our institution) for MR evaluation of the brain: 9 men ((26.8±2.1) years; range, 24–30 years) and 14 women ((24.94±2.75) years; range, 20–30 years). A preliminary neuropsychological evaluation included the Wechsler Adult Intelligence Scale (WAIS) III intelligence quotient (IQ) test validated for Mexican patients (considering an average IQ of 100 and a standard deviation of 15).<sup>20,21</sup> In addition, a validated, modified version of the Mini-Mental State Examination (MMSE) in Spanish was used (score greater than or equal to 25 points was considered normal),<sup>22</sup> and the presence of depression was assessed with the Beck's Depression Inventory-II (BDI) test (subjects with cutoff test values below 13 points were included).<sup>23</sup> The local Institutional Review Board approved the study, and all participants provided written informed consent.

### Brain image acquisition

Conventional MR evaluation of the brain was performed using a 3-Tesla Signa HDxt scanner (GE Healthcare, Waukesha, WI, USA) and a high-resolution eight-channel head coil (Invivo, Gainesville, FL, USA). Contraindications to magnetic resonance imaging (MRI) were claustrophobia and the presence of a pacemaker or metallic implant. Exclusion criteria considered any potential medical disorders that could affect brain

structure or function as well as subjects with brain-structural abnormalities on their MRI scans. All participants were included.

The examination included standard clinical sequences: sagittal T1-weighted Fluid-Attenuated Inversion Recovery (FLAIR) (TE/TR = 9.9 ms/2500 ms) with a 5/3-mm slice thickness/gap and a field of view (FOV) of 24 × 24; an axial Spoiled Gradient Echo (FSPGR) sequence (TE/TR = 3.9 ms/9.4 ms) with a 1.3/0-mm slice thickness/gap and an FOV of 24 × 18; a coronal T2-weighted fast spin-echo (FSE) sequence (TE/TR = 164.1 ms/2617 ms) with a 3/0-mm slice thickness/gap and an FOV of 22 × 16; and a FLAIR sequence (TE/TR = 115.8 ms/11002 ms) with a 5/1-mm slice thickness/gap and an FOV of 22 × 22. The DTI sequence resulted in 30 axial slices covering the entire brain and brainstem with 1.87 mm × 1.87 mm × 5.0 mm voxel size, acquiring 25 noncollinear diffusion directions with a b-value of 1000 s/mm<sup>2</sup>, as well as one with a b-value of 0 s/mm<sup>2</sup>.

### DTI analysis and FA measurements

We used two main tools for our imaging analysis: dcm2nii<sup>24</sup> to convert our data from DICOM to NIFTI formats and FMRIB Software Library (FSL).<sup>25,26</sup> to calculate the FA, normalize the data to Montreal Neurological Institute (MNI) space,<sup>27</sup> and select regions of interest (ROIs). Once we had obtained the subjects' diffusion images in DICOM format,<sup>28</sup> we proceeded to convert these files into the NIFTI format.<sup>29</sup>

DTI images were brain-extracted using the standard brain extraction tool (BET).<sup>30,31</sup> Eddy current effects were corrected by taking the first volume as a reference using FSL's Diffusion Toolbox. The diffusion tensor model was adjusted to generate FA images for each subject. All subjects' FA maps were then aligned into the MNI's common space using the nonlinear registration tool FNIRT, which uses a b-spline representation of the registration warp field.<sup>32</sup>

Eleven ROIs were selected on axial color-coded FA images, generating eleven masks. These eleven anatomic-landmarks corresponded approximately to the next coordinates in the space of the MNI brain atlas:<sup>27</sup> centrum semiovale (Z= +45 and Z= +55); corona radiata (Z= +35 and Z= +25); posterior limb of internal capsule (PLIC) (Z= +15 and Z= +05); mesencephalon (Z= -05 and Z= -15); pons (Z= -25 and Z= -35) and medulla oblongata (Z= -45); all these data points are shown in Figure 1. All ROIs were distributed along the PT according to the John Hopkins University Tractography Atlas.<sup>33</sup> Mean FA values for each subject were extracted from corresponding maps and masks using *fsstats*.<sup>26</sup> Figure 2 shows the algorithm used in DTI measurements.

### Clinical significance of DTI sequence and FA measurements

The use of the DTI sequence permits the noninvasive delineation of detailed anatomical and functional

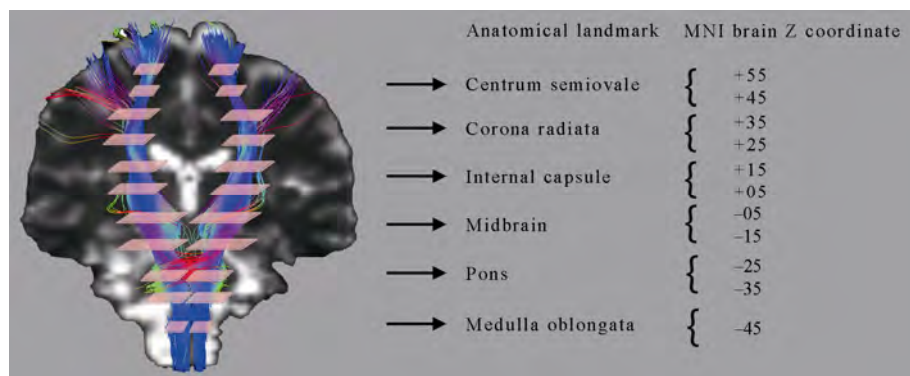


**Figure 1.** Selected anatomical landmarks for the DTI-derived FA measurements.

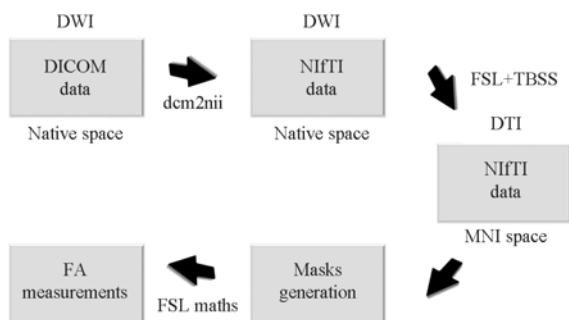


**Figure 2.** Algorithm showing the software used in DTI-derived FA measurements.

information of both normal and pathological brain tissues. DTI data can be used to visualize the major white matter (WM) tracts of the brain,<sup>34,35</sup> and indirectly evaluate the integrity of WM by measuring water diffusion and its directionality in three dimensions.<sup>36</sup>

FA provides information about the shape of the diffusion tensor in each voxel. The anisotropic fraction is based on the normalized variance of the core values of the main vectors of diffusion (corresponding to the eigenvectors of the tensor),<sup>37</sup> its values vary between 0 (isotropic diffusion) and 1 (infinite anisotropy).<sup>38</sup> Diffusion is anisotropic in WM fiber tracts, as axonal membranes and myelin sheaths present barriers to the motion of water molecules in directions not parallel to their own orientation. Based on previous reports,<sup>39</sup> we considered values  $>0.2$  as indication of oriented structure within the normal WM (myelination and axonal packing); however, we did not define superior or inferior limits to the expected FA values of PT, as these measurements were the purpose of this study. Reductions in FA values may result from fiber depletion (tumor destroy fibers, reducing their absolute number); fiber dilution (tumor or vasogenic edema spreads intact fibers apart, reducing their density); or fiber degradation (fibers degrade, fibers themselves become intrinsically less anisotropic and thus retain normal numbers and density).<sup>40</sup>

### Statistical analysis

A split-plot factorial analysis of variance (ANOVA)<sup>41,42</sup> was conducted to assess the influences of gender and the cerebral hemisphere on FA measures across the chosen anatomical landmarks along the PT. Subject age was used

as a covariate to control for individual differences. Preliminary checks were conducted to ensure that there was no violation of the general assumptions underlying univariate and multivariate ANOVA results, sphericity, and reliable measurement of the covariate. The effect size assessment (proportion of the variance in the dependent variable that can be explained by the independent variable) of each of the results was obtained by using the Partial Eta Squared ( $\eta^2$ ) proposed by Cohen,<sup>43</sup> where 0.01–0.06 = small effect; 0.06–0.14 = moderate effect; and a value greater than 0.14 = large effect.

Variation of the initial FA measurements was shown using descriptive statistics (mean  $\pm$  standard deviation (SD)); however, the final estimated marginal means of the factorial ANOVA analysis were reported using the mean  $\pm$  standard error (SE). Here we use SE instead of SD, as we consider that it is a probabilistic statement about how a specific number of samples would provide a better bound on estimates of the population mean, in light of the central limit theorem. SE was calculated by dividing the SD by the square root of N (the sample size),  $SE = SD/\sqrt{n}$ .<sup>44</sup>

All analyses were carried out using the IBM<sup>®</sup> SPSS<sup>®</sup> Statistics software (version 20.0.0 IBM Corporation; Armonk, NY, USA); for the graphics design, we used the STATISTICA data analysis software system (version 8.0; StatSoft, Inc.; Tulsa, OK, USA). Data were presented in accordance with the guidelines of the American Psychological Association.<sup>45,46</sup> Statistical significance was indicated by  $P < 0.05$  (two-tailed).

## RESULTS

### Subjects and FA measurements

Neuropsychological tests revealed that the corresponding IQs or other variables of mental status were comparable across the age range of the subjects. The PT was successfully traced from the medulla oblongata to the centrum semiovale with 11 FA measurements taken across the chosen anatomic landmarks. Forty-six PTs (from 23 subjects) representing a total of 506 FA measurements were included in the split-plot ANOVA analysis. The mean values and SD for the FA measurements totals across each anatomical landmark are

presented in Table 1.

**Interactions, main effects, and effect sizes on FA measurements**

The assumption of homogeneity of variance-covariance matrices was interpreted as non-significant (Box’s M value=109.137,  $P=0.330$ ), assuming the covariance matrices between the groups were equal.<sup>47</sup> The homogeneity of variance at each anatomical landmark was also non-significant ( $P >0.05$ ). The assumption of sphericity however, was found to be violated ( $P <0.05$ ). In light of this assumption violation, the findings of the multivariate testing were reported.

There were no significant interaction effects amongst anatomical landmark, gender, and cerebral hemisphere and the anatomical landmark and gender,  $P >0.05$ . However, there was a significant interaction effect between Anatomical landmark and cerebral hemisphere ( $F(10, 32)=4.516, P=0.001$ ; Wilks’ Lambda 0.415, with a large effect size (partial  $\eta^2=0.585$ )). The covariate age was non-significant in its interaction with the anatomical landmarks,  $P=0.055$ . Finally, there was a significant main effect of the anatomical landmarks ( $F(10, 32)=8.313, P <0.001$ ; Wilks’ Lambda 0.278, with the largest effect size (partial  $\eta^2=0.722$ )).

The between-subject effects depicted a non-significant main effect for groups; that is, there were not significant differences in the FA measurements for each group (cerebral hemisphere with  $P=0.297$  and gender with  $P=0.336$ ). Table 2 presents a summary of the within- and between-subjects effects assessment.

**Table 1.** Means and SD for FA measurements across the PT

Anatomical landmarks	N	Mean±SD
Medulla oblongata (Z = -45)	46	0.476±0.089
Pons (Z = -35)	46	0.493±0.070
Pons (Z = -25)	46	0.594±0.039
Midbrain (Z = -15)	46	0.639±0.068
Midbrain (Z = -05)	46	0.646±0.032
PLIC (Z = 05)	46	0.643±0.023
PLIC (Z = 15)	46	0.599±0.028
Corona radiata (Z = 25)	46	0.499±0.025
Corona radiata (Z = 35)	46	0.456±0.028
Centrum semiovale (Z = 45)	46	0.563±0.035
Centrum semiovale (Z = 45)	46	0.520±0.048

**Estimated marginal means**

Considering the significant interaction between anatomical landmarks and cerebral hemisphere, marginal means were clustered by groups. An inspection of the mean scores indicated that except for the pons ( $Z= -35$ ) and corona radiata ( $Z= +35$ ), FA measurements were significantly higher in the right cerebral hemisphere. The *post hoc* analyses (Bonferroni’s) revealed significant differences between mean comparisons across all eleven anatomical landmarks ( $P <0.05$ ). The trend analysis showed the FA measurements with a non-linear (cubic) trend,  $P=0.030$ , partial  $\eta^2=0.110$ . That is, on average, the midbrain and PLIC FA values were higher than those of the pons and medulla oblongata; centrum semiovale measurements were higher than those of the corona radiata but less than PLIC. Table 3 depicts the estimated marginal means and SE adjusted for cerebral hemispheres and the covariate age, and Figure 3 depicts the comparative graphs of marginal means.

**DISCUSSION**

Achieving a better understanding of normative regional FA values is of particular importance to those specialists participating in imaging the PT, especially considering that recent studies foster the use of DTI-derived measures alone as valid structural surrogates of motor impairment.<sup>5</sup>

The clinical relevance of our study, specifically, the evidence of normal variability of FA measurements across PT in a sample of healthy subjects, has three main components: (1) we accomplished the mapping and measurement of FA along fiber tracts in a reliable, standardized way by selecting a group of open-source software tools for DTI analysis (Figure 2); (2) we confirmed the existence of significant regional FA variability along the PT, which had a main effect behavior in our analysis; (3) we discovered evidence of the significant influences of the cerebral hemisphere in the FA measurements (interaction of anatomical-landmark and cerebral hemisphere). These findings are in agreement with previous reports of asymmetries in fiber density and FA values for the arcuate fasciculus,<sup>48</sup> a finding consistent with lateralization of brain functions in most humans. Also,

**Table 2.** Within- and between-subjects effects

Main effects and interaction	Wilks’ Lambda	F values	P values	Effect size (partial $\eta^2$ )
<b>Within-subjects effects</b>				
Anatomical landmark * Gender * Cerebral Hemisphere	0.672	1.563	0.163	0.328
Anatomical landmark * Gender	0.675	1.544	0.169	0.325
Anatomical landmark * Cerebral Hemisphere	0.415	4.516	0.001	0.585
Anatomical landmark * Age	0.604	2.099	0.055	0.396
Anatomical landmark	0.278	8.313	<0.001	0.722
<b>Between-subjects effects</b>				
Gender * Cerebral Hemisphere	–	0.029	0.865	0.001
Gender	–	0.946	0.336	0.023
Cerebral Hemisphere	–	1.116	0.297	0.027
Age	–	3.318	0.076	0.075

Design = Intercept + age + gender + cerebral hemisphere + gender \* cerebral hemisphere. \* = interaction.

**Table 3.** Means and SE adjusted for the significant interactions found in the study: anatomical landmarks and cerebral hemispheres

Anatomical landmarks	Right hemisphere		Left hemisphere	
	Mean±SE	95% CI	Mean±SE	95% CI
Medulla oblongata (Z = -45)	0.448±0.022	0.403–0.493	0.467±0.022	0.422–0.511
Pons (Z = -35)	0.496±0.018	0.460–0.532	0.511±0.018	0.474–0.547
Pons (Z = -25)	0.605±0.008	0.589–0.622	0.568±0.008	0.551–0.585
Midbrain (Z = -15)	0.647±0.018	0.611–0.683	0.637±0.018	0.601–0.673
Midbrain (Z = -05)	0.647±0.008	0.630–0.664	0.641±0.008	0.624–0.658
PLIC (Z = 05)	0.641±0.006	0.629–0.654	0.640±0.006	0.628–0.652
PLIC (Z = 15)	0.618±0.005	0.607–0.628	0.578±0.005	0.568–0.589
Corona radiata (Z = 25)	0.504±0.006	0.491–0.516	0.488±0.006	0.476–0.501
Corona radiata (Z = 35)	0.451±0.007	0.437–0.465	0.453±0.007	0.439–0.468
Centrum semiovale (Z = 45)	0.570±0.009	0.552–0.589	0.553±0.009	0.535–0.572
Centrum semiovale (Z = 45)	0.536±0.011	0.515–0.558	0.506±0.011	0.485–0.528

The covariate (age) was evaluated at the value of 25.22 years.

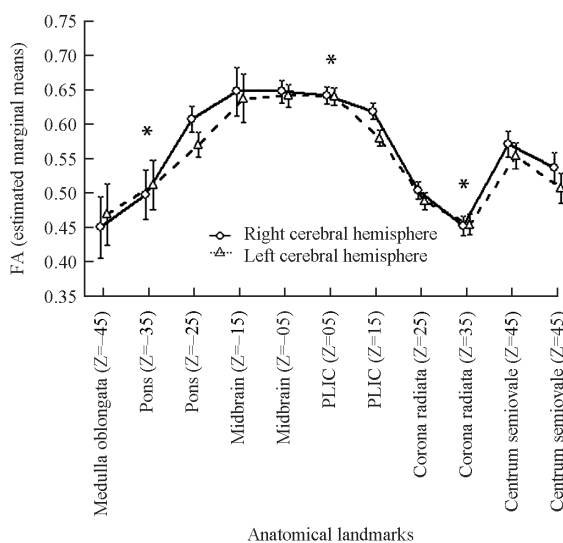


**Figure 3.** Estimated marginal means of FA at selected anatomical landmarks of the PT clustered by cerebral hemisphere (error bars = 95% CI). The crossing lines (\*) evidence the interactions between anatomical landmarks and cerebral hemispheres. These interactions support the influence of ROI location in the FA measurements.

our observations of similar measurements at certain anatomical landmarks, for example the FA values of PLIC at Z= +05, support previous reports of intact ascending and descending fiber tracts that traverse through the PT in close proximity.<sup>49,50</sup>

Although the image-processing pathway presented here are not at present well known by experts in the field, we considered it noteworthy to demonstrate that we were able to achieve standardized measurements. The use of FSL's tools and scripts,<sup>30</sup> predesigned ROIs from Johns Hopkins University's White Matter Atlas,<sup>33</sup> and drawings of our own ROIs (we preferred to draw specific masks around the desired ROIs instead of using the skeletonized image generated by the TBSS procedure<sup>51</sup> for some anatomic landmarks not included in the JHU atlas); permitted us to avoid common errors such as misidentification of cerebral structures and data alteration by other undesirable ROIs (e.g., gray-matter or adjacent white-matter tracts). The sequence of computational algorithms that we used here allowed us to conduct FA measurements within the same area and cerebral

landmarks in all patients; we sought the maximum accuracy in our final results, so variations in the results were only a reflection of the distribution of the FA values in the selected PT.

We considered the quality of our data reliable as normative values; we presented the corresponding FA values at each of the eleven-tier anatomical landmarks using mean, SE, and CI. To avoid confusion with SD, the reader must remember that SE represents how well the sample mean approximates the population mean (the larger the sample, the smaller the SE; the closer the sample mean approximates the population mean). In practical situations, because the true value of the SD is usually unknown, the SE is often used to refer to an estimate of this unknown quantity.<sup>44</sup> Also considering that the probability distribution of the values in this study was known, SE was used to calculate a good approximation to 95% exact CI.

Our study differs methodologically over previous ones, in that we used a split-plot ANOVA test controlling the age as a covariate; this analysis allowed us to identify the interaction between anatomical landmarks and the cerebral hemisphere, that is, the difference between FA measurements will depend on group membership; also, the significant main effect of the anatomical landmarks means that the imaging evaluation of the PT integrity should be conducted by reading the FA values at each landmark.

This kind of imaging analysis might be of special importance, considering that several previous publications have reported only main effects; however, a formal statistical analysis considering simultaneously independent variables that can influence results (age, cerebral hemisphere, and gender) has not been reported, to the best of our knowledge. These moderator variables are noteworthy because they might help explaining why some researchers obtain statistically significant results while others do not. Although the anatomical landmarks of our study depicted a large effect size, the observed 72.2% of variance should not stop neuroscientists and clinicians from considering additional interacting factors to discover additional variance.

Although it is currently accepted that axonal membranes and myelin sheets are the primary determinant of anisotropic diffusion along nerve fibers,<sup>14</sup> some reports consider that the variability of FA observed along the PT may be in fact associated with microstructural disruption of axonal transport; such disruption causes a significant disturbance of directed axonal protoplasmic flow.<sup>52</sup> The low FA values observed across some landmarks of the PT would mean that other tracts contribute to the diffusion signal decay in these healthy subjects. In this study, the higher FA values were observed in the regions between pons and internal capsule; the corona radiata, a region including crossing fibers from the superior longitudinal fasciculus (SLF), reflects a much lower FA; our explanation for this finding is that voxels do not represent just one tract but a sample of both the PT and the SLF (Figure 3).

In addition, when there is a nonuniform distribution of fiber directions, the eigenvector associated with the largest eigenvalue only corresponds to the averaged fiber direction within the voxel; this may not necessarily reflect the nerve fibers crossing the voxel.<sup>48</sup> Such mixture of tracts reflects a lower FA value because diffusion is not as anisotropic as it is in other regions where one single tract is represented, such as the PLIC. When PT is evaluated in patients, a low regional FA finding might not necessarily represent direct damage to the tract; other possibilities such as vasogenic edema and tract compression by a tumoral mass could be responsible for this FA finding.<sup>48</sup>

Some limitations to our study and factors that influence the accuracy of DTI in clinical applications need to be addressed, specifically: (1) Although the age range of our study subjects could seem limited, we intentionally did not compute a wider age group (young and elderly subjects). As age could be a variable that influences the calculation of FA, we wanted to study a group of young, healthy volunteers to help us understand the regional FA variability in a homogeneous sample prior to attaining measures of FA in pathological scenarios. The fact that even in this limited age-range group we found significant differences in FA measurements supports our statement that careful analysis must be taken into account by radiologists and/or bio-imaging experts when reporting DTI-derived measurements to clinicians (neurologists, neurosurgeons, psychiatrist, pediatricians, etc.), as these results might influence diagnosis and treatment. (2) The factorial ANOVA analysis of FA measurements was performed considering the number of pyramidal tracts — and not subjects — analyzed (after proof of normal distribution of the data), which should ease some concerns about the apparently limited sample size used in this study. (3) There are still some intrinsic limitations in DTI acceptance by the medical community, as this technique has not yet achieved the anatomic validity of myelo-architectonic studies and currently cannot differentiate individual axons or synaptic connections;<sup>53</sup> furthermore, there is still no gold standard for *in vivo*

fiber tracking.<sup>54-56</sup> Finally, although the path of PT is well known and can be reliably reconstructed,<sup>33</sup> there is a coexistence of alternate motor fibers,<sup>1</sup> and the course of these fibers is not yet based on anatomic studies in humans and were not discriminated in our study (the cortico-reticulo-spinal and cortico-rubro-spinal tracts).<sup>57,58</sup>

There is a normal variability of FA measurements along PT in healthy individuals, which is influenced by the location of ROIs (anatomical landmarks) and the cerebral hemisphere. The use of FA measurements as a biomarker in clinical settings will allow the follow-up of patients and comparison with controls by comparing only same-side and same-landmark PT. The comparisons of FA measurements with the contralateral PT ROI should be avoided when investigators are interested in accurate reports.

Ideally, normative values should exist for specific age and ethnic groups; further studies examining normal variations might provide additional understanding of brain physiology. Given the increased availability of open-source software in MRI units around the world, it is anticipated that DTI-derived FA measurement may become a low-cost and commonplace biomarker. A standardized package of selected DTI processing tools would allow tractography to be routinely performed in clinical settings. The combined use of DTI-derived FA measurements with other conventional MRI modalities such as 3D-volumetry, spectroscopy, and functional MRI Bold needs to have an integrative approach in order to obtain objective and reproducible results.

#### REFERENCES

1. Lang CE, Schieber MH. Human finger independence: limitations due to passive mechanical coupling versus active neuromuscular control. *J Neurophysiol* 2004; 92: 2802-2810.
2. Fries W, Danek A, Witt TN. Motor responses after transcranial electrical stimulation of cerebral hemispheres with a degenerated pyramidal tract. *Ann Neurol* 1991; 29: 646-650.
3. Platz T, Pinkowski C, van Wijck F, Kim IH, di Bella P, Johnson G. Reliability and validity of arm function assessment with standardized guidelines for the Fugl-Meyer Test, Action Research Arm Test and Box and Block Test: a multicentre study. *Clin Rehabil* 2005; 19: 404-411.
4. Wolf SL, Thompson PA, Morris DM, Rose DK, Winstein CJ, Taub E, et al. The EXCITE trial: attributes of the Wolf Motor Function Test in patients with subacute stroke. *Neurorehabil Neural Repair* 2005; 19: 194-205.
5. Lindenberg R, Renga V, Zhu LL, Betzler F, Alsop D, Schlaug G. Structural integrity of corticospinal motor fibers predicts motor impairment in chronic stroke. *Neurology* 2010; 74: 280-287.
6. Pineiro R, Pendlebury ST, Smith S, Flitney D, Blamire AM, Styles P, et al. Relating MRI changes to motor deficit after ischemic stroke by segmentation of functional motor

- pathways. *Stroke* 2000; 31: 672-679.
7. Schiemanck SK, Kwakkell G, Post MW, Kappelle LJ, Prevo AJ. Impact of internal capsule lesions on outcome of motor hand function at one year post-stroke. *J Rehabil Med* 2008; 40: 96-101.
  8. Duncan PW. Stroke disability. *Phys Ther* 1994; 74: 399-407.
  9. Cramer SC, Seitz RJ. Imaging functional recovery from stroke. *Handb Clin Neurol* 2009; 94: 1097-117.
  10. Chabert S, Scifo P. Diffusion signal in magnetic resonance imaging: origin and interpretation in neurosciences. *Biol Res* 2007; 40: 385-400.
  11. Basser PJ, Mattiello J, LeBihan D. MR diffusion tensor spectroscopy and imaging. *Biophys J* 1994; 66: 259-267.
  12. Konishi J, Yamada K, Kizu O, Ito H, Sugimura K, Yoshikawa K, et al. MR tractography for the evaluation of functional recovery from lenticulostriate infarcts. *Neurol* 2005; 64: 108-113.
  13. Nelles M, Gieseke J, Flacke S, Lachenmayer L, Schild HH, Urbach H. Diffusion tensor pyramidal tractography in patients with anterior choroidal artery infarcts. *AJNR Am J Neuroradiol* 2008; 29: 488-493.
  14. Beaulieu C. The basis of anisotropic water diffusion in the nervous system — a technical review. *NMR Biomed* 2002; 15: 435-455.
  15. Mukherjee P. Diffusion tensor imaging and fiber tractography in acute stroke. *Neuroimaging Clin N Am* 2005; 15: 655-665.
  16. Bhagat YA, Emery DJ, Shuaib A, Sher F, Rizvi NH, Akhtar N, et al. The relationship between diffusion anisotropy and time of onset after stroke. *J Cereb Blood Flow Metab* 2006; 26: 1442-1450.
  17. Liang Z, Zeng J, Liu S, Ling X, Xu A, Yu J, et al. A prospective study of secondary degeneration following subcortical infarction using diffusion tensor imaging. *J Neurol Neurosurg Psychiatry* 2007; 78: 581-586.
  18. Hua K, Zhang J, Wakana S, Jiang H, Li X, Reich DS, et al. Tract probability maps in stereotaxic spaces: analyses of white matter anatomy and tract-specific quantification. *Neuroimage* 2008; 39: 336-347.
  19. Heiervang E, Behrens TE, Mackay CE, Robson MD, Johansen-Berg H. Between session reproducibility and between subject variability of diffusion MR and tractography measures. *Neuroimage* 2006; 33: 867-877.
  20. Wechsler D. Manual for the Wechsler adult intelligence scale, 3rd ed. San Antonio, TX: Psychological Corporation; 1997.
  21. Wechsler D. Wechsler adult intelligence scale-revised. San Antonio, TX: Psychological Corporation; 1981.
  22. Reyes-de-Beaman S, Beaman PE, Garcia-Pena C, Angel-Villa MA, Heres J, Cordova A, et al. Validation of a modified version of the Mini-Mental State Examination (MMSE) in Spanish. *Aging Neuropsychol Cogn* 2004; 11: 1-11.
  23. Beck AT, Steer RA, Brown GK. Manual for the Beck Depression Inventory-II. San Antonio, TX: Psychological Corporation; 1996.
  24. Rorden C, Karnath HO, Bonilha L. MRICron dicom to nifti converter. *Neuroimaging Informatics Tools and Resources Clearinghouse (NITRC)*. (Accessed 2011 at <http://www.cabiatl.com/mricro/mricron/index.html>.)
  25. Woolrich MW, Jbabdi S, Patenaude B, Chappell M, Makni S, Behrens T, et al. Bayesian analysis of neuroimaging data in FSL. *Neuroimage* 2009; 45: S173-S186.
  26. Smith SM, Jenkinson M, Woolrich MW, Beckmann CF, Behrens TE, Johansen-Berg H, et al. Advances in functional and structural MR image analysis and implementation as FSL. *Neuroimage* 2004; 23 Suppl 1: S208-S219.
  27. Chau W, McIntosh AR. The Talairach coordinate of a point in the MNI space: how to interpret it. *Neuroimage* 2005; 25: 408-416.
  28. DICOM. Digital Imaging and Communication in Medicine. NEMA — National Electrical Manufacturers Association. 1993.
  29. NIFTI-1. Neuroimaging Informatics Technology Initiative.
  30. Smith SM. Fast robust automated brain extraction. *Hum Brain Mapp* 2002; 17: 143-155.
  31. Jenkinson MP, Smith S. BET2: MR-based estimation of brain, skull and scalp surfaces. Eleventh Annual Meeting of the Organization for Human Brain Mapping, 2005.
  32. Rueckert D, Sonoda LI, Hayes C, Hill DL, Leach MO, Hawkes DJ. Nonrigid registration using free-form deformations: application to breast MR images. *IEEE Trans Med Imaging* 1999; 18: 712-721.
  33. Wakana S, Jiang H, Nagae-Poetscher LM, van Zijl PC, Mori S. Fiber tract-based atlas of human white matter anatomy. *Radiology* 2004; 230: 77-87.
  34. Bammer R, Acar B, Moseley ME. *In vivo* MR tractography using diffusion imaging. *Eur J Radiol* 2003; 45: 223-234.
  35. Ciccarelli O, Toosy AT, Parker GJ, Wheeler-Kingshott CA, Barker GJ, Miller DH, et al. Diffusion tractography based group mapping of major white-matter pathways in the human brain. *Neuroimage* 2003; 19: 1545-1555.
  36. Basser PJ. Inferring microstructural features and the physiological state of tissues from diffusion-weighted images. *NMR Biomed* 1995; 8: 333-344.
  37. Holodny AI, Korneinko VN, Pronin IN, Zhukovskiy ME, Gor DM, Ulug A. Diffusion tensor tractography of the motor white matter tracts in man: current controversies and future directions. *Ann N Y Acad Sci* 2005; 1064: 88-97.
  38. Pierpaoli C, Basser PJ. Toward a quantitative assessment of diffusion anisotropy. *Magn Reson Med* 1996; 36: 893-906.
  39. Gupta RK, Hasan KM, Mishra AM, Jha D, Husain M, Prasad KN, et al. High fractional anisotropy in brain abscesses versus other cystic intracranial lesions. *AJNR Am J Neuroradiol* 2005; 26: 1107-1114.
  40. Field AS. Diffusion tensor imaging at the crossroads: fiber tracking meets tissue characterization in brain tumors. *AJNR Am J Neuroradiol* 2005; 26: 2168-2169.
  41. Jones B, Nachtshiem CJ. Split-Plot Designs: What, Why, and How. *J Qual Technol* 2009; 41: 340-361.
  42. Pallant J. Mixed between-within subjects analysis of variance. In: Pallant J, ed. *SPSS survival manual*, 4th ed. Crows Nest, NSW, Australia: Allen & Unwin; 2011: 274-282.
  43. Cohen JW. *Statistical power analysis for the behavioral sciences*, 2nd ed. Hillsdale, NJ: Lawrence Erlbaum Associates; 1988.
  44. *The Cambridge Dictionary of Statistics*, 3rd ed. London: King's College; 2006. Standard error.
  45. Wilkinson L. *Statistical Methods in Psychology Journals*. Task Force on Statistical Inference. APA Board of Scientific



- Affairs. *Am Psychol* 1999; 54: 594-604.
46. APA. *Publication Manual of the American Psychological Association*. American Psychological Association, 6 ed. 2009.
47. Huberty CJ, Petroskey MD. Multivariate analysis of variance and covariance. In: Tinsley H, Brown S, eds. *Handbook of applied multivariate statistics and mathematical modeling*. New York: Academic Press; 2000.
48. Ahn S, Lee SK. Diffusion tensor imaging: exploring the motor networks and clinical applications. *Korean J Radiol* 2011; 12: 651-661.
49. Kretschmann HJ. Localisation of the corticospinal fibres in the internal capsule in man. *J Anat* 1988; 160: 219-225.
50. Zarei M, Johansen-Berg H, Jenkinson M, Ciccarelli O, Thompson AJ, Matthews PM. Two-dimensional population map of cortical connections in the human internal capsule. *J Magn Reson Imaging* 2007; 25: 48-54.
51. Smith SM, Jenkinson M, Johansen-Berg H, Rueckert D, Nichols TE, Mackay CE, et al. Tract-based spatial statistics: voxelwise analysis of multi-subject diffusion data. *Neuroimage* 2006; 31: 1487-1505.
52. Radlinska B, Ghinani S, Leppert IR, Minuk J, Pike GB, Thiel A. Diffusion tensor imaging, permanent pyramidal tract damage, and outcome in subcortical stroke. *Neurology* 2010; 75: 1048-1054.
53. Jones DK. Studying connections in the living human brain with diffusion MRI. *Cortex* 2008; 44: 936-952.
54. Scollan DF, Holmes A, Winslow R, Forder J. Histological validation of myocardial microstructure obtained from diffusion tensor magnetic resonance imaging. *Am J Physiol* 1998; 275 (6 Pt 2): H2308-H2318.
55. Lin CP, Tseng WY, Cheng HC, Chen JH. Validation of diffusion tensor magnetic resonance axonal fiber imaging with registered manganese-enhanced optic tracts. *Neuroimage* 2001; 14: 1035-1047.
56. Okada T, Mikuni N, Miki Y, Kikuta K, Urayama S, Hanakawa T, et al. Corticospinal tract localization: integration of diffusion-tensor tractography at 3-T MR imaging with intraoperative white matter stimulation mapping – preliminary results. *Radiology* 2006; 240: 849-857.
57. Lawrence DG, Kuypers HG. The functional organization of the motor system in the monkey. II. The effects of lesions of the descending brain-stem pathways. *Brain* 1968; 91: 15-36.
58. Schmähmann JD, Ko R, MacMore J. The human basis pontis: motor syndromes and topographic organization. *Brain* 2004; 127: 1269-1291.

(Received December 16, 2011)

Edited by JI Yuan-yuan

中藥醫學會

# Diagnostic performance of regional DTI-derived tensor metrics in glioblastoma multiforme: simultaneous evaluation of p, q, L, Cl, Cp, Cs, RA, RD, AD, mean diffusivity and fractional anisotropy

David Cortez-Conradis · Rafael Favila ·  
Keila Isaac-Olive · Manuel Martinez-Lopez ·  
Camilo Rios · Ernesto Roldan-Valadez

Received: 19 July 2012 / Accepted: 30 September 2012 / Published online: 21 October 2012  
© European Society of Radiology 2012

## Abstract

**Objectives** Almost a dozen diffusion tensor-imaging (DTI) variables have been used to evaluate brain tumours with scarce information about their diagnostic ability. We aimed to perform a comprehensive evaluation of tensor metrics reported in the last decade.

**Methods** Retrospective case control study performed in 14 patients with glioblastoma multiforme (GBM) and 28 controls. Conventional brain MR sequences and image postprocessing of DTI allowed the calculation of: MD, FA, p, q, L, Cl, Cp, Cs, RA, RD and AD, classified into five regions:

normal appearance white matter (NAWM), immediate and distant oedema, enhancing rim and cystic cavity. ANOVA and AUROC analyses were performed.

**Results** ANOVA depicted a significant difference among all metrics ( $p < 0.05$ ). RA had the highest performance in the NAWM and cystic cavity; immediate and distant zones of oedema were best diagnosed by RD and Cp respectively; q was the best biomarker of the enhancing rim zone;  $p < 0.001$  for all metrics.

**Conclusions** FA and MD, accepted biomarkers of brain injury, were surpassed by other metrics. RA, together with Cs, Cl and CP, might be the new leaders in the evaluation of brain tumours. DTI tensor metrics depict different clinical applicability at each tumour region.

## Key Points

- DTI-derived tensor metrics can characterise the regional impairment of intraaxial brain tumours.
- A performance evaluation of new diagnostic tests should follow the STARD initiative.
- Each tumour region in GBM is detected by a different tensor metric.
- FA and MD are not the best biomarkers of tumour infiltration.
- The diagnostic performance of some tensor metrics allows them to be used interchangeably.

D. Cortez-Conradis · M. Martinez-Lopez · E. Roldan-Valadez (✉)  
Section of Research and Innovation in MRI,  
Magnetic Resonance Unit, Medica Sur Clinic & Foundation,  
Puente de Piedra # 150. Col. Toriello Guerra. Deleg. Tlalpan.,  
14050, Mexico City, Mexico  
e-mail: ernest.rolan@usa.net

D. Cortez-Conradis · K. Isaac-Olive  
Medical Physics Department, Autonomous University  
of State of Mexico,  
Toluca City, Mexico

R. Favila  
GE Healthcare,  
Mexico City, Mexico

C. Rios  
Department of Neurochemistry, National Institute of Neurology  
and Neurosurgery,  
Mexico City, Mexico

**Keywords** Brain neoplasms · Diffusion tensor imaging ·  
Magnetic resonance imaging · Sensitivity and specificity ·  
Statistics as topic

**Abbreviations**

AD	axial diffusivity
ADC	apparent diffusion coefficient
Anova	analysis of variance
AUROC	area under the ROC curve
CI	confidence interval
Cl	linear tensor
Cp	planar tensor
Cs	spherical tensor
DTI	diffusion tensor imaging
FA	fractional anisotropy
GBM	glioblastoma multiforme
L	total magnitude of the diffusion tensor
MD	mean diffusivity
NAWM	normal-appearing white matter
p	pure isotropic diffusion
q	pure anisotropic diffusion
RA	relative anisotropy
RD	radial diffusivity
ROC	receiver operating characteristic
SE	standard error
STARD	Standards for Reporting of Diagnostic Accuracy initiative
VEGF	vascular endothelial growth factor
WM	white matter

**Introduction**

Advanced MR techniques that produce image contrast reflecting attributes of tissue physiology and microstructure have begun to be widely applied in clinical brain tumour imaging at major academic centres [1]. Diffusion tensor imaging (DTI) provides quantitative measures of the molecular motion of water in a three-dimensional space [2]. The measure of this directionality [3] has been accepted as a quantitative index for diffusion anisotropy that correlates with microstructural integrity of myelinated fibre tracts [4]. Three eigenvectors and three eigenvalues are used to represent the main diffusion directions and magnitudes, respectively [5], by combining the eigenvalues  $\lambda_1$ ,  $\lambda_2$  and  $\lambda_3$ ; several scalar measures of diffusion have been proposed: mean diffusivity (MD), fractional anisotropy (FA), pure isotropic diffusion (p), pure anisotropic diffusion (q), the total magnitude of the diffusion tensor (L), linear tensor (Cl), planar tensor (Cp), spherical tensor (Cs), relative anisotropy (RA), axial diffusivity (AD) and radial diffusivity (RD) [6–10]. Some of these DTI-derived variables have been studied in brain tumours [7, 8]; however, there is still scarce information about the performance of most of these

tensor metrics in the diagnosis of the infiltration zones caused by glioblastoma multiforme (GBM).

We conducted this study to compare the diagnostic accuracy among DTI-derived tensor metrics in the detection of regional tumour infiltration by using the infiltration pattern observed in the T2- and T1-weighted post-contrast images as the reference standard [11]. Our data intend to be a small contribution in understanding the clinical applicability of these available quantitative biomarkers of brain-tumour impairment, which could accelerate the adoption of these image-data analyses in clinical settings.

**Material and methods****Subjects**

Retrospective study using a case and control design. Inclusion criteria considered preoperative brain MR examinations between January 2011 and May 2012 of patients with at first (suspected) diagnosis and later pathological confirmation of primary GBM. Exclusion criteria applied to corticosteroid or antibiotic treatment, lesions with areas related to calcification and/or haemorrhage and previous brain surgery. A control group included young and elderly healthy volunteers recruited among the enrolled interns and medical residents of the hospital as well as elderly subjects from our Geriatrics unit. All volunteers received detailed health examinations; exclusion criteria considered major neurological, psychiatric or cardiovascular diseases. Two radiologists (E.R.V., M.M.L.) interpreted the MR images blinded to the patient's history. MRI examinations with other structural abnormalities were excluded. The local Institutional Review Board approved the study (project no. 2011.044).

**Brain image acquisition**

MR sequences included conventional axial T2-weighted imaging, axial fluid-attenuated inversion recovery (FLAIR), axial spoiled gradient echo (FSPGR), DWI and axial T1-weighted imaging, using 0.1 mmol/kg of body weight of gadopentetate dimeglumine (Magnevist; Schering, Berlin, Germany). DTI was performed using a single-shot SE EPI sequence. Diffusion gradients were applied in 25 directions with b-values of 700 s/mm<sup>2</sup> and an image without diffusion weighting with b-value of 0 s/mm<sup>2</sup>. DTI sequences were acquired in the axial

plane with 44 contiguous sections, 2.4-mm section thickness, no intersection gap, TR/TE of 17,000/80 ms, with imaging in parallel for decreasing the time of acquisition, 25×25 cm FOV and 128×128 matrix size.

MR was performed on a single occasion by using a 3-T unit (Signa HDxt, GE Healthcare, Waukesha, WI, USA) and a high-resolution eight-channel head coil (Invivo, Gainesville, FL, USA).

Image postprocessing and data analysis (DTI tensor-metric formulas) [6–10]

$$\begin{aligned}
 MD = D &= \frac{\lambda_1 + \lambda_2 + \lambda_3}{3} & p &= \sqrt{3D} = \frac{\lambda_1 + \lambda_2 + \lambda_3}{\sqrt{3}} & AD &= \lambda_1 \\
 L &= \sqrt{p^2 + q^2} = \sqrt{\lambda_1^2 + \lambda_2^2 + \lambda_3^2} & q &= \sqrt{(\lambda_1 - D)^2 + (\lambda_2 - D)^2 + (\lambda_3 - D)^2} & C_l &= \frac{\lambda_1 - \lambda_2}{\lambda_1 + \lambda_2 + \lambda_3} \\
 RA &= \frac{q}{p} = \frac{\sqrt{(\lambda_1 - D)^2 + (\lambda_2 - D)^2 + (\lambda_3 - D)^2}}{\sqrt{3D}} & FA &= \sqrt{\frac{3}{2}} \frac{q}{L} = \sqrt{\frac{3}{2}} \sqrt{\frac{(\lambda_1 - D)^2 + (\lambda_2 - D)^2 + (\lambda_3 - D)^2}{\lambda_1^2 + \lambda_2^2 + \lambda_3^2}} & C_p &= \frac{2(\lambda_2 - \lambda_3)}{\lambda_1 + \lambda_2 + \lambda_3} \\
 C_s &= \frac{3\lambda_3}{\lambda_1 + \lambda_2 + \lambda_3} & RD &= \frac{\lambda_2 + \lambda_3}{2}
 \end{aligned}$$

We used the software dcm2nii [12] and the FMRIB Software Library (FSL) v. 4.1.9 [13]; for extraction of DTI images, we used the *Brain Extraction Tool (BET)* v. 2.1 [14]. Eddy currents were corrected using the *FMRIB's Diffusion Toolbox v. 2.0*; the *Reconstruct Diffusion Tensor (DTIFIT)* and the *fslmaths tool* generated the eigenvector and eigenvalue maps for each tensor metric. The *fslstats tool* calculated the scalar measures (mean values) of the selected regions.

For each tumour region, three regions of interest (ROI) with a maximum average size of 10 mm<sup>2</sup> were drawn and manually segmented using *DTIFIT* at three different locations, separated at least 10 mm from the adjacent one: cystic cavity, enhancing rim, an immediate zone of oedema (oedema most adjacent to the enhancing rim, it was arbitrarily chosen as a 10-mm-wide band) and a distant zone of oedema (oedema adjacent to the immediate zone of oedema, chosen also as a 10-mm-wide band). Each enhancing-rim zone was matched with three measurements of normal-appearing white matter (NAWM): one drawn in the patient's contralateral hemisphere and two additional ones drawn in the ipsilateral hemisphere of two healthy volunteers. A total of 15 ROIs were obtained from each patient with four additional ROIs of NAWM matched from normal subjects. An example of the sequences and regions of interest is shown in Fig. 1a–d.

#### Statistical analysis

*Sample size* had two considerations: First, our research was defined as phase I, “exploratory phase” [15], in which a new diagnostic test is first evaluated in a clinical setting to determine whether the test has any ability to discriminate diseased from nondiseased patients. Second, we matched this phase I with the summarised list of computed sample sizes needed for an exploratory retrospective study as

reported by Obuchowski et al. [16]. At least ten diseased patients and ten control patients are required to keep statistical validation in a receiver-operating characteristic (ROC) curve analysis assuming the type I error rate is set at 0.05 and type II error rate is ≤ 0.10, with power ≥ 0.90. Our study included 14 patients and 28 controls.

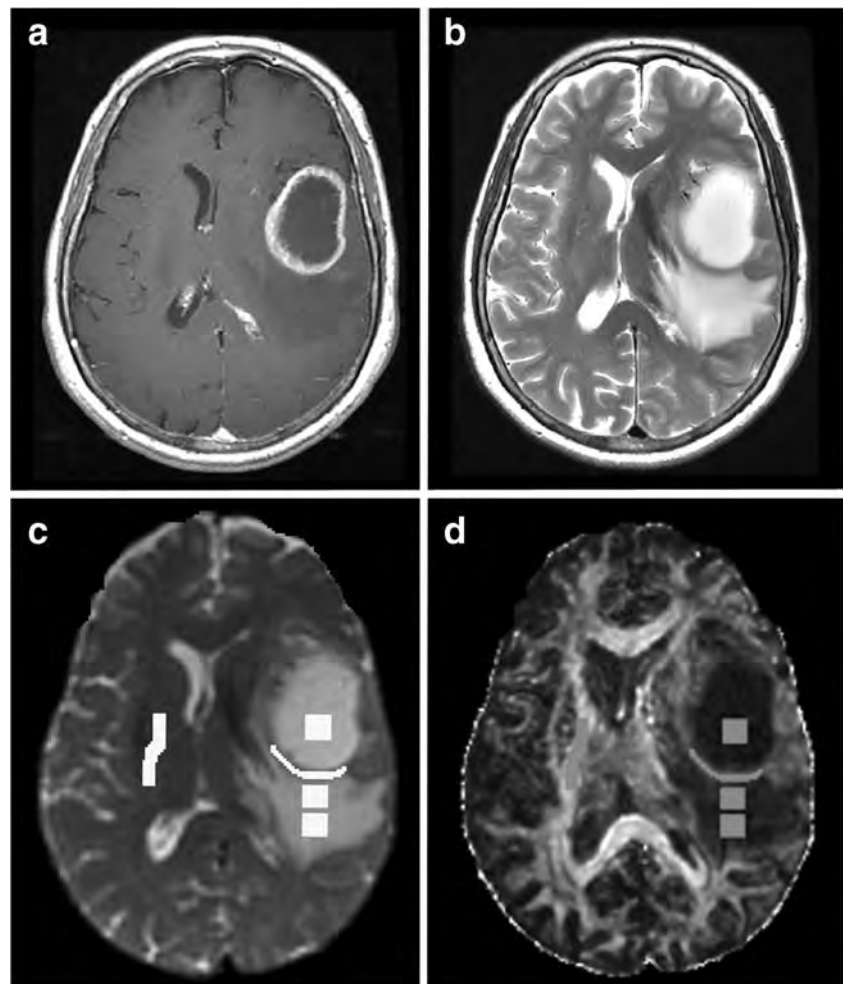
*Evaluations of diagnostic tests* used one-way analysis of variance (ANOVA) [17] and the Student-Newman-Keuls test [18–20] for pairwise comparison of subgroups. The *effect size* was obtained for each ANOVA result using the Eta squared value [21]. It considered 0.01 as a small effect, 0.06 as a medium effect and 0.14 as a large effect [22].

The area under the ROC curve (AUROC) was considered the measure of the overall performance of each tensor metric [23–25]; standard error (SE), p value and its 95 % confidence interval (CI) were also reported. The method of Delong [26] was used for the calculation of SE and pairwise comparisons. Values of sensitivity, specificity, (+) and (–) predictive value, and (+) and (–) likelihood ratios were also displayed. Cutoff ranges represented the optimal cutoff to maximise sensitivity plus specificity for assessment of the presence of the five selected brain regions. The accuracy was determined using a traditional academic point-system classification: 0.90–1 = excellent (A), 0.80–0.90 = good (B), 0.70–0.80 = fair (C), 0.60–0.70 = poor (D) and 0.50–0.60 = fail (F) [27].

*Software* All analyses were carried out using MedCalc® (version 12.2.1 MedCalc Software bvba, Mariakerke, Belgium). Statistical significance was indicated by a *P*-value < 0.05.

*Presentation of data* followed the Standards for Reporting of Diagnostic Accuracy (STARD) initiative [28]. General presentation of the manuscript was prepared in accordance with the guidelines set by the International Committee of Medical Journal Editors [29].

**Fig. 1** **a, b** Conventional MR sequences used in the MRI evaluation of brain tumours showing axial plane T1-weighted post-contrast and T2-weighted images. **c** T2-weighted image in the axial plane generated by the FSL showing the drawn ROIs corresponding to each tumour region. **d** Example of ROI location on FA maps



## Results

### Demographic and quantitative DTI tensor maps

The study was conducted in 14 patients: 6 men (mean age, SD; 51.50±17.74 years; range, 33–78 years) and 8 women (mean age, SD; 49.75±16.54 years; range, 31–73 years). There were 28 controls: 9 men (mean age, SD; 45.78±21.57 years; range, 24–72 years) and 19 women (mean age, SD; 27.21±10.25 years; range, 20–68 years). Ninety-eight ROIs of the NAWM region (from all tensors) and 40 ROIs from each tumour region added 258 measurements included in the analysis.

### Anova analyses and pairwise comparison of subgroups

There was a statistically significant difference with a large effect size for all tensor metrics: MD=0.418; FA=0.532;  $p=0.515$ ;  $q=0.238$ ;  $L=0.461$ ;  $Cl=0.554$ ;  $Cp=0.366$ ;  $Cs=0.627$ ;  $RA=0.616$ ;  $RD=0.576$  and  $AD=0.345$ . Post-hoc tests also showed significant pairwise comparisons within

subgroups of all tensor metrics. Table 1 presents the means and SD within the subgroups of each tensor metric.

### Diagnostic performance of tensor metrics

Among the 55 ROC curves calculated for each patient, the highest performer for each region corresponded to: RA in the NAWM and cystic cavity with an excellent fit (0.944 and 0.829 respectively); RD in the immediate zone of oedema with fair performance (0.708); Cp was the highest for the distant zone of oedema with a fair performance (0.785); q depicted a poor fit (0.642) in the enhancing rim zone. Tables 2 and 3 and Figs. 2 and 3 show the values of the AUROC analyses and the interactive dot diagrams corresponding to the three best performers for each tumour region.

### Pairwise comparison of ROC curves

Significant differences of the tensor metrics in each region were observed only between: RA with Cp, p, MD, L and q in the NAWM; RD with AD in the immediate zone of

**Table 1** Means and SD within subgroups for each tensor metric

Tensor metric	NAWM		Immediate zone of oedema		Distant zone of oedema		Enhancing rim		Cystic cavity	
	Mean	SD	Mean	SD	Mean	SD	Mean	SD	Mean	SD
MD	0.000832	0.000147	0.001519	0.000420	0.001608	0.000253	0.001138	0.000332	0.001951	0.001093
FA	0.513454	0.143641	0.195618	0.122330	0.177375	0.081779	0.241313	0.100363	0.202516	0.215315
p	0.001440	0.000255	0.002630	0.000726	0.002783	0.000438	0.001970	0.000574	0.003698	0.001693
q	0.000666	0.000202	0.000376	0.000150	0.000394	0.000156	0.000384	0.000192	0.000422	0.000483
L	0.001609	0.000240	0.002669	0.000703	0.002819	0.000428	0.002019	0.000581	0.003677	0.001755
CI	0.267629	0.114121	0.082389	0.065540	0.081726	0.047998	0.096443	0.051993	0.058288	0.051932
Cp	0.228388	0.110703	0.099713	0.064011	0.070233	0.032118	0.138498	0.062885	0.080032	0.103336
Cs	0.520621	0.130280	0.819050	0.116676	0.851493	0.061990	0.770997	0.093871	0.861679	0.141119
RA	0.480533	0.155383	0.166486	0.114198	0.147988	0.070564	0.205776	0.091396	0.124237	0.117666
RD	0.000575	0.000190	0.001380	0.000441	0.001456	0.000271	0.000999	0.000313	0.001977	0.000893
AD	0.001352	0.000192	0.001799	0.000402	0.001911	0.000268	0.001417	0.000410	0.002452	0.001226

oedema; Cp with Cs, FA, RA, CI and q at the *distant zone of oedema*; q with FA, RA, Cs and RD in the *enhancing rim zone*; RA with q in the *cystic cavity zone*.

**Discussion**

Diagnostic accuracy studies are a vital step in the evaluation of new diagnostic technologies [30]. They compared results from one or more tests with the results obtained with the reference standard evaluated with the purpose of detecting the target condition [30]. Our findings allowed us to identify which DTI-derived tensor metrics better classified each

selected tumour region in a group of patients with GBM and healthy volunteers.

The clinical relevance of our study has several components: first, we report a comprehensive diagnostic evaluation for each selected region; the top three tensor metrics presented in each region (largest AUROC) did not show statistically significant differences in the pairwise comparisons, meaning they could be used interchangeably. Our study has differences from the one published by Toh et al. [7]: we only compared GBM with a control group of healthy volunteers. The NAWM included measurements of matched ROIs (to the enhancing rim area) from the contralateral hemisphere of patients and the ipsilateral hemisphere of

**Table 2** AUROC analyses of the three best biomarkers at each tumour region

Tumour region	Best DTI-tensor performers	Cutoff value	AUROC	SE	P-value	95 % CI	
						Lower bound	Upper bound
NAWM	RA	>0.3079	0.944	0.0146	<0.0001	0.908	0.969
	Cs	≤0.6286	0.944	0.0153	<0.0001	0.908	0.969
	CI	>0.1518	0.933	0.0153	<0.0001	0.895	0.96
Immediate zone of oedema	RD	>0.0009	0.708	0.0387	<0.0001	0.648	0.764
	FA	≤0.2595	0.700	0.0373	<0.0001	0.640	0.756
	MD	>0.0011	0.695	0.0439	<0.0001	0.635	0.751
Distant zone of oedema	Cp	≤0.0929	0.785	0.0304	<0.0001	0.73	0.835
	MD	>0.0012	0.769	0.028	<0.0001	0.713	0.819
	p	>0.0021	0.765	0.0284	<0.0001	0.708	0.816
Enhancing rim	q	≤0.0005	0.642	0.0434	0.0011	0.580	0.701
	AD	≤0.002	0.614	0.0482	0.0177	0.551	0.675
	CI	≤0.1865	0.613	0.0384	0.0033	0.550	0.673
Cystic cavity	RA	≤0.1623	0.829	0.0385	<0.0001	0.777	0.874
	Cs	>0.8392	0.828	0.0404	<0.0001	0.776	0.873
	CI	≤0.0711	0.821	0.0363	<0.0001	0.768	0.866

**Table 3** Evaluation of diagnostic tests for the three best biomarkers at each tumour region

Tumour region	Best DTI-Tensor performers	Sensitivity		Specificity		+LR		-LR		+PV		-PV	
		Value	95 % CI	Value	95 % CI	Value	95 % CI	Value	95 % CI	Value	95 % CI	Value	95 % CI
NAWM	RA	86.60	78.2–92.7	90.97	85.3–95.0	9.59	8.7–10.5	0.15	0.07–0.3	85.7	77.2–92.0	91.6	86.0–95.4
	Cs	84.54	75.8–91.1	96.13	91.8–98.6	21.84	19.9–23.9	0.16	0.06–0.4	93.2	85.7–97.5	90.9	85.4–94.8
	CI	81.44	72.3–88.6	89.03	83.0–93.5	7.43	6.7–8.3	0.21	0.1–0.4	82.3	73.2–89.3	88.5	82.4–93.0
Immediate zone of oedema	RD	84.62	69.5–94.1	56.07	49.1–62.8	1.93	1.6–2.3	0.27	0.1–0.6	26.0	18.6–34.5	95.2	89.9–98.2
	FA	84.62	69.5–94.1	59.63	52.8–66.2	2.10	1.8–2.5	0.26	0.1–0.5	27.3	19.6–36.1	95.6	90.6–98.4
	MD	87.18	72.6–95.7	57.80	50.9–64.4	2.07	1.8–2.4	0.22	0.10–0.5	27.0	19.5–35.6	96.2	91.3–98.7
Distant zone of oedema	Cp	88.89	73.9–96.9	68.52	61.9–74.7	2.82	2.4–3.3	0.16	0.06–0.4	32.0	23.0–42.1	97.4	93.4–99.3
	MD	100.0	90.3–100	64.25	57.6–70.6	2.8	2.5–3.1	0.00	0.0–0.0	31.3	22.9–40.7	100.0	97.4–100.0
	P	100.0	90.3–100	63.59	56.8–70.0	2.73	2.5–3.0	0.0	0.0–0.0	31.3	23.0–40.6	100.0	93.1–100.0
Enhancing rim	q	73.81	58.0–86.1	49.77	42.9–56.6	1.47	1.2–1.8	0.53	0.3–0.9	22.3	17.7–30.1	90.7	83.9–95.3
	AD	97.62	87.4–99.9	28.91	22.9–35.5	1.37	1.1–1.7	0.082	0.01–0.6	21.5	15.9–28.0	98.4	91.2–100.0
	CI	97.62	87.4–99.9	37.14	30.6–44.1	1.55	1.3–1.9	0.064	0.009–0.4	23.7	17.6–30.7	98.7	93.1–100.
Cystic cavity	RA	84.21	68.7–94.0	71.50	64.9–77.4	2.95	2.5–3.5	0.22	0.1–0.5	34.4	24.9–45.0	96.2	92.0–98.6
	Cs	81.58	65.7–92.3	73.36	66.9–79.2	3.06	2.6–3.6	0.25	0.1–0.5	35.2	25.3–46.1	95.7	91.4–98.3
	CI	81.58	65.7–92.3	72.43	65.9–78.3	2.96	2.5–3.5	0.25	0.1–0.5	34.4	24.7–45.2	95.7	91.3–98.2

healthy volunteers; we followed the basic requisites of a diagnostic test to obtain validity in its results [25].

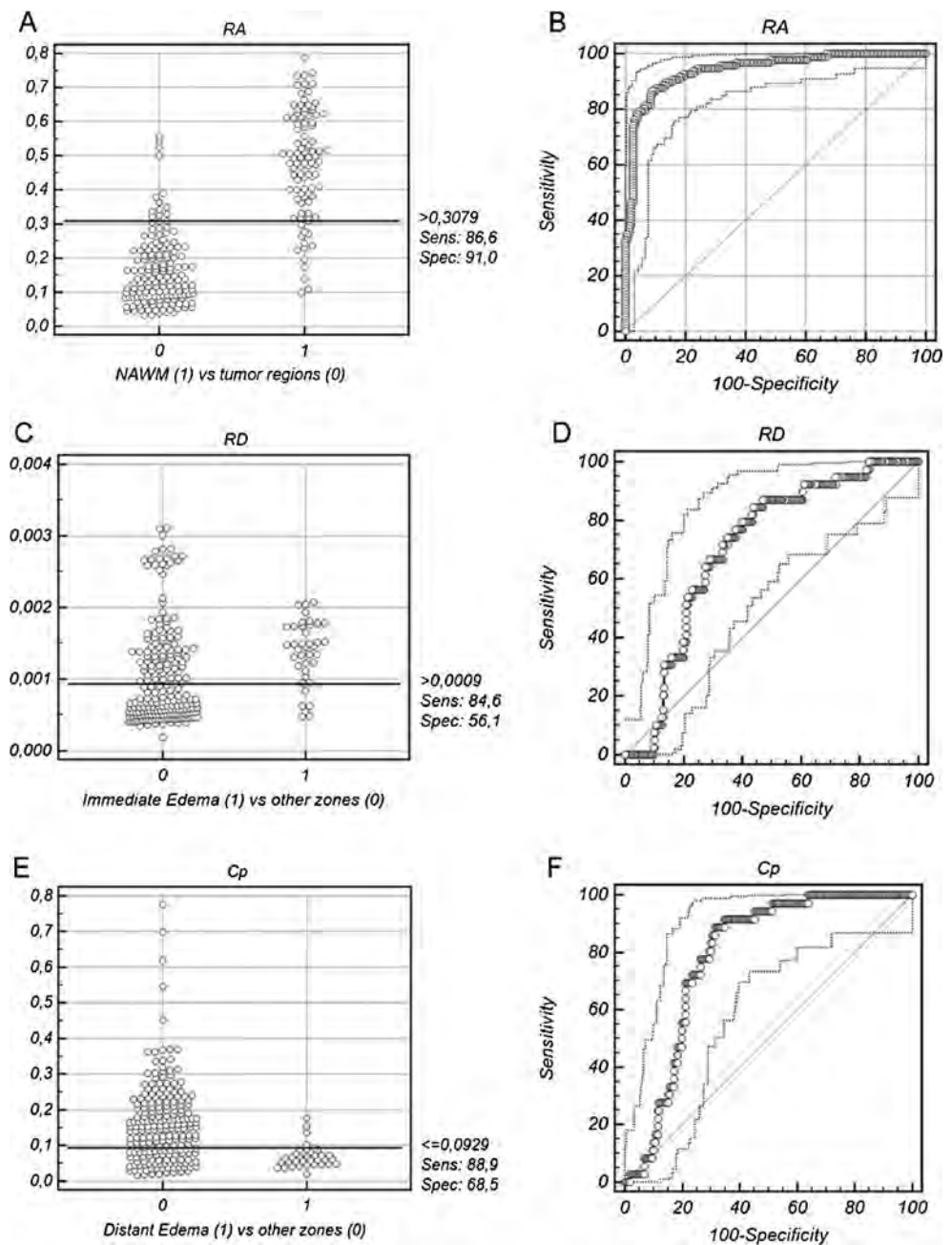
Second, each diagnostic evaluation followed the STARD initiative [28], reporting AUROC, CI, SE and p-values as well as the sensitivity and specificity, (+) and (–) predictive values and (+) and (–) likelihood ratios with their corresponding CI. To the best of our knowledge, although just a few studies have followed this initiative [7, 8], comprehensive evaluations like the one presented in this study are scarce in imaging reports.

Third, we obtained evidence that FA and MD are not the best tensor metrics in any of the five selected regions for this study. These results differ from those presented by Toh et al. [7]. They found that FA was the best biomarker for the cystic cavity and enhancing-rim zones and ADC for the immediate oedema zone. Our results are not necessarily contradictory but might complement the current available information: our pairwise analysis of ROC curve comparisons showed that the top sorted biomarkers for each region could be clinically interchangeable. Our results provide additional hints to clarify tensor metrics' abilities and might unveil underlying behaviours of these biomarkers. An integrative approach could explain why some researchers found significant relationships while others did not.

Fourth, there is still a significant amount of empiricism surrounding the understanding of tensor metrics in each tumour region and their expected cutoff values. In the MR-DTI literature, usually FA and MD are displayed as the accepted biomarkers of brain microstructure; however, the caveat to exclusively using MD and FA to characterise pathology in clinical applications is that it is still not known a priori which tensor measure is the most appropriate to quantify pathological changes in brain tissue [6]. Eventually, there will be a deeper understanding as more studies are reported, especially those including multivariate analysis of biological features presented in patients with brain tumours (gender, age, regional location of tumour, race, etc.).

A grading of the peritumoral oedema in MR images is relevant, considering its role as an independent prognostic factor has been proved. We supported our classification of immediate and distant oedema with the study by Schoenegger et al. [31], who found that when oedema is classified as minor (<1 cm) and major (>1 cm), patients with the presence of major oedema had significantly shorter overall survival compared to patients with minor oedema; also, distant oedema has been correlated with a higher degree of necrosis and vascular endothelial growth factor (VEGF) expression [11]. The higher performance of FA observed in the immediate zone of oedema could explain its mechanism of decrement related to an increase in extracellular space

**Fig. 2** a, c and e Images correspond to the interactive dot diagrams. b, d, and f ROC curves from the NAWM, immediate and distant zones of oedema respectively



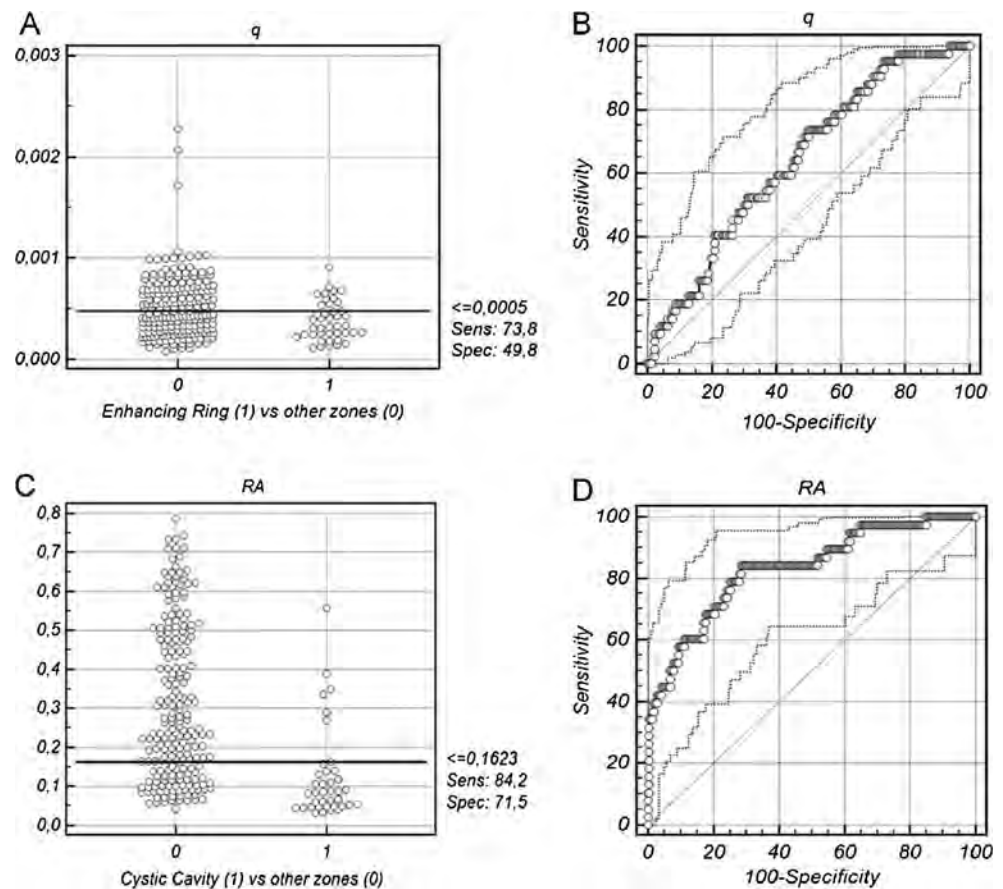
secondary to neuronal and fibre tract destruction [32] or to a reduction in extracellular space secondary to tumour infiltration [33]. The best performance of MD in both oedema zones is explained by its measuring the magnitude of the molecular motion of water, although it does not depend directly on the integrity of myelinated fibre tracts [9].

The best biomarker for the enhancing rim zone was  $q$ , followed by AD and CI. Previous studies on the features of FA have mentioned that the inclusion of the parameter  $q$  may be able to provide a more complete picture of the diffusion profile of a brain tumour

[6]. Price et al. [34] found that in brain tumours, compared with normal white matter, there is a less markedly decreased  $q$  (mean 14 %) in infiltrated white matter, with marked reduction in  $q$  (mean 42 %) in disrupted white matter. AD describes microscopic water movement parallel to axonal tracts and has been associated with acute axonal injury [35]. CI had the worst performance among FA, MD, Cs and Cp in the study by Toh et al. [7]. We hypothesise that the geometric component of linearity in CI accounts for its better discriminant ability for the enhancing rim zone compared with other tensor metrics.



**Fig. 3** **a, c** Images correspond to the interactive dot diagrams. **b** and **d** ROC curves from to the enhancing rim and cystic cavity respectively



For the cystic cavity and the NAWM, RA was the best biomarker followed by Cs and Cl; seven metrics outperformed FA and MD in the former zone and four tensor metrics did in the latter zone. RA is a ratio of the normalised standard deviations between the anisotropic part of the diffusion coefficient and its isotropic part [9]. It is a function of the variance of the eigenvalues of the diffusion tensor, which is not equal to the variance of the diffusivities along all directions [36]. There have not been publications about the clinical applicability of RA in brain tumours; RA has been found to have inferior noise immunity (lower signal-to-noise ratio) than FA for any tensor anisotropy value [37]. We believe the features of the RA definition and the spherical geometric properties of the Cs tensor allowed them to better characterise the cystic cavity and NAWM. The performance of Cs (second position) after RA agrees with the results for Cs published by Toh et al. [7].

Some limitations in this study need to be addressed: DTI's acceptance by the medical community is still limited, mainly because it does not yet reach the anatomic validity of the myeloarchitectonic studies and currently cannot differentiate individual axons or synaptic connections [38]. We consider this project a phase-I study; it was not our purpose to either correlate clinical features of our subjects or to explore prognostic abilities; some readers would like to

know which combinations of metrics increase the sensitivity in a specific region. A binary logistic regression might unveil this answer, but it would require additional analyses and explanations. Thus, the clinical value of our findings has yet to be determined, and the biological impact of the different metrics should be explained in more detail in clinical journals.

There is still scarce information regarding the potential of tensor metrics as biomarkers. This is perhaps because several publications have shown contradictory results for some biomarkers such as FA and MD [8, 39–41]. Our control and patient groups had differences between gender and age distributions; this could influence our measurements, as has been proved for FA and AD with aging. Also, variability due to the size of the selected ROIs should be considered; some papers reported ROIs encompassing the whole enhancing rim or oedema that varied at each subject; in a previous publication from our group [41], we proved the existence of significant FA variability across normal pyramidal tracts, which is influenced by anatomic landmarks and the cerebral hemisphere. Small ROIs (no larger than 10 mm in diameter) might provide less variability by encompassing a smaller number of axonal tracts (each one hypothetically with significantly different DTI values) and explain the lack of agreement among previous reports. A complex

mathematical explanation of the differences in AUROCs for each selected region is beyond the scope of this manuscript, which was written for clinical researchers. Further studies should address if the theoretical definitions of each tensor metric can explain the intricacies of brain tumour behaviour affected by the ratio of extracellular to intracellular space, vascularity, oedema, microcysts and extracellular matrix [42]. This study is part of an on-going project trying to understand the role of tensor metrics in characterising GBM. We are aware of the omission in this study of metabolic data provided by MRI using spectroscopy and perfusion; however, we limited our definitions of regional tumour infiltration and oedema boundaries to those patterns observed in the T1-weighted post-contrast and T2-weighted images, as they have been used as the reference for diagnosis in previous reports [11, 31]. Additional studies including metabolic sequences might help to understand which approach offers the best performance.

Our study makes a contribution toward understanding the fundamentals of the tensors' relationships; this information may help radiologists and/or bio-imaging experts to explain their clinical applicability to clinicians (neurologists, neurosurgeons, oncologists, psychiatrist, paediatricians, etc.). Almost 20 years after the initial definitions of FA and MD [43], there is incomplete understanding of the relationships between brain structure and tensor metrics; they might answer different questions. Also, variations in DTI measures are not specific to one histological type of tumour, which broadens the application of these biomarkers to a wide variety of intracranial lesions. Nowadays, DTI-derived biomarkers can characterise the regional impairment of intraaxial brain tumours; in the short term we expected that an advanced quantitative analysis of DTI-derived tensor metrics might be accepted in clinical practice, depending on the interest of the clinicians, for screening of patients, triaging patients presenting with symptoms suggestive of progression and/or follow-up to evaluate treatment response (radiotherapy).

**Acknowledgments** David Cortez-Conradis received a scholarship from the Autonomous University of Mexico State, UAEMex (*Becca Enlace de investigacion*), from August 2010 to July 2012.

Rafael Favila is an expert in advanced MRI applications from GE Healthcare. He participated in the planning of brain MRI, image post-processing with the FSL software and manuscript preparation.

The authors thank to Arturo Arrieta, Carlos Cobos and the rest of the MRI technologists from the MRI Unit at Medica Sur Clinic & Foundation for their assistance with brain MR acquisitions.

**Conflict of interest** The authors who have taken part in this study declared that they do not have anything to disclose regarding funding or conflict of interest with respect to this manuscript. The authors who have taken part in this study did not have a relationship with the manufacturers of the drugs involved in either the past or present and did not receive funding from the manufacturers to carry out their research.

## References

1. Young GS (2007) Advanced MRI of adult brain tumors. *Neurol Clin* 25:947–973
2. Basser PJ, Pierpaoli C (1996) Microstructural and physiological features of tissues elucidated by quantitative-diffusion-tensor MRI. *J Magn Reson B* 111:209–219
3. Lu S, Ahn D, Johnson G, Law M, Zagzag D, Grossman RI (2004) Diffusion-tensor MR imaging of intracranial neoplasia and associated peritumoral edema: introduction of the tumor infiltration index. *Radiology* 232:221–228
4. Chenevert TL, Brunberg JA, Pipe JG (1990) Anisotropic diffusion in human white matter: demonstration with MR techniques in vivo. *Radiology* 177:401–405
5. Basser PJ, Mattiello J, LeBihan D (1994) MR diffusion tensor spectroscopy and imaging. *Biophys J* 66:259–267
6. Pena A, Green HA, Carpenter TA, Price SJ, Pickard JD, Gillard JH (2006) Enhanced visualization and quantification of magnetic resonance diffusion tensor imaging using the p:q tensor decomposition. *Br J Radiol* 79:101–109
7. Toh CH, Wei KC, Ng SH, Wan YL, Lin CP, Castillo M (2011) Differentiation of brain abscesses from necrotic glioblastomas and cystic metastatic brain tumors with diffusion tensor imaging. *AJNR Am J Neuroradiol* 32:1646–1651
8. Wang W, Steward CE, Desmond PM (2009) Diffusion tensor imaging in glioblastoma multiforme and brain metastases: the role of p, q, L, and fractional anisotropy. *AJNR Am J Neuroradiol* 30:203–208
9. Le Bihan D, Mangin JF, Poupon C et al (2001) Diffusion tensor imaging: concepts and applications. *J Magn Reson Imaging JMRI* 13:534–546
10. Freund P, Wheeler-Kingshott C, Jackson J, Miller D, Thompson A, Ciccarelli O (2010) Recovery after spinal cord relapse in multiple sclerosis is predicted by radial diffusivity. *Mult Scler* 16:1193–1202
11. Seidel C, Dorner N, Osswald M et al (2011) Does age matter?—A MRI study on peritumoral edema in newly diagnosed primary glioblastoma. *BMC Cancer* 11:127
12. Rorden C, Karnath HO, Bonilha L MRICron dicom to nifti converter(ed)(eds). Neuroimaging Informatics Tools and Resources Clearinghouse (NITRC). <http://www.mccauslandcenter.sc.edu/mricro/mricron/dcm2nii.html> Accessed June 07, 2012
13. Smith SM, Jenkinson M, Woolrich MW, Beckmann CF, Behrens TEJ, Johansen-Berg H, Bannister PR, De Luca M, Drobnjak I, Flitney DE, Niazy R, Saunders J, Vickers J, Zhang Y, De Stefano N, Brady JM, Matthews PM (2004) Advances in functional and structural MR image analysis and implementation as FSL. *NeuroImage* 23(S21):208–221
14. Smith SM (2002) Fast robust automated brain extraction. *Hum Brain Mapp* 17:143–155
15. Zhou XH, Obuchowski NA, McClish DK (2002) Statistical methods in diagnostic medicine. Wiley & Sons Interscience, New York
16. Obuchowski NA, McClish DK (1997) Sample size determination for diagnostic accuracy studies involving binormal ROC curve indices. *Stat Med* 16:1529–1542
17. Pallant J (2011) One-way analysis of variance. In: Pallant J (ed) SPSS Survival Manual, 4th edn. Allen & Unwin, Crows Nest, pp 249–264
18. Student (1927) Errors of routine analysis. *Biometrika* 19:151–164
19. Newman D (1939) The distribution of range in samples from a normal population, expressed in terms of an independent estimate of standard deviation. *Biometrika* 31:20–30
20. Keuls M (1952) The use of the “studentized range” in connection with an analysis of variance. *Euphytica* 1:112–122
21. Pallant J (2011) Calculating effect size. In: Pallant J (ed) SPSS Survival Manual, 4th edn. Allen & Unwin, Crows Nest, pp 254–255
22. Cohen JW (1988) Statistical power analysis for the behavioral sciences. Lawrence Erlbaum Associates, Hillsdale

23. Park SH, Goo JM, Jo CH (2004) Receiver operating characteristic (ROC) curve: practical review for radiologists. *Korean J Radiol* 5:11–18
24. Hanley JA, McNeil BJ (1982) The meaning and use of the area under a receiver operating characteristic (ROC) curve. *Radiology* 143:29–36
25. Obuchowski NA (2003) Receiver operating characteristic curves and their use in radiology. *Radiology* 229:3–8
26. DeLong ER, DeLong DM, Clarke-Pearson DL (1988) Comparing the areas under two or more correlated receiver operating characteristic curves: a nonparametric approach. *Biometrics* 44:837–845
27. Metz CE (1978) Basic principles of ROC analysis. *Semin Nucl Med* 8:283–298
28. Bossuyt PM, Reitsma JB, Bruns DE et al (2003) The STARD statement for reporting studies of diagnostic accuracy: explanation and elaboration. *Ann Intern Med* 138:W1–W12
29. (1997) Uniform requirements for manuscripts submitted to biomedical journals. International Committee of Medical Journal Editors. *N Engl J Med* 336:309–315
30. Guyatt GH, Tugwell PX, Feeny DH, Haynes RB, Drummond M (1986) A framework for clinical evaluation of diagnostic technologies. *CMAJ Can Med Assoc J J Assoc Med Can* 134:587–594
31. Schoenegger K, Oberndorfer S, Wuschitz B et al (2009) Peritumoral edema on MRI at initial diagnosis: an independent prognostic factor for glioblastoma? *Eur J Neurol Off J Eur Fed Neurol Soc* 16:874–878
32. Wieshmann UC, Clark CA, Symms MR, Franconi F, Barker GJ, Shorvon SD (1999) Reduced anisotropy of water diffusion in structural cerebral abnormalities demonstrated with diffusion tensor imaging. *Magn Reson Imaging* 17:1269–1274
33. Stadlbauer A, Ganslandt O, Buslei R et al (2006) Gliomas: histopathologic evaluation of changes in directionality and magnitude of water diffusion at diffusion-tensor MR imaging. *Radiology* 240:803–810
34. Price SJ, Pena A, Burnet NG et al (2004) Tissue signature characterisation of diffusion tensor abnormalities in cerebral gliomas. *Eur Radiol* 14:1909–1917
35. Budde MD, Xie M, Cross AH, Song SK (2009) Axial diffusivity is the primary correlate of axonal injury in the experimental autoimmune encephalomyelitis spinal cord: a quantitative pixelwise analysis. *J Neurosci Off J Soc Neurosci* 29:2805–2813
36. Ozarslan E, Vemuri BC, Mareci TH (2005) Generalized scalar measures for diffusion MRI using trace, variance, and entropy. *Magn Reson Med* 53:866–876
37. Hasan KM, Alexander AL, Narayana PA (2004) Does fractional anisotropy have better noise immunity characteristics than relative anisotropy in diffusion tensor MRI? An analytical approach. *Magn Reson Med* 51:413–417
38. Jones DK (2008) Studying connections in the living human brain with diffusion MRI. *Cortex J Devoted Stud Nerv Syst Behav* 44:936–952
39. Tsuchiya K, Fujikawa A, Nakajima M, Honya K (2005) Differentiation between solitary brain metastasis and high-grade glioma by diffusion tensor imaging. *Br J Radiol* 78:533–537
40. van Westen D, Latt J, Englund E, Brockstedt S, Larsson EM (2006) Tumor extension in high-grade gliomas assessed with diffusion magnetic resonance imaging: values and lesion-to-brain ratios of apparent diffusion coefficient and fractional anisotropy. *Acta Radiol* 47:311–319
41. Roldan-Valadez E, Rios-Piedra E, Favila R, Alcauter S, Rios C (2012) Diffusion tensor imaging-derived measures of fractional anisotropy across the pyramidal tract are influenced by the cerebral hemisphere but not by gender in young healthy volunteers: a split-plot factorial analysis of variance (ANOVA). *Chin Med J* 125:2180–2187
42. Brunberg JA, Chenevert TL, McKeever PE et al (1995) In vivo MR determination of water diffusion coefficients and diffusion anisotropy: correlation with structural alteration in gliomas of the cerebral hemispheres. *AJNR Am J Neuroradiol* 16:361–371
43. Basser PJ (1995) Inferring microstructural features and the physiological state of tissues from diffusion-weighted images. *NMR Biomed* 8:333–344

# Global diffusion tensor imaging derived metrics differentiate glioblastoma multiforme vs. normal brains by using discriminant analysis: introduction of a novel whole-brain approach

Ernesto Roldan-Valadez<sup>1</sup>, Camilo Rios<sup>2</sup>, David Cortez-Conradis<sup>1</sup>, Rafael Favila<sup>3</sup>, Sergio Moreno-Jimenez<sup>4</sup>

<sup>1</sup> Magnetic Resonance Unit, Medica Sur Clinic & Foundation, Mexico City, Mexico

<sup>2</sup> Department of Neurochemistry, National Institute of Neurology and Neurosurgery, Mexico City, Mexico

<sup>3</sup> GE Healthcare, Mexico city. Mexico

<sup>4</sup> Radioneurosurgery Unit, National Institute of Neurology and Neurosurgery, Mexico City, Mexico

Radiol Oncol 2014; 48(0): 000-00.

Received 15 October 2013

Accepted 21 December 2013

Correspondence to: Ernesto Roldan-Valadez, Coordination of Research & Innovation, Magnetic Resonance Unit, Medica Sur Clinic & Foundation, Puente de Piedra 150, Toriello Guerra, Tlalpan, CP 14050, Mexico City, Mexico. E-mail: ernest.roldan@usa.net

Disclosure: No potential conflicts of interest were disclosed.

**Background.** Histological behavior of glioblastoma multiforme suggests it would benefit more from a global rather than regional evaluation. A global (whole-brain) calculation of diffusion tensor imaging (DTI) derived tensor metrics offers a valid method to detect the integrity of white matter structures without missing infiltrated brain areas not seen in conventional sequences. In this study we calculated a predictive model of brain infiltration in patients with glioblastoma using global tensor metrics.

**Methods.** Retrospective, case and control study; 11 global DTI-derived tensor metrics were calculated in 27 patients with glioblastoma multiforme and 34 controls: mean diffusivity, fractional anisotropy, pure isotropic diffusion, pure anisotropic diffusion, the total magnitude of the diffusion tensor, linear tensor, planar tensor, spherical tensor, relative anisotropy, axial diffusivity and radial diffusivity. The multivariate discriminant analysis of these variables (including age) with a diagnostic test evaluation was performed.

**Results.** The simultaneous analysis of 732 measures from 12 continuous variables in 61 subjects revealed one discriminant model that significantly differentiated normal brains and brains with glioblastoma: Wilks'  $\lambda = 0.324$ ,  $\chi^2(3) = 38.907$ ,  $p < .001$ . The overall predictive accuracy was 92.7%.

**Conclusions.** We present a phase II study introducing a novel global approach using DTI-derived biomarkers of brain impairment. The final predictive model selected only three metrics: axial diffusivity, spherical tensor and linear tensor. These metrics might be clinically applied for diagnosis, follow-up, and the study of other neurological diseases.

Key words: brain neoplasms; diffusion tensor imaging; discriminant analysis; magnetic resonance imaging; predictive value of tests

## Introduction

Some pathologic and magnetic resonance (MR) imaging characteristics of astrocytomas grades II to IV (highest degree known as glioblastoma multiforme, GBM) suggest these tumors would benefit from the use of a global measurement of brain impairment.<sup>1</sup>

The first imaging approaches to characterize high-grade glial lesions, especially GBM, were fraught with pitfalls resulting from the marked heterogeneity of both glial-infiltrated and normal brains.<sup>2,3</sup> These tumors frequently contain multiple areas of variable histologic features, so that a sampling error in a biopsy may mean that the degree of

malignancy seen by the neuropathologist may not reflect the degree of malignancy present elsewhere in the tumor, resulting in significant undergrading of some lesions.<sup>2</sup> Thus, even when all radiologically visible portions of a tumor have been excised, the surgical margins may not be “clean”, and further neoplastic growth can (and usually does) occur in the adjacent brain tissue, leading from microscopic residual to gross recurrence.<sup>4</sup> Therefore, none of the MR protocols for GBM in every day practice should be only morphologic.<sup>3,5,6</sup> As a consequence, surgery usually only reduces the tumor; this information is relevant as recent evidence has proved gross total resection (surgical margin status) significantly correlates with progression-free, recurrence pattern and overall survival in patients with GBM.<sup>7,8</sup>

GBM is considered a whole brain disease. Radiotherapy and chemotherapy follow surgery.

Although MR perfusion and spectroscopy<sup>9</sup>, and sometimes diffusion tensor imaging (DTI)<sup>10</sup> are routinely used methods to locate parts of the tumor-GBM with high malignancy that should be biopsied, the development of specific and sensitive biomarkers remains a critical unmet need.<sup>11</sup>

Our purpose in this study was to explore the diagnostic ability of a *global* (whole brain) assessment of DTI-derived tensor metrics in normal and infiltrated brains with GBM. We used the multivariate technique of linear discriminant analysis (DA), previously reported in MRI diagnosis<sup>12</sup>, to classify the study participants into groups, describe group differences and to assess the relative importance of DTI variables for discriminating between groups. This analysis might unveil findings and associations that cannot, in a partial-regional assessment, be recognized at surgery, neurologic, MRI and/or pathologic examination. Considering there is still scarce information in the medical literature about the global calculation of tensor metrics<sup>13,14</sup>, a predictive discriminating model may offer an innovative diagnostic approach to the surgical-neuro-oncology team.

## Subjects and methods

### Subjects

This was a case-control study. We included patients with suspected diagnosis and later pathological confirmation of primary GBM who had undergone preoperative brain MR examinations between January 2010 and September 2012. Exclusion criteria were corticosteroid or antibiotic treatment,

lesions with areas related to calcification and/or hemorrhage and previous brain surgery. A control group included young and elderly healthy volunteers recruited from the enrolled interns and medical residents of the hospital, and elderly subjects from our Geriatrics unit. All volunteers received detailed health examinations; exclusion criteria were major neurological, psychiatric, or cardiovascular diseases. A radiologist interpreted the MR images blinded to the patient's history and MRI examinations with other structural abnormalities were excluded. The local institutional review board approved the study (Project #2011-EXT-05).

### Brain image acquisition

MR sequences included conventional axial T2-weighted imaging, axial Fluid-Attenuated Inversion Recovery (FLAIR), axial Spoiled Gradient Echo (SPGR), DWI and axial T1-weighted imaging, using 0.1 mmol/kg of body weight of gadopentetate dimeglumine (Magnevist; Schering, Berlin, Germany). Healthy volunteers did not receive endogenous contrast. DTI was performed using a single-shot SE EPI sequence. Diffusion gradients were applied in 25 directions with b-values of 1000 s/mm<sup>2</sup> and an image without diffusion weighting with b-value of 0 s/mm<sup>2</sup>. DTI sequences were acquired in the axial plane with 44 contiguous sections, 2.4 mm section thickness, no intersection gap; TR/TE of 17,000/80 ms, with parallel imaging to reduce off-resonance artifacts (PI factor was 2); 25 × 25 cm FOV; and 128 × 128 matrix/pixel size. MR was performed on a single occasion using a 3T unit (Signa HDxt, GE Healthcare, Waukesha, WI, USA); and a high-resolution eight-channel head coil (Invivo, Gainesville, FL, USA).

### Image postprocessing and data analysis

We used the software dcm2nii<sup>15</sup> and the FMRIB Software Library (FSL) v. 4.1.9.<sup>16</sup> DTI images were extracted using the *Brain Extraction Tool (BET)* v. 2.1.<sup>17</sup> Eddy currents were corrected using the *FMRIB's Diffusion Toolbox v. 2.0*; the *Reconstruct Diffusion Tensor (DTIFIT)* and the *fslmaths* tool generated the eigenvector and eigenvalue maps for each tensor metric. The *fslstats* tool calculated the scalar measures (mean values) of each whole-brain calculation. The apparent diffusion coefficient (ADC) value, a simple index calculated from diffusion-weighted images<sup>18</sup>, was considered equivalent to the MD (mean diffusivity) metric, as it was obtained from the DTI sequence.<sup>19</sup> DTI-derived tensor

TABLE 1. Correlations of tensor metrics, controlled for the effect of diagnosis, age and gender

Tensor metric											
FA	Pearson's R	-.552	FA								
	p-value	< .001									
RA	Pearson's R	-1.000	RA								
	p-value	< .001		< .001							
Cp	Pearson's R	-.937	Cp								
	p-value	< .001		< .001	< .001						
CI	Pearson's R	-.898	CI								
	p-value	< .001		< .001	< .001	< .001					
L	Pearson's R	.211	L								
	p-value	.165		.596	.256	.213	.999				
p	Pearson's R	.195	p								
	p-value	.205		.580	.240	.214	.972	< .001			
AD	Pearson's R	.034	AD								
	p-value	.826		.137	.958	.989	.508	< .001	< .001		
MD	Pearson's R	.195	MD								
	p-value	.206		.589	.241	.214	.968	< .001	< .001	< .001	
RD	Pearson's R	.213	RD								
	p-value	.151		.103	.163	.316	.502	< .001	< .001	< .001	< .001
q	Pearson's R	-.306	q								
	p-value	.031		< .001	.030	.016	.026	.003	.046	< .001	.044

AD = axial diffusivity; CI = linear tensor; Cp = planar tensor; Cs = spherical tensor; FA = fractional anisotropy; L = the total magnitude of the diffusion tensor; MD = mean diffusivity; p = pure isotropic diffusion; q = pure anisotropic diffusion; RA = relative anisotropy; RD = radial diffusivity

metrics formulas using the major ( $\lambda_1$ ), intermediate ( $\lambda_2$ ), and minor ( $\lambda_3$ ) eigenvalues allowed the calculation of the eleven most common tensor metrics for brain imaging; mean diffusivity (MD), fractional anisotropy (FA), pure isotropic diffusion (p), pure anisotropic diffusion (q), the total magnitude of the diffusion tensor (L), linear tensor (CI), planar tensor (Cp), spherical tensor (Cs), relative anisotropy (RA), axial diffusivity (AD) and radial diffusivity (RD)<sup>10</sup>; each one representing a single global measure of the whole-brain. Figure 1A shows the algorithm for measuring the DTI-derived tensor metrics.

**Statistical analysis**

*Study design*

The study was considered a Phase II aimed to determine the capacity of DTI-derived biomarkers to

distinguish between people with cancer and those without.<sup>20</sup>

*Sample size*

Considering our predictive model to discriminate between normal brains vs. brains infiltrated with GBM underwent a diagnostic performance assessment, the adequacy of the sample size to expect validity from our results was based on matching this phase with the summarized list of computed sample sizes needed for an exploratory retrospective study reported by Obuchowski *et al.*<sup>21</sup>, at least 10 diseased patients and 10 control patients were required to maintain statistical validation in a diagnostic test evaluation where the type I error rate was set at 0.05, type II error rate was  $\leq 0.10$ , and power  $\geq 0.90$ . Our study included 27 patients and 34 controls.

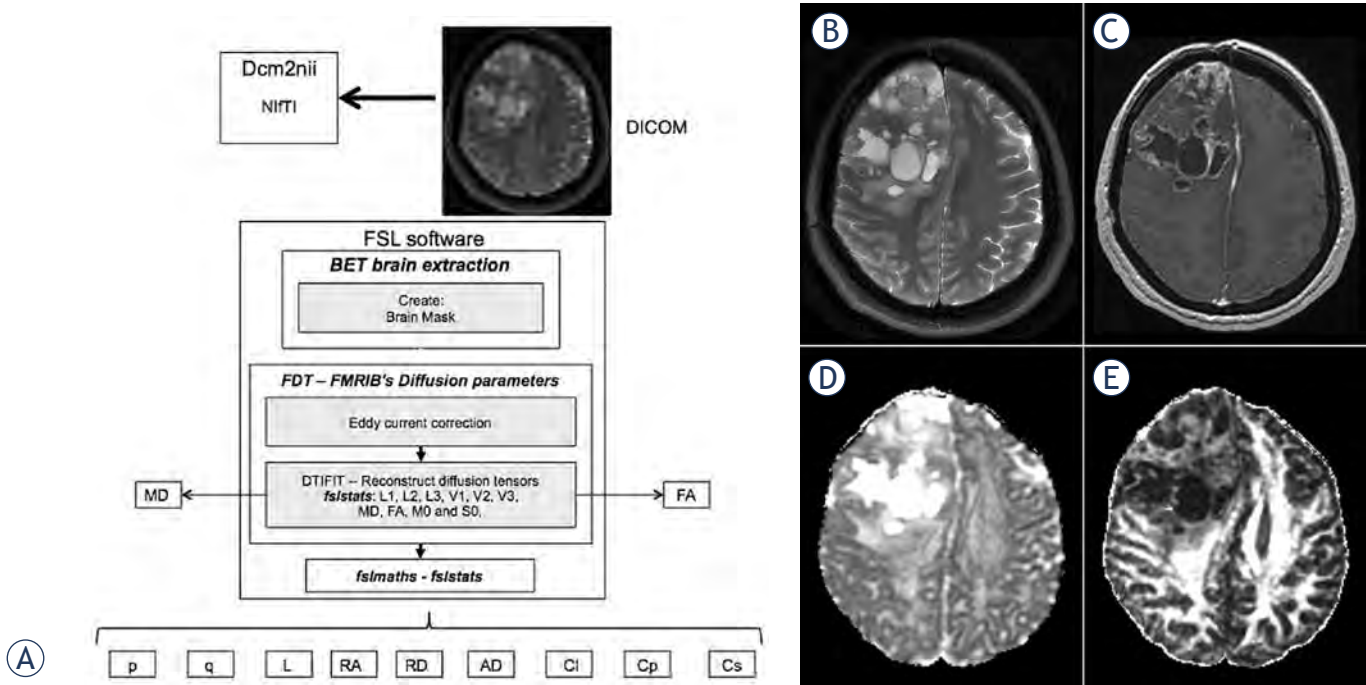


**FIGURE 1.** (A), FSL software algorithm used in the image postprocessing and data analyses. (B-E), Examples of acquired sequences in a patient with GBM and the tensor-metric maps generated for the data analyses: (B), axial T2-weighted; (C), post contrast axial T1-weighted; (D), axial diffusivity (AD) tensor map; and (E), fractional anisotropy (FA) tensor map. Notice how it might not be possible to perform an imaging diagnosis based only on a visual inspection of these maps.

### Multivariate DA

We ran a DA, which was optimal under the same conditions where Manova was optimal; then attempted to detect any deviation from Manova assumptions that might distort the tests of statistical significance.<sup>22</sup> We assessed the normality of the distribution of the DTI-derived scores using the Kolmogorov-Smirnov's and Shapiro-Wilk normality tests<sup>23</sup>; eliminated significant outliers, evaluated multivariate normality and linearity, and tested the homogeneity of variance-covariance matrices using the Box's M test.<sup>24</sup> Considering the similarity of the tensor-metric formulae, we ran scatterplots and correlations to check the strength of correlations among the dependent variables in order to detect the presence of multicollinearity and singularity (Table 1). Partial correlation analyses were carried out to calculate the Pearson's correlation coefficient ( $r$ ) controlling for the effect of age, gender and clinical diagnosis. The strength of the linear relationship corresponding to each correlation coefficient value was interpreted as very strong (at least of 0.8), moderately strong (0.6 up to 0.8), fair (0.3 up to 0.6) and poor (less than 0.3). A squared  $r$  value represented the coefficient of determination, the proportion of variance that each two compared variables had in common.<sup>25</sup>

We applied the stepwise method in DA, it considered the value of Wilk's lambda and changing criteria: minimum partial F to enter of 3.84 and minimum partial F to remove of 2.71.<sup>22</sup> Continuous variables were included with the predictive aim to identify specific tensor-metric attributes in GBM and normal brains. The dependent variable (DV) used in the DA was the clinical diagnosis, which classified subjects as patients or controls. The independent variables (IVs) included 11 DTI-derived tensor metrics: MD, FA,  $p$ ,  $q$ ,  $L$ ,  $CI$ ,  $Cp$ ,  $Cs$ ,  $RA$ ,  $RD$  and  $AD$ , and the patients' age (in years). The effect-size measure for discriminant analysis was calculated using the squared canonical correlation as the equivalent of the  $R^2$  in regression.<sup>26</sup> By convention, effect sizes of 0.02, 0.15, and 0.35 are termed small, medium, and large, respectively.<sup>27</sup> For all analyses, statistical significance was indicated by a  $p$ -value < 0.05.

### Diagnostic model evaluation

The cross-validated contingency Table generated by the DA was used to evaluate the diagnostic performance of the DA model. We reported values of sensitivity, specificity, positive and negative likelihood ratios, and positive and negative predictive values, with their corresponding confidence in-

**TABLE 2.** Multivariate analysis (between-groups) of diffusion tensor imaging (DTI)-derived tensor metrics and age showing the statistical differences between means of normal-brain and brain-with- as glioblastoma multiforme (GBM) groups for the independent variables included in the analysis

Variable	Healthy brains		Brains with GBM		Wilks' Lambda	F test	p-value
	Mean	SD	Mean	SD			
Cs (spherical tensor)	.747091	.026938	.768395	.042299	.915	3.341	.076
FA (fractional anisotropy)	.287029	.011517	.254082	.026761	.607	23.341	< .001
RA (relative anisotropy)	.233436	.025491	.209370	.033559	.855	6.088	.018
Cp (planar tensor)	.138366	.013823	.136635	.036218	.999	.036	.850
Cl (linear tensor)	.114543	.013991	.098463	.011930	.711	14.621	.001
L (total magnitude of the diffusion tensor)	.002277	.000087	.002117	.000147	.691	16.077	< .001
p (pure isotropic diffusion)	.002107	.000077	.001959	.000134	.681	16.893	< .001
AD (axial diffusivity)	.001548	.000044	.001399	.000087	.461	42.052	< .001
MD (mean diffusivity)	.001217	.000044	.001132	.000078	.685	16.526	< .001
RD (radial diffusivity)	.001051	.000050	.000997	.000078	.852	6.237	.017
q (pure anisotropic diffusion)	.000452	.000036	.000367	.000047	.483	38.529	< .001
Age	40.333	21.502	47.150	15.187	.965	1.294	.263

SD = standard deviation

tervals (CI). Evaluation of the diagnostic tests followed the Standards for Reporting of Diagnostic Accuracy (STARD) initiative.<sup>28</sup>

#### Software

All analyses were carried out using the IBM® SPSS® Statistics software (version 22.0.0.0 IBM Corporation; Armonk, NY, USA). Diagnostic performance was assessed using MedCalc® (version 12.3.0.0 MedCalc Software bvba, Mariakerke, Belgium).

## Results

### Subjects and MRI acquisition

The study was conducted in 61 subjects; 27 patients: 13 females (mean age 50.0 ± 15.400 years, range 31–73 years) and 14 males (mean age 46.93 ± 15.403 years, range 18–78 years); and 34 controls: 26 females (mean age 41.04 ± 22.37 years, range 21–80 years) and 8 males (mean age 42.88 ± 21.89 years, range 24–72 years). The eleven DTI tensor-maps plus the age (per subject) added up 732 measurements included in the analyses. Figure 1 B-E shows examples of some of the MR sequences and tensor-metric maps used in the data analyses.

### Partial correlation analyses

A scatterplot showed no serious violation of the assumptions of linearity, homoscedasticity, and

outliers. Among 55 pairs of bivariate correlations, we found only 15 with a significantly very strong (at least 0.8) r value: Cs↔RA (-), Cs↔Cp (-), Cs↔L (-), FA↔q (+), RA↔Cp (+), RA↔Cl (+), L↔p (+), L↔AD (+), L↔MD (+), L↔RD (+), p↔AD (+), p↔MD (+), p↔RD (+), AD↔MD (+), and MD↔RD (+). Table 1 and Figure 2 depict correlation values and the scatterplot of the eleven tensor-metrics.

### Discriminant analysis

Although some r values were calculated at > 0.8, we included all variables in the DA, as we found evidence the stepwise variant of this method protects against multicollinearity and singularity;<sup>29</sup> a brief explanation is presented in the discussion section. The assumption of homogeneity of variance-covariance matrices was interpreted as significant (Box's M value = 35.110, F = 5.317, df (6, 9087.738), p = < .001). In the stepwise statistics, at each step, the best variable that minimized the overall Wilks' Lambda was entered: AD was entered at Step 1, F = 42.052 (1, 36) p < .001; Cl entered at Step 2, F = 29.609 (2, 35) p < .001; and Cs entered at Step 3, F = 23.672 (3, 34) p < .001.

DA revealed one discriminant function that significantly differentiated the normal brains and GBM brains: Wilks' λ = 0.324, χ<sup>2</sup> (3) = 38.907, p < .001. By indicating the significance of the discriminant function, Wilks' lambda provided a moderate proportion of total variability not explained by the model of 10.49%. A canonical correlation of 0.822



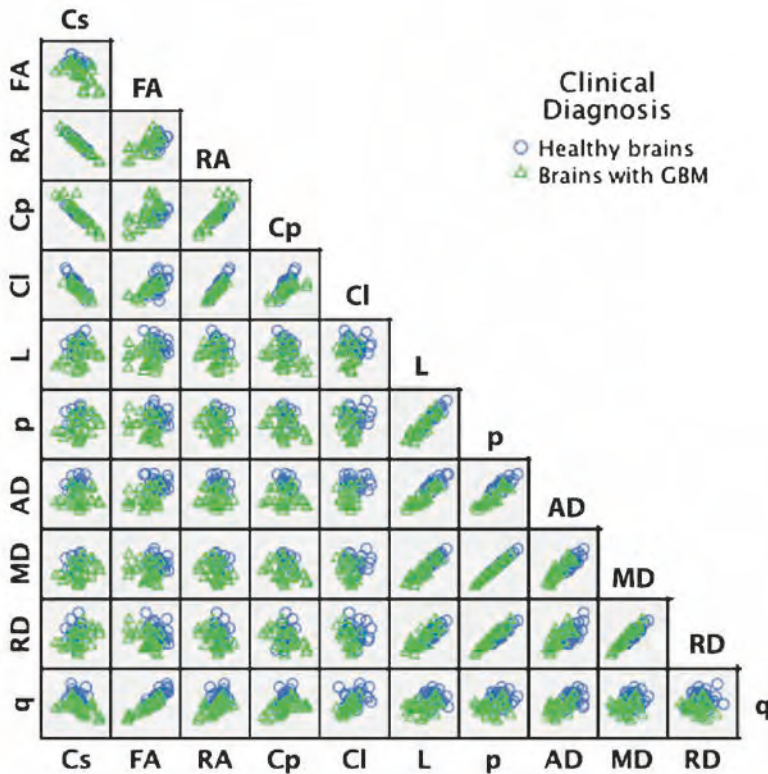


FIGURE 2. Scatter matrix of the data variables grouped by diagnosis.

suggested the model explains 67.56% of the variation in the grouping variable.

### Summary of discriminant functions

The tests of equality of group means provided statistical evidence of significant differences between means of normal brains and brains with GBM in 9 of the IVs, with AD producing the highest F's value; Table 2 depicts the means, standard deviations (SD) and F's tests values (between-groups multivariate analysis).

*Standardized canonical discriminant function coefficients* showed an index of the importance of each predictor for diagnosis with the sign indicating the direction of the relationship. A significant increase in values of Cs (spherical tensor), Cl (linear tensor) and AD (axial diffusivity) were the strongest diagnostic predictors. The variable coefficients stood out (for these data) as those that strongly predicted allocation to the normal-brain or tumor-brain group. The coefficient score decrement was proportional to less successful diagnostic predictors (Table 3A).

*Structure Matrix Data* provided another way of indicating the relative importance of the diagnostic predictors by showing the correlations (Pearson

coefficients) of each variable with each discriminate function. Many researchers consider the structure matrix correlations more accurate than the standardized canonical discriminant function coefficients.<sup>26</sup> By identifying the largest loadings for each discriminate function, different patterns of loading variables can be seen. We found AD, MD, p, q, Cl, RD and FA, as the functions that best discriminate between normal brains and brains with tumor. A value of 0.30 was considered as the cut-off between important and less important variables (Table 3B).<sup>30</sup>

The canonical discriminant function coefficients Table showed the unstandardized coefficients (b) that were used to create the discriminant function (equation), they operated just like a regression equation, allowing us to build a predictive model of brain status:

*Brain status (normal brain vs. tumor infiltration) = -48.295 +11,443.557 (axial diffusivity, AD) +105.124 (longitudinal tensor, Cl) +26.804 (spherical tensor, Cs)*

The discriminant function coefficients (b) indicated the partial contribution of each variable to the discriminate function controlling all other variables in the equation (Table 3C).

The group centroids values described each group in terms of its profile, using the group means of the predictor variables called centroids. The cut-off value was defined as the mean of the two centroids; if the discriminant score of the function of a new case was less than or equal to the cut-off, the case was classed as 1 (brain with tumor), whereas if it was above the cut-off, it was classed as 0 (normal brain). In our study, normal brains had a mean of 1.483 while brains with GBM produced a mean of -1.334; the cut-off for the function at group centroids showed a calculated value of 0.149.

For the final part of the DA we performed a classification phase using the cross-validated set of data to present the power of the discriminant function. These results revealed that 92.7% of patients were classified correctly into "normal brain" or "brain with GBM" groups, this value corresponded to the overall predictive accuracy of the discriminant function. Additional results of diagnostic tests performance including the 95% confidence intervals (C.I.) showed: sensitivity = 100.00 (80.49 – 100.00); specificity = 87.50 (67.64 – 97.34); (+) likelihood ratio = 8.00 (82.78 – 23.06); (-) likelihood ratio = 0.00 (-); (+) predictive value = 85.00 (62.11 – 96.79); and (-) predictive value = 100.00 (83.89 – 100.00).

The average discriminant (D) scores for each group and the group centroids were used as visual demonstrations of the effectiveness of the dis-

**TABLE 3.** Independent variables included in the discriminant analysis. A, ordered by their Standardized Canonical Discriminant Function Coefficients (variables with larger coefficients stand out as those that strongly predict allocation to each diagnosis). B, Within-groups correlation matrix depicts the participant variables ordered by absolute size of correlation (Pearson coefficients) within function. The largest loadings for each discriminate function (AD was the largest) suggest the preference of diffusivity values that discriminates between normal- and brain-tumor groups. A value of 0.30 is considered as the cut-off between important and less important variables, notice that variables with (\*) were not used in the analysis. C, unstandardized coefficients used to create a discriminant function operating just like a regression equation. Coefficients indicate the partial contribution of each variable to the discriminate function controlling for all other variables in the equation

A		B		C	
Standardized Canonical Discriminant Function Coefficients		Structure Matrix		Canonical Discriminant Function Coefficients	
Variable	Function	Variable	Function	Variable	Function
	1		1		1
CI (linear tensor)	1.361	AD (axial diffusivity)	.748	AD (axial diffusivity)	11443.557
Cs (spherical tensor)	.962	MD (mean diffusivity)*	.568	CI (linear tensor)	105.124
AD (axial diffusivity)	.806	p (pure isotropic diffusion)*	.566	Cs (spherical tensor)	26.804
		L (total magnitude of the diffusion tensor)*	.553	(Constant)	- 48.295
		q (pure anisotropic diffusion)*	.533		
		CI (linear tensor)	.441		
		RD (radial diffusivity)*	.427		
		FA (fractional anisotropy)	.320		
		RA (relative anisotropy)*	.278		
		Cs (spherical tensor)	-.211		
		Age*	.124		
		Cp (planar tensor)*	.020		

criminant function. Histograms and box plots of the average D scores for each group were used as graphical demonstrations of the effectiveness of the discriminant function, the absence of overlap of the plots revealed an excellent discrimination (Figure 3 A-B).

## Discussion

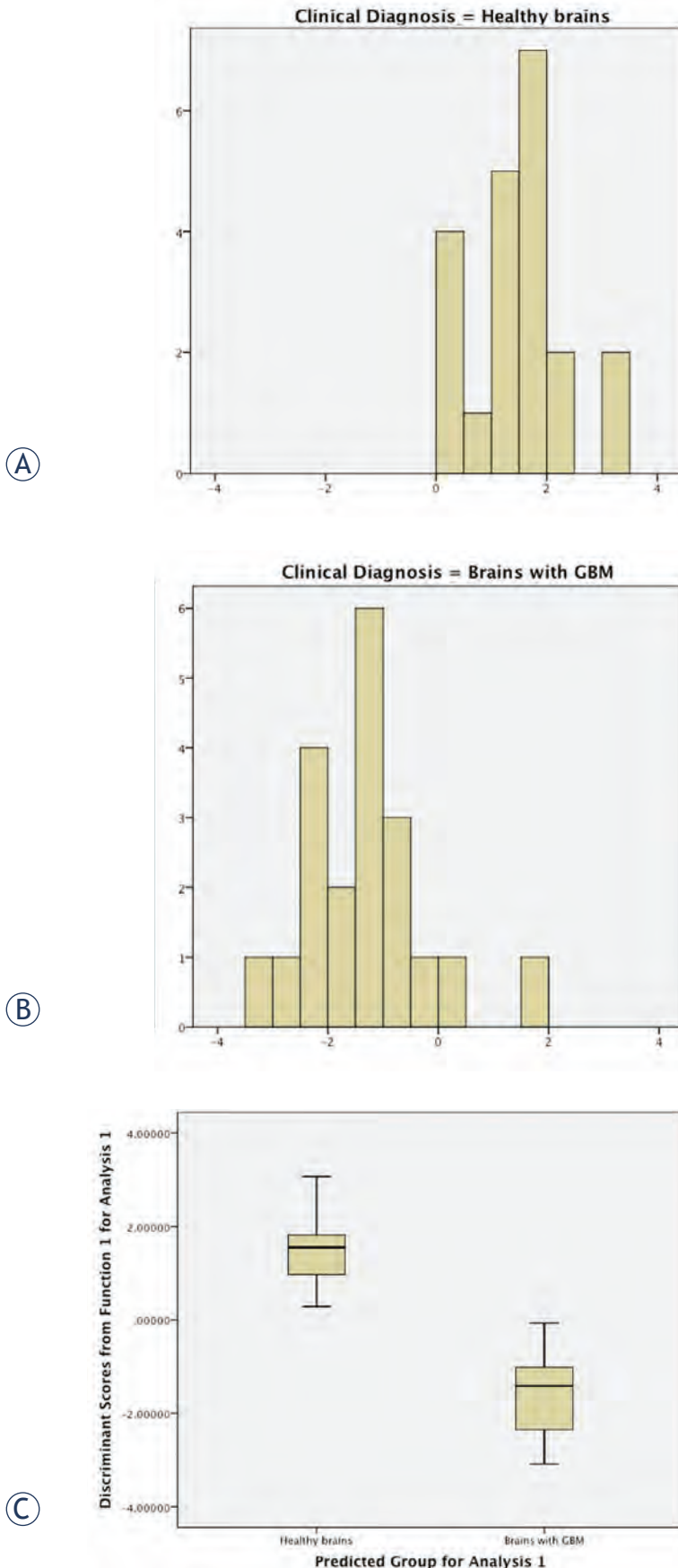
The lack of consensus regarding which DTI-derived tensor metrics are the most meaningful<sup>31</sup>, and the scarce information about their diagnostic abilities, compelled us to evaluate whether a *global* approach might have clinical applicability. We consider our study an introduction to the method and proof-of-principle that a *global* approach using selected DTI-derived tensor metrics can differentiate normal brains from brains infiltrated with GBM, the selected metrics may function as biomarkers assembling a predictive model of tumor infiltration.

The relevant findings in our study showed that a multivariate DA of global measurements excluded the pair-wise comparisons from conventional tumor-region evaluations; the assembled statistically

significant discriminant model of tumor brain impairment (for these data) needed only three *global* DTI-derived metrics: AD, CI, and Cs.

Some advantages of a global approach using DTI metrics need to be mentioned: it decreases the bias associated with manual placement of a region of interest encompassing tumor regions; the tumor and edema regions are implicitly included in the evaluation; lesions not perceived by the radiologist's eye on conventional sequences would be included in a global assessment; it may avoid problems associated with partial volume effects, and inaccurate image coreregistrations; DTI biomarkers can be applied to other tumors/neurological diseases; its acquisition does not need contrast, and its post processing method can be semiautomatic; these facts broaden the clinical applicability with no significant increase in the cost of MRI examinations.

The selected biomarkers in our final model deserve a brief explanation: AD depicted the main influence (larger value of its b unstandardized coefficient); it represents the directional diffusivity describing the microscopic water movement parallel to axonal tracts. AD is one of the best biomarkers in the diagnosis of enhancing rim in GBM, but not for other tumor regions<sup>10</sup>; (this fact provides evidence



that a *regional* measurements may not be the most effective way to use DTI metrics in brain tumor imaging).<sup>14</sup> AD has been studied in animal models of encephalomyelitis of the spinal cord<sup>32,33</sup>, in unfixed *ex vivo* human brains with multiple sclerosis<sup>34</sup>, in a model of axonal injury caused by stroke<sup>35</sup>, and in optic neuritis. CI and Cs on the other hand, along with FA, have been reported among the biomarkers with best overall performance in differentiating the cystic cavity in abscess from GBM.<sup>13</sup> They show best diagnostic performance in the detection of normal-appearance white matter (NAWM) and the cystic cavity in brains with GBM.<sup>10</sup> Cs represents spherical normalized coordinates of a non-orthogonal DTI-derived tensor for each voxel, and CI corresponds to the linear case.<sup>36</sup>

Several limitations in this study need to be addressed: because there have not been studies investigating a whole set of tensor metrics (not only FA and ADC) in a global approach<sup>1,37,38</sup>, it is difficult to compare our results with others in the literature. Further studies might include comparisons with other brain tumors, the influence of variables like radiation necrosis, inflammatory and demyelinating diseases; and tumor infiltration categories such as post-surgery and post-radiotherapy; all of them were beyond the scope of this study. A concern of using DTI-metric values with high correlations (correlations up 0.8 or 0.9), as we observed in our data, might be raised because in those situations one variable is a near-linear combination of the other variable (the variable provides information that is redundant to the information available in one or more of the others, making matrix inversion unreliable).<sup>29</sup> The usual solution is a deletion of the redundant variable, however, because we have a compelling theoretical reason to retain all variables in this study (to evaluate the simultaneous discriminant ability of 11 global tensor metrics), the IBM® SPSS® Statistics software protects against multicollinearity and singularity through computation of pooled within-cell tolerance (1-squared multiple correlation, SMC) for each variable. SMC is the squared multiple correlation of a variable where it serves as the dependent variable (DV) with the rest

**FIGURE 3.** Visual demonstration of the effectiveness of the discriminant function. (A), histograms showing the distribution of discriminant scores for normal- and tumor-brains. (B), box plots of the average D scores. Both kinds of plots illustrate the distribution of the discriminant function scores for each group. The box-plots depict a visual demonstration of the excellent discrimination of the model by showing no overlap between groups.

as independent variables (IV) in multiple correlation. Variables with insufficient tolerance are deleted from the analysis; this procedure is a part of the stepwise method in DA.<sup>22</sup> Our discriminant model was able to explain a significant proportion of the variability in the data (67.56%), but may still have some errors in predicting individual diagnosis, so model validation should be done in subsequent studies. We acknowledge the linking of tensor-metric values with the axonal-integrity status represents an oversimplification with respect to what is happening in brains with GBM, where complex tissue changes occur and affect water diffusivity: density of fiber, average diameters, degree of myelination, directional similarity, cellularity, viscosity, permeability, and histologic architecture; the DTI-tensor values are the effects of the summation of all these microstructural barriers.<sup>13</sup>

Several questions remain unanswered, for example, what is the relation of these tumor-DTI biomarkers with those of MR perfusion and spectroscopy? What is the association of DTI-biomarkers with the pattern of relapse and extension of resection in GBM? So far, only one study, to the best of our knowledge, has correlated a few regional DTI-tensor metrics with the survival of patients with GBM<sup>39</sup>; thus the clinical value of global DTI-metrics in predicting the overall survival has yet to be determined. As a phase II study, our research line will look for a sequel, applying the proven concepts in the follow-up of tumor-infiltration categories (post-surgery, post-radiotherapy, etc.) and in differential diagnoses (primary brain tumors vs. metastasis vs. demyelinating diseases).

## Conclusions

Although we cannot affirm the superiority of global vs. regional DTI-derived tensor metrics in the evaluation of GBM yet, we can ascertain with certainty that there **is** an immediate clinical applicability of these biomarkers in assembling statistically significant predictive models able to announce the conversion of normal tissue to tumor infiltrated tissue before the conventional MR sequences show conspicuous findings. These principles could easily be extended to other neurological diseases. A first step in the advanced evaluation of brain tumors might include a global measurement of DTI-biomarkers able to pick up major infiltration zones. Due to the large number of variables (qualitative and quantitative) that must be analyzed in contemporary brain MRI by radiologists and neuro-

scientists conducting research on novel imaging biomarkers; multivariate techniques, like DA, may help in the generalization of knowledge beyond one setting.

## References

- Zolal A, Hejcl A, Malucelli A, Novakova M, Vachata P, Bartos R, et al. Distant white-matter diffusion changes caused by tumor growth. *J Neuroradiol* 2013; **40**: 71-80.
- Rees JH, Smirniotopoulos JG, Jones RV, Wong K. Glioblastoma multiforme: radiologic-pathologic correlation. *Radiographics* 1996; **16**: 1413-38.
- Watanabe M, Tanaka R, Takeda N. Magnetic resonance imaging and histopathology of cerebral gliomas. *Neuroradiology* 1992; **34**: 463-9.
- Zimmerman RA. Imaging of adult central nervous system primary malignant gliomas. Staging and follow-up. *Cancer* 1991; **67**: 1278-83.
- Johnson PC, Hunt SJ, Drayer BP. Human cerebral gliomas: correlation of postmortem MR imaging and neuropathologic findings. *Radiology* 1989; **170**: 211-7.
- DeAngelis LM. Brain tumors. *N Engl J Med* 2001; **344**: 114-23.
- Smets T, Lawson TM, Grandin C, Jankovski A, Raftopoulos C. Immediate post-operative MRI suggestive of the site and timing of glioblastoma recurrence after gross total resection: a retrospective longitudinal preliminary study. *Eur Radiol* 2013; **23**: 1467-77.
- De Bonis P, Anile C, Pompucci A, Fiorentino A, Balducci M, Chiesa S, et al. The influence of surgery on recurrence pattern of glioblastoma. *Clin Neurol Neurosurg* 2013; **115**: 37-43.
- Young GS. Advanced MRI of adult brain tumors. *Neurol Clin* 2007; **25**: 947-73.
- Cortez-Conradis D, Favila R, Isaac-Olive K, Martinez-Lopez M, Rios C, Roldan-Valadez E. Diagnostic performance of regional DTI-derived tensor metrics in glioblastoma multiforme: simultaneous evaluation of p, q, L, Cl, Cp, Cs, RA, RD, AD, mean diffusivity and fractional anisotropy. *Eur Radiol* 2013; **23**: 1112-21.
- Chaudhry NS, Shah AH, Ferraro N, Snelling BM, Bregy A, Madhavan K, et al. Predictors of long-term survival in patients with glioblastoma multiforme: advancements from the last quarter century. *Cancer Invest* 2013; **31**: 287-308.
- Lopez-Acevedo ML, Martinez-Lopez M, Favila R, Roldan-Valadez E. Secondary MRI-findings, volumetric and spectroscopic measurements in mesial temporal sclerosis: a multivariate discriminant analysis. *Swiss Med Wkly* 2012; **142**: w13549.
- Toh CH, Wei KC, Ng SH, Wan YL, Lin CP, Castillo M. Differentiation of brain abscesses from necrotic glioblastomas and cystic metastatic brain tumors with diffusion tensor imaging. *Am J Neuroradiol* 2011; **32**: 1646-51.
- Wang W, Steward CE, Desmond PM. Diffusion tensor imaging in glioblastoma multiforme and brain metastases: the role of p, q, L, and fractional anisotropy. *Am J Neuroradiol* 2009; **30**: 203-8.
- Rorden C, Karnath HO, Bonilha L. MRICron dicom to nifti converter. In: Neuroimaging Informatics Tools and Resources Clearinghouse (NITRC). Available at: <http://www.mccauslandcenter.sc.edu/mricro/mricron/dcm-2nii.html> Accessed June 07, 2012.
- Smith SM, Jenkinson M, Woolrich MW, Beckmann CF, Behrens TE, Johansen-Berg H, et al. Advances in functional and structural MR image analysis and implementation as FSL. *Neuroimage* 2004; **23**: 208-21.
- Smith SM. Fast robust automated brain extraction. *Hum Brain Mapping* 2002; **17**: 143-55.
- Moseley ME, Cohen Y, Kucharczyk J, Mintorovitch J, Asgari HS, Wendland MF, et al. Diffusion-weighted MR imaging of anisotropic water diffusion in cat central nervous system. *Radiology* 1990; **176**: 439-45.
- Le Bihan D, Mangin JF, Poupon C, Clark CA, Pappata S, Molko N, et al. Diffusion tensor imaging: concepts and applications. *J Magn Reson Imaging* 2001; **13**: 534-46.

20. Brown SR, Gregory WM, Twelves CJ, Buyse M, Collinson F, Parmar M, et al. Designing phase II trials in cancer: a systematic review and guidance. *Br J Cancer* 2011; **105**: 194-9.
21. Obuchowski NA, McClish DK. Sample size determination for diagnostic accuracy studies involving binormal ROC curve indices. *Stat Med* 1997; **16**: 1529-42.
22. Tabachnik BG, Fidell SL. Discriminant analysis. In: Tabachnik BG, Fidell SL, editors. *Using multivariate statistics*. Boston: Pearson Education Inc.; 2013. p. 377-438.
23. Pallant J. Assessing normality. In: Pallant J, editor. *SPSS survival manual*. Crows Nest: Allen & Unwin; 2011. p. 59-64.
24. Pallant J. Multivariate analysis of variance. In: Pallant J, editor. *SPSS survival manual*. Crows Nest: Allen & Unwin; 2011. p. 283-96.
25. Chan YH. Biostatistics 104: correlational analysis. *Singapore Med J* 2003; **44**: 614-9.
26. Field A. Output from the discriminant analysis. In: Field A, editor. *Discovering statistics using SPSS*. London: SAGE Publications Ltd; 2009. p. 618-21.
27. Cohen JW. *Statistical power analysis for the behavioral sciences*. 2nd edition. Hillsdale: Lawrence Erlbaum Associates; 1988.
28. Bossuyt PM, Reitsma JB, Bruns DE, Gatsonis CA, Glasziou PP, Irwig LM, et al. The STARD statement for reporting studies of diagnostic accuracy: explanation and elaboration. *Ann Int Med* 2003; **138**: W1-12.
29. Tabachnik BG, Fidell SL. Multicollinearity and singularity. In: Tabachnik BG, Fidell SL, editors. *Using multivariate statistics*. Boston: Pearson Education Inc.; 2013. p. 88-91.
30. Field A. Discriminant function variates. In: Field A, editor. *Discovering statistics using SPSS*. London: SAGE Publications Inc.; 2009. p. 599-624.
31. Pena A, Green HA, Carpenter TA, Price SJ, Pickard JD, Gillard JH. Enhanced visualization and quantification of magnetic resonance diffusion tensor imaging using the p:q tensor decomposition. *Br J Radiol* 2006; **79**: 101-9.
32. Budde MD, Xie M, Cross AH, Song SK. Axial diffusivity is the primary correlate of axonal injury in the experimental autoimmune encephalomyelitis spinal cord: a quantitative pixelwise analysis. *J Neurosci* 2009; **29**: 2805-13.
33. Feng S, Hong Y, Zhou Z, Jinsong Z, Xiaofeng D, Zaizhong W, et al. Monitoring of acute axonal injury in the swine spinal cord with EAE by diffusion tensor imaging. *J Magn Reson Imaging* 2009; **30**: 277-85.
34. Schmierer K, Wheeler-Kingshott CA, Boulby PA, Scaravilli F, Altmann DR, Barker GJ, et al. Diffusion tensor imaging of post mortem multiple sclerosis brain. *Neuroimage* 2007; **35**: 467-77.
35. Song SK, Yoshino J, Le TQ, Lin SJ, Sun SW, Cross AH, et al. Demyelination increases radial diffusivity in corpus callosum of mouse brain. *Neuroimage* 2005; **26**: 132-40.
36. Westin CF, Maier SE, Mamata H, Nabavi A, Jolesz FA, Kikinis R. Processing and visualization for diffusion tensor MRI. *Med Image Anal* 2002; **6**: 93-108.
37. Woodworth DC, Pope WB, Liao LM, Kim HJ, Lai A, Nghiemphu PL, et al. Nonlinear distortion correction of diffusion MR images improves quantitative DTI measurements in glioblastoma. *J Neurooncol* 2013. [Epub ahead of print]
38. Saksena S, Jain R, Schultz L, Jiang Q, Soltanian-Zadeh H, Scarpace L, et al. The corpus callosum Wallerian degeneration in the unilateral brain tumors: evaluation with diffusion tensor imaging (DTI). *J Clin Diagn Res* 2013; **7**: 320-5.
39. Saksena S, Jain R, Narang J, Scarpace L, Schultz LR, Lehman NL, et al. Predicting survival in glioblastomas using diffusion tensor imaging metrics. *J Magn Reson Imaging* 2010; **32**: 788-95.

## Conclusiones

- La medición de biomarcadores avanzados de resonancia magnética en pacientes con glioblastoma multiforme permiten la construcción de modelos predictivos de supervivencia. En nuestro proyecto, obtuvimos un modelo con significancia estadística que seleccionó tres biomarcadores avanzados:
  - Cholina/N-acetil-aspartato
  - Lípidos-Lactato/Creatina
  - Edad
- El resto de variables utilizadas en nuestro modelo (derivados de secuencias convencionales) no fueron seleccionadas.
- Es posible calcular 11 biomarcadores diferentes, derivadas de la secuencia tensor de difusión en el encéfalo de sujetos sanos y en pacientes con glioblastoma multiforme.
- Existe una variabilidad significativa en mediciones derivadas del tensor de difusión en diferentes regiones y a lo largo de trayectos axonales de estructuras nerviosas del encéfalo normal. Conocer esta variabilidad permitirá una correcta interpretación de hallazgos en el estado normal y patológico.
- Cada uno de estos nuevos biomarcadores muestra un desempeño diagnóstico diferente dependiendo de la región tumoral evaluada: tumor viable, necrosis, edema y tejido normal. Este hallazgo limita la realización de un abordaje regional para medir la infiltración tumoral en pacientes con glioblastoma multiforme y justifica la necesidad de un método global para detectar la infiltración tumoral.
- El análisis multivariado discriminante aplicado a los biomarcadores avanzados globales también permiten calcular un modelo significativo que permite la diferenciación de tejido sano y enfermo y que tiene capacidad predictiva.
- El proyecto de investigación permitió crear una línea de investigación original y con gran potencial para producción científica de calidad, no existente actualmente en México y que podría traer beneficio inmediato al diagnóstico y tratamiento de pacientes.
- Nuestra línea de investigación continuará su tarea de responder varias preguntas referentes al uso de las técnicas avanzadas de resonancia magnética en el estudio de los tumores cerebrales, entre las más inmediatas se incluyen:
  - ¿Cuál es la correlación entre espectroscopia, difusión, perfusión y tensor de difusión como biomarcadores de una misma región tumoral?
  - ¿Cuál es la capacidad diagnóstica multivariada de estos biomarcadores para la supervivencia en GBM en un abordaje global versus regional?